POLITECNICO DI TORINO

Master's Degree course in Energy and Nuclear Engineering

Master’s degree thesis

ENHANCING BUILDING ENERGY FLEXIBILITY THROUGH DYNAMIC ENVELOPE COMPONENTS

Supervisors:

Prof. Perino Marco

Prof. Favoino Fabio

Candidate:

Marmo Federico

Co-Supervisor:

Eng. Li Castri Ginevra

Academic year: 2025-2026

Summary

ABSTRACT

The transition towards a decarbonised energy system, driven by European objectives such as the Green Deal and the 'Fit for 55' package, increasingly relies on the integration of intermittent renewable energy sources. This requires shifting from a paradigm in which generation adapts to demand to one where demand also supports grid balancing, through Demand Side Management strategies and, in particular, building energy flexibility. Given the high share of electricity consumption in the building sector and the growing diffusion of electrified HVAC systems, buildings represent a key resource for Demand Response programmes. In this context, the building envelope, traditionally considered passive, can become an active component, here referred to as an Advanced Building Envelope (ABE), capable of supporting flexibility while maintaining indoor comfort.

The literature shows that direct technology-independent comparisons of ABE solutions in terms of energy flexibility remain limited, especially for transparent components, which have mostly been studied from an energy-saving rather than flexibility perspective. This thesis addresses this gap by proposing a comparative method to quantify how heterogeneous envelope technologies contribute to maintaining acceptable indoor conditions during DR events.

Three advanced building-envelope elements operating across different physical domains were analysed: transparent double-skin façades, phase-change materials integrated into internal walls, and traditional and dual-band electrochromic glazing. The technologies were implemented in a BESTEST-based room served by an ideal HVAC system. Their energy performance was evaluated in EnergyPlus and compared with a reference case without advanced building-envelope technologies.

One-hour energy flexibility events were scheduled during peak electricity prices identified using the SAX technique and implemented by modifying temperature and relative humidity setpoints together with technology-specific control strategies. Reference climatic conditions were defined through a standardised sinusoidal parameterisation of outdoor temperature and solar radiation, calibrated against meteorological data from four locations representative of a broad climatic range: Trondheim, Turin, Florence, and Messina. This approach makes the methodology generalisable beyond site-specific weather conditions.

A dedicated set of Key Performance Indicators was used to quantify and compare each technology's performance against its corresponding reference case. These indicators

include autonomy, degree of partialisation, peak-shaving capacity, rebound energy, pre-charge energy, and DR energy balance.

The results show that implementing ABEs can improve a building's energy performance during flexibility events. PCM-enhanced walls significantly extend the system runtime and reduce rebound loads, especially during the coldest months. The performance of the DSF system is strongly linked to solar radiation levels, delivering significant benefits when used correctly while limiting both operational autonomy and peak-shaving capacity when used improperly, highlighting the close correlation between building envelope elements and the control system. The electrochromic glazing used did not perform optimally under any conditions, confirming that its primary purpose is to serve as a system for controlling thermal and light radiation, mainly to ensure occupant comfort and long-term energy savings.

1 INTRODUCTION

The need to achieve the objectives established by the Paris Agreement [1] adopted during the 2015 Conference of the Parties (COP 21) has led to increasing attention towards renewable and low-carbon energy sources. These sources are essential for reducing greenhouse gas emissions and limiting the environmental impact of energy production. However, many renewable energy sources, such as solar and wind power, are intermittent and non-dispatchable, creating new challenges for the management of both energy supply and demand.

At the European level, the energy transition is framed by the European Green Deal[2], an agreement reached in December 2019, which sets the objective of achieving climate neutrality by 2050. This long-term target was complemented by the European Climate Law, the 'Fit for 55' [3] and by the intermediate goal of reducing net greenhouse gas emissions by at least 55% by 2030, compared with 1990 levels. The 55% target was endorsed by the European Council in December 2020 and subsequently incorporated into the European Climate Law.

The regulations provide major reforms in sectors with high CO_2 emissions, such as industry, transport and energy production. The building sector and energy consumption linked to air conditioning are also addressed, with a push to improve the energy efficiency of the existing building stock, introduce stricter requirements for new construction, and digitalise key systems.

Although the integration of renewable energy sources is essential for reducing greenhouse gas emissions and the environmental footprint of energy generation, their intermittent, highly variable nature poses new challenges and requires changes to supply and demand management.

In this context, it is necessary to move beyond the traditional energy system paradigm, in which generation is adjusted to meet demand, and to actively involve consumers through demand-side management (DSM) strategies to adjust their consumption over time. As a growing number of consumers become prosumers by installing small-scale renewable energy systems such as solar panels and micro-wind turbines, there is an increasing need to develop a dynamic system that aligns generation with demand and vice versa. It will therefore be necessary to manage energy demand not only by reducing total consumption but also by reducing peak demand and shifting peak-load periods over time so that they coincide as closely as possible with periods of highest Renewable Energy Sources (RES) production.

The ongoing expansion of heat pump air-conditioning systems, together with the significant share of electricity consumption in residential and non-residential buildings, means that this category of consumers is an excellent candidate for implementing DSM programmes, which in this field are known as Energy Flexibility programmes. By modifying the operating parameters of HVAC systems managed by comprehensive control systems that can receive and evaluate signals from the electricity distribution network, it is possible to shift electricity loads over time, making greater use of Renewable Energy Sources (RES) and reducing strain on the grid during periods of peak demand. Even with this change in HVAC system operation, it remains imperative to maintain occupant comfort in indoor environments; this must be ensured through control methods for the air-conditioning systems themselves and, as discussed in the following study, by utilising the building envelope and its characteristics.

1.1. MODERN ELECTRICAL GRIDS

The current national and European electricity system is based on a centralised production model, relying on large fossil fuel-fired generation plants and a consumer network spread across the country.

Renewable electricity generation facilities, including photovoltaic and wind power, are inherently dispersed throughout the country and often require multiple connection points for small and medium-sized producers. This new configuration presents substantial challenges for network operators and consequently necessitates infrastructure modernisation, with an emphasis on increased interconnections among regions and states to enhance resilience.

Furthermore, the effort to electrify air conditioning and transport is driving increasing electricity demand. To address this issue, transmission lines must be properly expanded and adapted to ensure continuous, accessible service to all consumers.

On this issue, the European Commission, during Plenary session 604, approved the *European grids package* [4] aimed at updating the regulatory framework for *Trans-European Networks for Energy (TEN-E)* to better align with EU climate goals and regional needs. The main objectives include:

- Support for decentralised production

- Greater coordination at the European level
- Digitalisation of electricity networks

This final point is of great importance for facilitating greater interconnection among all stakeholders and for developing a smart grid capable of integrating distributed generation systems, renewable energy production, energy storage, and flexible buildings, all of which are elements needed to achieve the objectives set out by the Green Deal.

1.2. PRODUCTION AND CONSUMPTION OF ELECTRICAL ENERGY

According to Eurostat [5] data for 2024, electricity accounts for 23% of all energy consumed in Europe; 48% of this electricity is generated from renewable sources, including wind turbines (17%), hydropower plants (13%), solar power (11%) and biofuels (nearly 6%), with the remainder coming from fossil fuels (28%) and nuclear power (23%). These figures represent the European average, but there are still significant differences between individual countries.

According to the IEA [6] during 2023, in Europe, transport accounted for the largest share of total energy consumption (29%), followed by the residential sector (24%). However, in terms of electricity consumption, the industrial sector was the largest consumer (35%), followed by the residential sector (30%).

These figures show that the residential sector, and more broadly the building sector, is a major consumer of energy and, consequently, a key sector for developing and implementing energy flexibility programmes to balance energy demand and supply, which is increasingly dominated by renewable and intermittent sources.

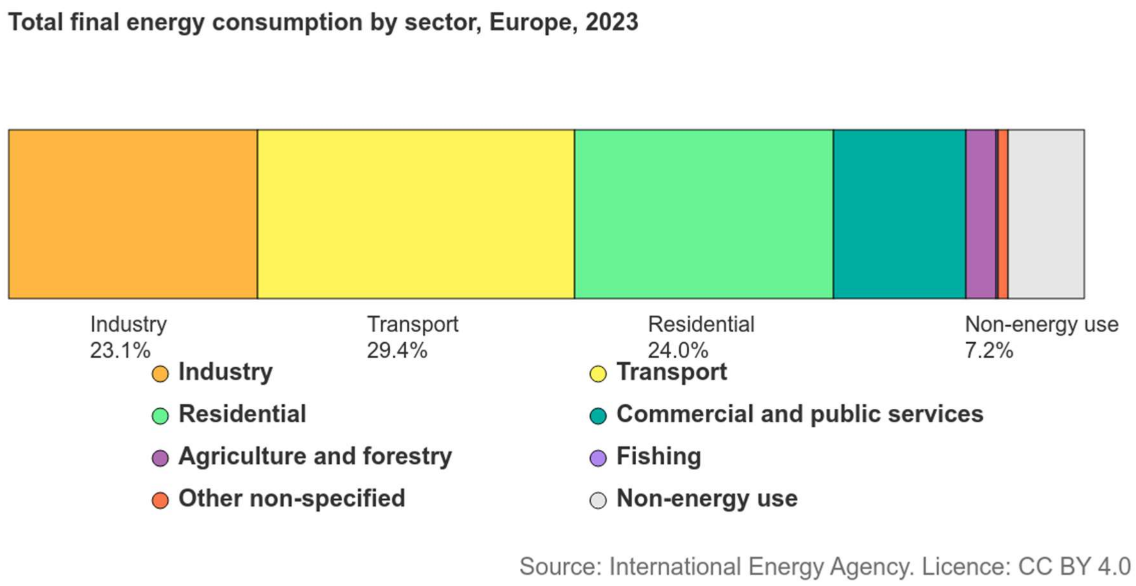

Figure 1: Total final energy consumption by sector, Europe, 2023 [6]

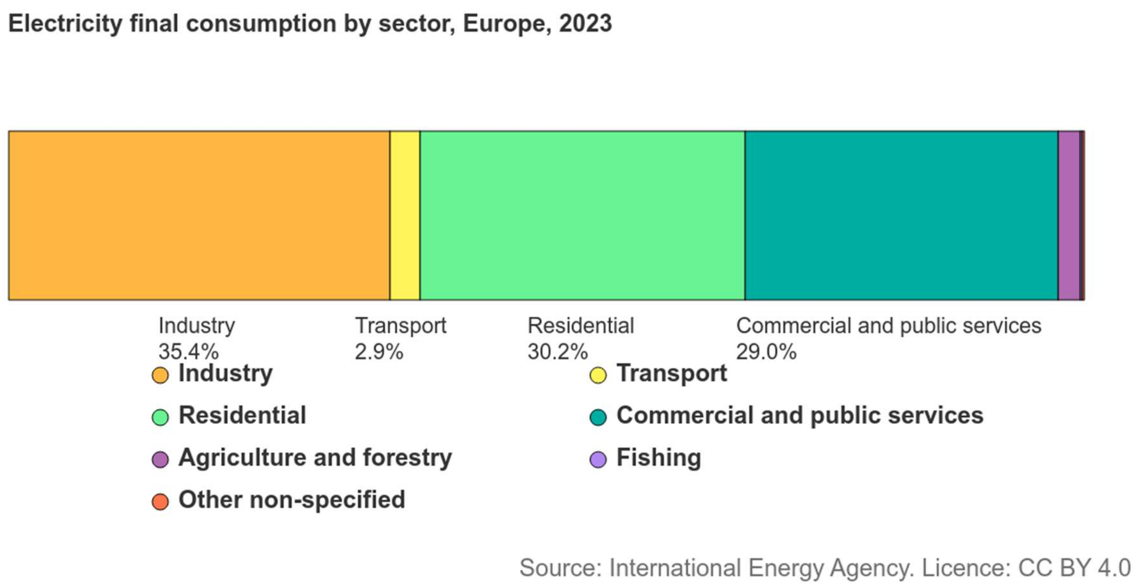

Figure 2: Total electrical energy consumption by sector, Europe, 2023 [6]

1.3. AIMS OF THE STUDY AND RESEARCH QUESTIONS

Building-related energy flexibility, as described in [7], has been an established field of research since 2019; it is also reported that more than 160 articles on this topic were published between 2019 and 2023. Various have set out to identify standard parameters for measuring a building's capacity to provide energy flexibility, using categories [8] and numerical values, thereby providing a method for comparing different buildings under varying boundary conditions. There are also many articles on innovative building envelope elements, especially opaque ones, that are linked to both energy savings and energy flexibility.

The literature review summarised in Chapter 2 revealed that direct comparisons of different building envelope technologies in relation to energy flexibility events have not been extensively examined; furthermore, regarding transparent building envelopes, the studies have primarily focused on energy savings, with few references to energy flexibility and direct comparisons. The main focus of this work was therefore to quantify the contribution these technologies can make to maintaining acceptable indoor conditions during Demand Response events. Several parameters were specifically developed to characterise the most relevant energy values, quantify the contribution of the different technologies, evaluate the control method, and assess the influence of the external climate.

In order to meet these challenges, the following research questions are raised:

RQ1. How can the energy flexibility potential of advanced building envelope technologies operating through different physical domains be assessed and compared using a common simulation-based framework?

The objective of this question is to explore the feasibility of using a common methodology to assess the contributions of heterogeneous envelope solutions that act through different physical mechanisms and to compare them fairly.

RQ2. How can standardised climatic boundary conditions be defined to support a generalisable assessment of building energy flexibility?

The objective is to develop a standardised method for identifying climate parameters representative of the climate under analysis and to apply them to model-based simulations of flexibility events.

RQ3. Which Key Performance Indicators are most appropriate for quantifying the flexibility services provided by advanced building envelope technologies?

The goal is to define a set of metrics able to capture all the different aspects of flexibility performance: peak-demand reduction, load-shifting capacity, energy use and indoor thermal comfort.

2 LITERATURE REVIEW

A building's façade is the first barrier separating the interior from the external environment; it is therefore responsible for heat exchange and for controlling incoming solar radiation. Buildings with large, glazed façades are aesthetically appealing and widely used; they allow high solar gain and good lighting. However, these features also result in higher cooling loads and, during colder periods, poor insulation, which in turn leads to high heating loads; finally, if not properly controlled, sunlight can cause glare.

Given the significant influence of the building envelope on a building's energy consumption, advanced façade technologies have attracted increasing attention. By dynamically regulating heat transfer and solar gains, these systems can transform the building envelope from a passive boundary into an active and controllable element. As a result, they can contribute not only to improving energy efficiency but also to enhancing energy flexibility by adapting the building's energy demand according to grid requirements and flexibility-oriented control strategies. This chapter presents a literature review to assess the current state of these technologies, their potential contributions to energy flexibility, and prior studies on them.

2.1. ENERGY FLEXIBILITY DEFINITION

Regarding the subject of energy flexibility in buildings, the pioneering study that initially aimed to raise awareness within the scientific community and establish a shared foundation is the one conducted between 2016 and 2019 by the International Energy Agency (IEA), titled "IEA EBC ANNEX 67: Energy Flexible Buildings." Energy flexibility is defined as: "Energy flexibility of a building is the ability to manage its demand and generation according to local climate conditions, user needs, and grid requirements. Energy flexibility of buildings will thus allow for demand-side management/load control and thereby demand response based on the requirements of the surrounding grids and on the availability of RES, in order to minimize CO2 emissions"[9].

In accordance with European policies aimed at reducing climate-altering gas emissions and the widespread adoption of RES, the distinction between energy flexibility and energy savings is emphasised. In fact, the issue of reducing total consumption is not addressed; rather, the focus is on strategically shifting energy loads to align with periods of high energy production from environmentally sustainable sources.

In accordance with Reynders et al. [10], three general properties are defined to characterise a building's degree of energy flexibility:

1. Capacity: the amount of energy that can be diverted per unit of time

2. Temporal aspects: duration of flexibility events, start time, and system response time

3. Cost: potential economic and energy savings associated with the flexibility event.

These aspects are necessary to quantify a building's behaviour and energy consumption when it is subject to flexibility events, compared with a reference case.

2.1.1. Penalty signal

The method identified in [9] for communicating the start, duration and characteristics of a demand response event in a standardised manner amongst all stakeholders is to implement a penalty signal. This is issued by the grid and may have different objectives depending on the situation and requirements, such as:

- Minimising costs
- Minimising CO_2 emissions
- Maximising the utilisation of RES generation

The signal is generated to pursue one or more objectives simultaneously, and it is the responsibility of the controller of the individual system or a cluster of systems/buildings to adjust operating parameters to best meet the requirements represented by the penalty signal.

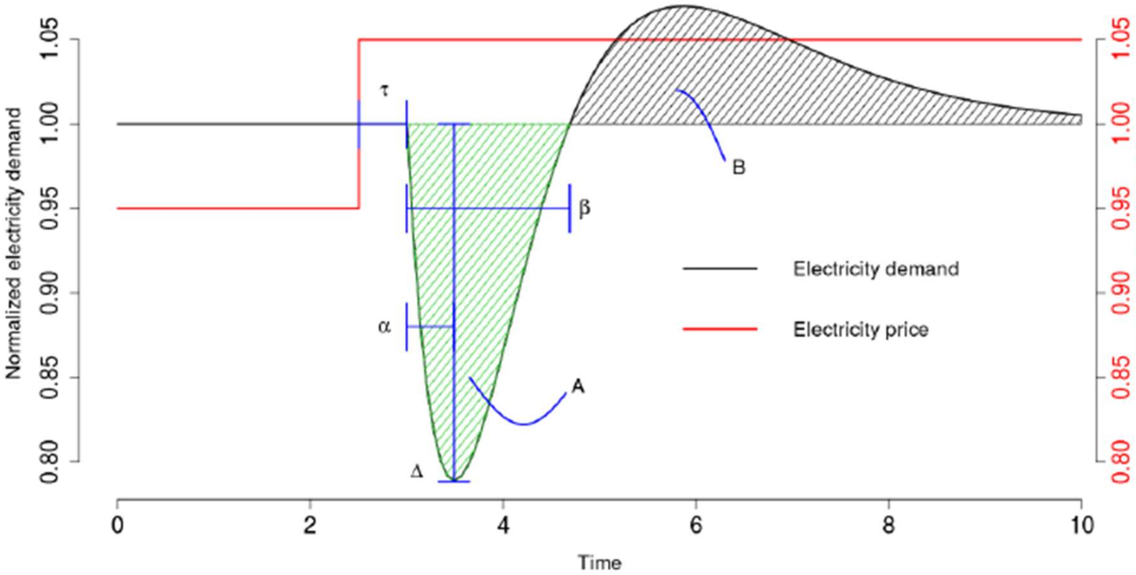

Figure 3: From [9] electrical load example of a building subject to a penalty signal: τ is the time delay from when the signal is submitted to an action start, α is the time from start of the response to maximum response, A is a shifted amount of energy, and B is the rebound effect.

2.1.2. Energy flexibility strategies

Energy flexibility can be driven by one or more objectives and can therefore be achieved through various methods, which adjust the timing and level of energy demand in response to grid requirements or changes in energy availability. The main methods are:

- **Peak shaving:** aims to reduce peak energy demand during critical periods, thereby reducing the strain on the grid and limiting peak power requirements.
- **Valley filling:** involves increasing energy demand at times when there is little need for it, in order to make the most of periods of high renewable energy production and/or to store energy.
- **Load shedding:** involves temporarily reducing energy demand, even at the expense of certain services.
- **Load shifting:** comprising a coordinated use of these techniques, it aims to shift energy loads from periods of high demand to times when demand is lower, whilst keeping total energy consumption unchanged.

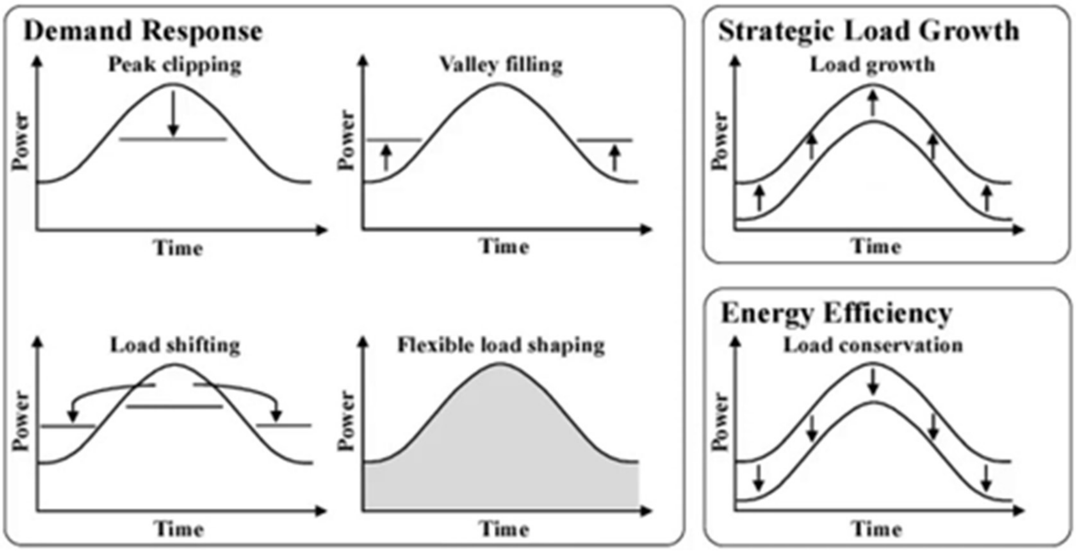

Figure 4: Typical demand response strategies

2.2. ADVANCED BUILDING ENVELOPE

Historically, the building envelope has been designed as a passive, static element based on the ‘energy conservation approach’ [11], whose main objective is to reduce energy consumption and maintain occupant comfort, without the ability to respond to dynamic events such as changing weather conditions and the availability of internal systems.

To support the evolution of a building’s energy system from the traditional demand-driven model to one with greater adaptability, the building envelope must also become an active system capable of adjusting its parameters and energy input to the interior spaces. This is the role of Advanced Building Envelopes (ABEs), “Envelope systems and technologies that can ensure high building performance across a wide range of physical domains … using a combination of advanced material properties, advanced components and advanced integrated control strategies” [12]. These technologies enable dynamic control of certain energy vectors to which the building is constantly subjected, but which, without the appropriate systems, remain dictated solely by external conditions; for this reason, they are also referred to in the literature as “responsive building elements” [11]. *Figure 5* shows the diagram presented by [12], which illustrates the main existing systems that are classifiable as ABEs and the energy vectors on which they can exert influence.

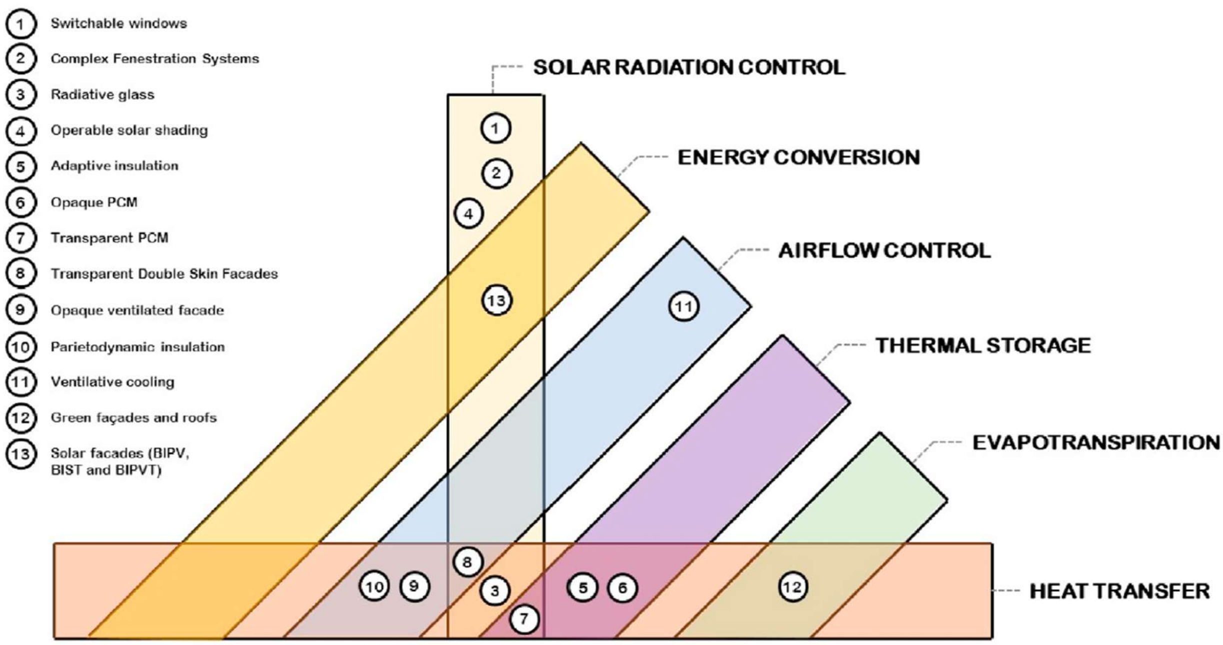

Figure 5: The relationship between ABEs and the physical domains [12]

2.3. SELECTION FOR THE CASE STUDY

Based on the literature review and on the classification presented in Figure 4, three advanced building envelope technologies were selected for the case study. These technologies were chosen because they operate primarily in different physical domains, allowing the analysis to cover a broader range of possible envelope contributions to energy flexibility. This choice necessitated the development of universal parameters not directly linked to individual energy contributions from external sources, which are essential for developing a comparison methodology that is theoretically applicable to any ABE technology.

The following physical domains and related ABEs have been chosen for this analysis:

- **Airflow control:** Transparent double skin façade
- **Thermal storage:** Opaque phase change materials (PCM)
- **Solar radiation control:** Switchable windows

This selection supports the development of a comparison methodology that is not limited to a single type of energy exchange or to a specific technology. Instead, it enables the assessment of different envelope strategies using common performance parameters that can theoretically be applied to different ABE systems.

For the sake of simplicity, each technology has been assigned to a single physical domain. As is well known, in reality all the physical elements present in a building and the various physical domains are, at least in part, interconnected; for example, Transparent Double Skin Facades fall under both the 'Solar radiation control' and 'Airflow control' categories. Therefore, the classification adopted here should not be interpreted as rigid, but rather as a way to identify the dominant contribution of each technology and to structure the comparative analysis.

2.4. DOUBLE SKIN FACADES

Safer et al. define this technology as: "A double-skin façade is a special type of building envelope, where a second 'skin', usually transparent glazing, is placed in front of a standard building façade". The space between the second skin and the façade is known as a 'channel' and can range in thickness from a few centimetres up to 0.8–1 meter, depending on design choices [13]

There are essentially two types of DSF design: in the first, the outer layer creates a series of cavities, one for each floor of the building, each separate and independent of the others; in the second, a single cavity connects all the floors [14]. The study presents a further categorisation of DSFs, as shown in *Figure 6*:

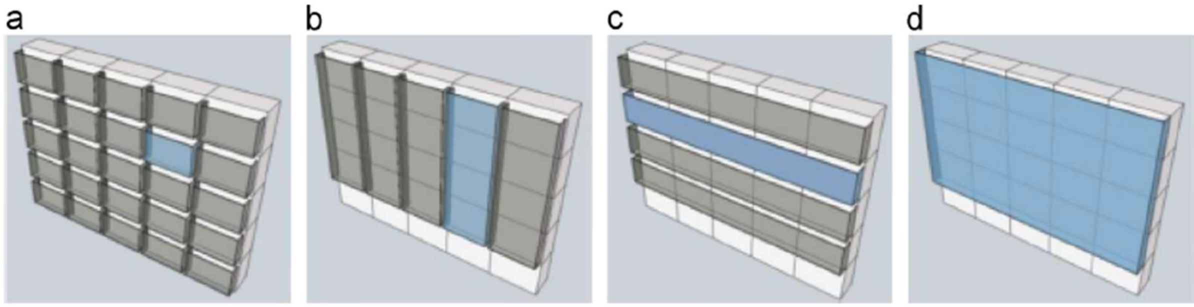

Figure 6: Another categorization of DSFs: (a) Box window, (b) shaft-box, (c) corridor and (d) multi-storey double skin facade from [14]

The most interesting feature of a DSF is undoubtedly the internal cavity through which air can circulate via natural or forced ventilation; the latter is independent of weather conditions, providing greater control and flexibility for the technology, although it does increase its complexity [15]. The airflow rate and turbulence affect the heat transfer coefficients of the building façade, making this technology highly dynamic.

A DSF may have two or four openings; the second allows guided air exchange between the interior and exterior, enabling ventilation air to be supplied to the interior spaces. Regardless of the design choice, a common feature of a DSF system is an adjustable shading system, most often a roller blind or a Venetian blind. These elements allow control of solar gain, significantly influencing the amount of light entering the space and regulating how much solar radiation is transmitted to the interior or converted into heat within the cavity [15].

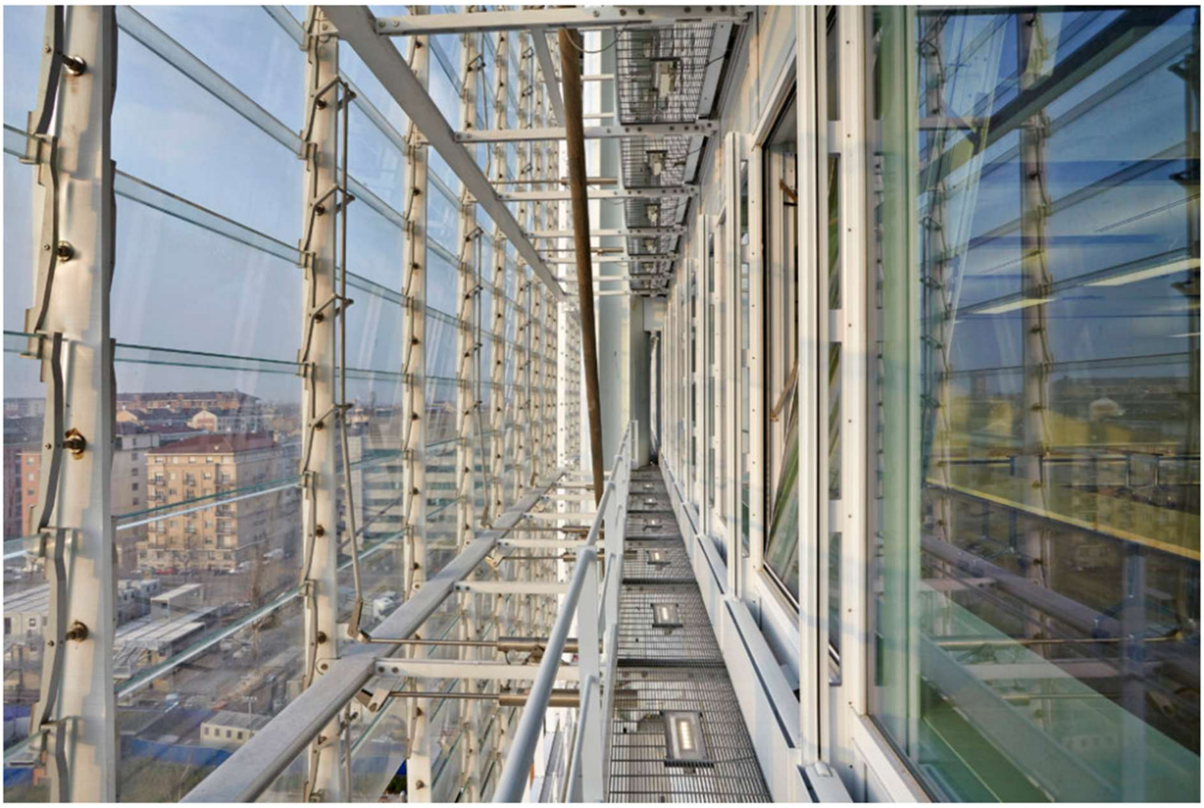

Figure 7: Interior view of the DSF installed on San Paolo's skyscraper in Turin

DSF systems were originally developed to improve thermal insulation and energy performance in buildings in cold climates [14]; thanks to their adaptability, these systems also perform well in hot climates, where the greatest energy demands relate to cooling [16]. The latter also assesses how this technology can be applied in retrofit projects for existing buildings to improve energy performance, a topic of great interest in Europe, where, according to an article published in 2019 [17] "The building stock in the EU Member States is relatively old; on average, 21.6% of the building stock was built before 1945, 45.4% before 1969 and 75.4% before 1990".

[14]One of the main limitations of these systems is their very low thermal inertia; to overcome this problem and reduce overheating, [18] considers the advantages of incorporating phase-change materials (PCMs) into the slats of the Venetian blinds.

2.4.1. Cavity ventilation type

As presented by Li Castri et al. [19] there are primarily four operating modes for a four-opening DSF with mechanical ventilation:

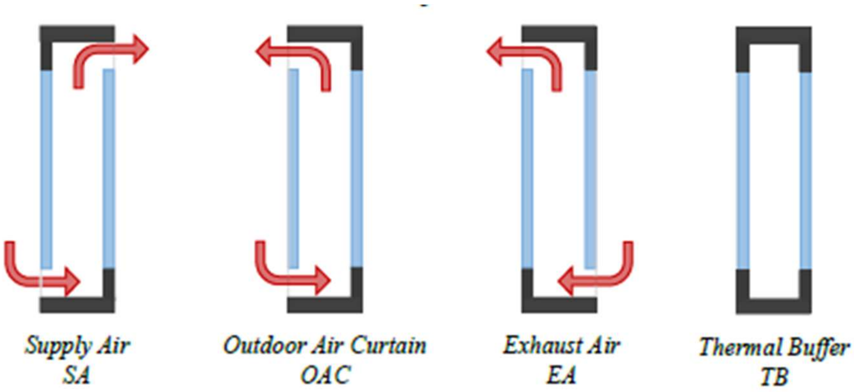

Figure 8: DSF ventilation mode from [19]

- **Supply air (SA):** air drawn in from outside is channelled through the cavity to be preheated before being released into the interior; this method is used in winter to maximise the capture and conversion of solar radiation into thermal energy.
- **Outdoor air curtain (OAC):** air is forced through the cavity and expelled through the top opening; this is used during the cooling season to limit solar gain and prevent overheating of the cavity and shading systems.
- **Exhaust air (EA):** The interior air is passed through the cavity before being expelled; this method uses temperature-controlled air—which is laden with pollutants—to extract heat from the cavity, thereby preventing overheating.
- **Thermal buffer (TB):** In this mode, all openings are closed, reducing airflow to zero and thereby minimising heat loss during the heating season by lowering the total heat exchange through the façade**.**

This technology can also be integrated with the air-conditioning system and a heat recovery unit to make the most of all available heat flows.

2.4.2. Façade Total Heat Transfer

To best describe the thermal behaviour of this technology and to take all energy-related factors into account, the paper by Li Castri et al. [19] introduces the Façade Total Heat Transfer (FTHT) parameter, which comprises the following elements:

- $Q_{\Delta T}$: Heat transferred between the inner surface of the façade and the air by convection and radiation due to the temperature difference, including solar heat absorbed by the façade
- $Q_{s,dir}$: refers to short-wave solar radiation transmitted directly into the indoor environment
- Q_v , Q_{v_dsf} , Q_{v_hr} : The heat gain or loss due to ventilation air, depending on the chosen strategy.

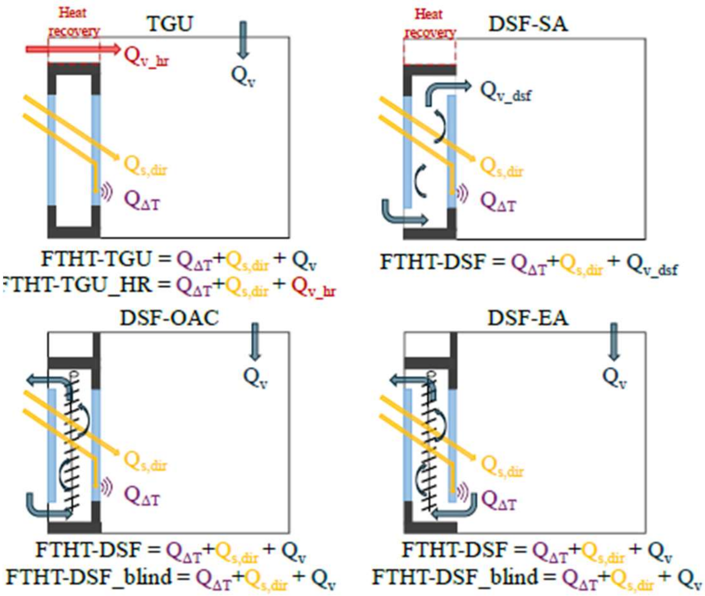

Figure 9: Schematic representation of the FTHT indicator from [19]

2.5. PHASE CHANGE MATERIALS

One of the key issues accompanying the development of renewable energy sources is energy storage, which is necessary to meet energy demand when production is insufficient or to store surplus energy during periods of overproduction. These systems can take many forms and operate on different principles, storing energy in thermal, chemical or potential forms. One of the main obstacles to the adoption of these technologies is their high costs and long payback periods.

In the domain of building energy management, the most widely used energy storage technologies are electric batteries and water tanks for sensible heat storage. When adequately managed by a control system, these devices facilitate the maximisation of renewable energy use where available and enable decoupling of periods when the building's internal systems require electrical and/or thermal power from periods when the building draws this energy from the grid.

The systems described above can be costly and difficult to implement; however, buildings naturally store thermal energy in the form of sensible heat within all their structural components, a concept known as Structural Thermal Energy Storage (STES) [10]. Defining a building’s thermal storage capacity and the charging and discharging efficiency of its thermal mass is less straightforward than with traditional energy storage; these parameters depend on the physical characteristics of the structures, the external climate and the behaviour of the occupants [10]. They also depend on the presence of interior furnishings within the rooms [20], which will not be considered in this study, as the focus is on the building envelope elements.

As a general principle, the capacity for thermal storage is directly related to the building's mass; this is determined by the mass and specific heat of the structures in contact with indoor air. Heavy materials such as bricks or concrete, placed in the innermost layer of the building envelope, can exchange heat with the indoor air efficiently and store large amounts of heat; conversely, if the envelope consists of lightweight materials, it will not be able to store sensible heat. The positioning of the various layers of material making up the building envelope is also crucial: if the insulating layer is placed on the inside, it will be harder for the indoor air to exchange heat with the elements comprising the wall, thus limiting the amount of heat present in the structures that can be recovered; conversely, if the insulation layer is placed on the outside, the heavier structures and the indoor air will be able to exchange heat.

Lightweight buildings with poor insulation have limited capacity to adapt to energy flexibility schemes, as they entail high energy loads and virtually no energy storage capacity [20]; however, it is precisely in these buildings where significant reductions in energy consumption could be achieved. In this case, to significantly increase thermal mass without introducing large, heavy elements, the walls can be integrated with elements containing phase-change materials (PCMs) which, thanks to their ability to store large quantities of heat within a small volume, through latent heat associated with phase transition processes, can absorb and release thermal energy under limited temperature variations compared to sensible heat storage systems, thereby helping to make the building more flexible, “modulate the peak energy demand and provide load shedding and shifting capacity” [21].

The most commonly used materials include eutectics, hydrated salts and paraffins [22]. When applied to the building envelope, these can be macro-encapsulated – that is, enclosed within sealed panels, often modular [23] – or micro-encapsulated, with the materials dispersed within a matrix material, such as plasterboard panels.

2.5.1. Properties of phase change materials

PCMs can store large amounts of thermal energy during phase transitions whilst maintaining a relatively stable temperature. When this process occurs in a pure material, the melting and solidification temperatures coincide, and the material's temperature remains constant throughout the process. When industrial-grade PCMs such as those listed above are used, undesirable phenomena may occur; the two main ones are a widening of the temperature range over which the phase change occurs and hysteresis.

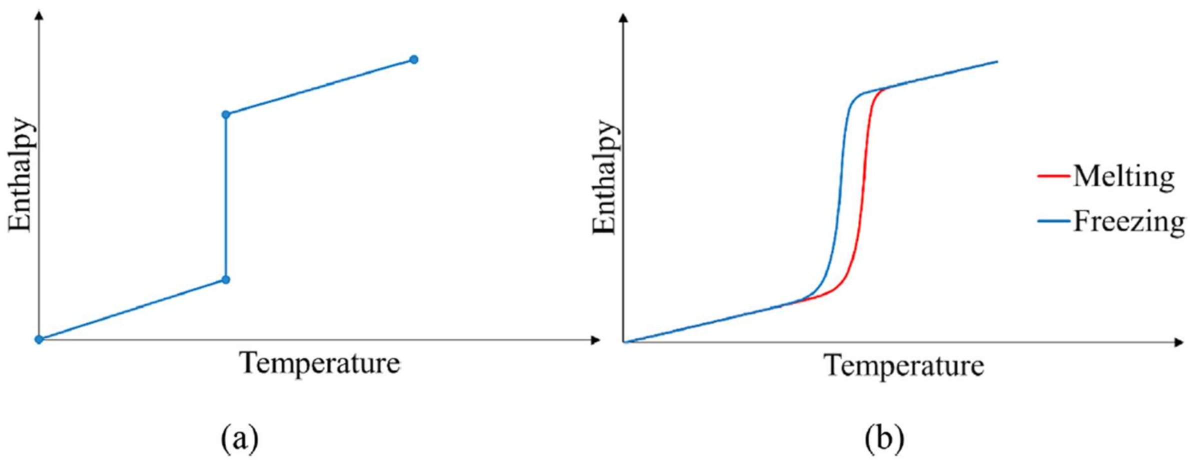

Figure 10: Enthalpy-temperature curves for (a) ideal/pure PCMs and (b) industrial-grade PCMs, from [24]

Thermal hysteresis in PCMs is the temperature lag between a material's melting and freezing points. The melting temperature will thus be higher than the solidification temperature, resulting in a deviation of the enthalpy curves during the phase change. Furthermore, this behaviour is not fixed but depends on the material's state and its past history. As described by Feng et al. [24], this phenomenon "is mainly due to primary nucleation and crystal growth mechanisms, which lower the crystallisation temperature compared to the melting temperature". Other undesirable phenomena that particularly affect hydrated salts include phase separation, volume changes and supercooling, which result in a significant loss of usable latent heat [21].

These characteristics pose significant challenges that have limited the widespread adoption of this technology; furthermore, simulation-based assessments of material behaviour are particularly difficult, requiring specialised calculation methods and careful attention to descriptive parameters.

2.5.2. Control method and parameters

The main purpose of this technology is to store heat and shift air-conditioning loads over time; thermal inertia helps maintain stable indoor conditions by releasing or absorbing heat, thereby reducing the system's workload. This behaviour can be considered passive, similar to the conditions normally found in a building without advanced controls or systems. To make the best use of this technology, the most commonly used technique is pre-heating or pre-cooling, depending on requirements. In anticipation of a flexibility event, the internal temperature setpoint will be adjusted; as a result, the PCM in the walls will undergo a partial phase change due to hysteresis, exchanging heat as required.

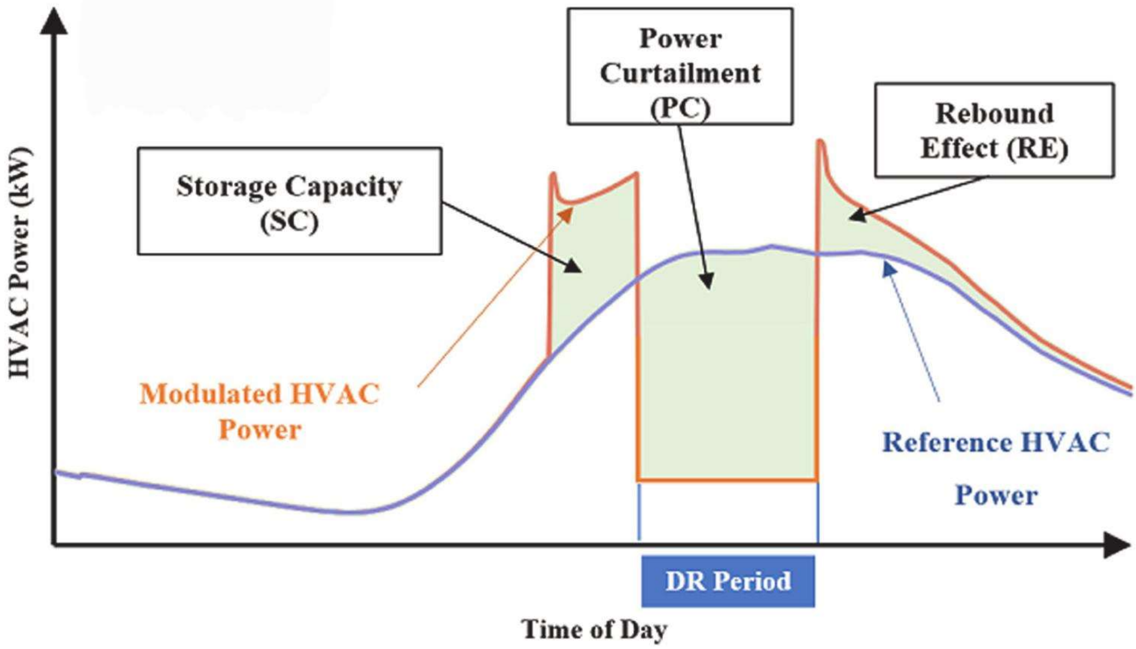

Figure 11: Sample graph comparing normal system load with pre-loading followed by a flexibility event from [22]

Saffari et al. [22] describe how the ability of PCMs to maintain indoor conditions during energy-flexibility events depends primarily on the event duration, but also on the temperature and duration of the preheating phase. The variation in internal temperature must allow the material to be preheated while maintaining comfortable conditions for the occupants; therefore, it will be necessary to limit the variation based on the preheating period.

Time period	0.25 h	0.5 h	1 h	2 h	4 h
Max. operative temperature change allowed	1.1 °C	1.7 °C	2.2 °C	2.8 °C	3.3 °C

Figure 12: Allowed temperature change in a thermal zone from[22]

The selection of specific parameters is crucial for achieving the material's desired performance during demand response events and for accounting for total energy consumption.

The study conducted by Wijesuriya [21] presents a parametric analysis which shows that:

- Energy flexibility increases with PCM thickness and reaches saturation at over 1.91 cm
- Energy flexibility increases with latent heat capacity and saturates at 200 $^{kj}/_{kg}$
- The heat transfer coefficient between the air and the walls plays a crucial role in the charging and discharging of the material; however, above a value of 5 $^{W}/_{m^2k}$ total energy consumption increases.

Another important parameter is the material's thermal conductivity; if this value is very low, the interaction between the material and the environment will be limited. Consequently, particularly during short pre-loading and flexibility events, it will not be possible to transfer sufficient heat to or from the material, thereby limiting its effectiveness. As reported in [25] increasing thermal conductivity increases the material's thermal contribution, but beyond 0,5 $^{W}/_{mK}$ no significant changes are observed.

Finally, the melting temperature is the last parameter that significantly influences the material's behaviour, as reported by Saffari et al. [22]. The optimal temperature depends on the building's energy requirements: "PCM with a low melting temperature of 21 °C is best suited for a building that requires a heating input, whilst a PCM with a higher melting temperature of 25 °C is more effective for a building that requires a cooling input". Whilst correct, this statement does not account for the hysteresis characteristics analysed previously; these must be considered when selecting the material, as they can significantly widen the temperature range over which the total phase change occurs.

2.6. ADAPTABLE GLAZING TECHNOLOGIES

Windows in buildings are essential for ensuring a comfortable environment for occupants; they provide a connection to the outside world, allow sunlight to illuminate rooms, contribute to acoustic comfort, and, where no dedicated ventilation system is present, enable ventilation. Due to significant differences relative to the opaque building envelope, glazed enclosures account for approximately 50% of the building's heat loss; furthermore, artificial lighting, which is directly linked to window characteristics, accounts for approximately 19% of total electricity consumption in Europe [26].

There is considerable room for improvement in this area to reduce the energy consumption associated with glazed enclosures, making them more adaptable and responsive to occupants' needs and the building system; this is made possible by advanced smart glazing technologies.

As with opaque glazing, one of the key characteristics used to describe the performance of transparent glazing is its thermal transmittance, typically referred to as the U-value $\left[{W}/{m^2K}\right]$. Alongside the optical properties of glass are also crucial when assessing its performance. The key parameter is the Solar Heat Gain Coefficient (SHGC), or g-value, which ranges from 0 to 1. It represents the fraction of solar energy entering through the transparent glazing, comprising both the energy transmitted directly and that absorbed by the glass and then re-emitted into the interior.

In their review of established and innovative glazing technologies, Michael et al. [27] identify two main categories: static and dynamic technologies.

2.6.1. Static glazing technologies

Static technologies are characterised by fixed properties; among the most common are single glazing units (SGU), now found only in older buildings and with very low thermal insulation values, multi-layer units, including double glazing units (DGU), the most common in Europe [28], and triple glazing units (TGU). A greater number of layers and thicker glass increase the panes' thermal resistance; to further increase this value, the air between the panes can be replaced by a noble gas such as argon, krypton or xenon, which are, however, very expensive; alternatively, the cavity can be completely evacuated to create a vacuum, in which case it is known as an evacuated glazing unit (EGU).

The g-value and light transmittance depend both on the composition of the glass, which can be modified by adding small amounts of metal oxides (cobalt, titanium, manganese, etc.) during the manufacturing process, and on the surface treatments usually applied "by chemical dipping of the glass panes or by evaporating metals onto the surfaces of the glass panes in a vacuum"[27].

These coatings can be designed to selectively reflect electromagnetic radiation within a specific range; low-e coatings are characterised by their ability to reflect long-wave radiation. When applied to buildings with predominantly heating loads, "short-wave solar heat enters the building, whereas long-wave heat re-radiated from warm indoor surfaces is reflected by the low-e coating and retained within the building. In cooling-dominated climates, low-e coatings prevent long-wave radiation from warm surfaces outside from entering through the glass" [27].

2.6.2. Dynamic glazing technologies

To adapt as effectively as possible to external conditions, occupant needs, and transient events, such as those related to energy flexibility, it is necessary to adjust the characteristic parameters of a transparent glazing system as described above. In dynamic glazing technologies, also known as switchable glazing, it is possible to alter the properties passively or actively, thereby adjusting the amount of energy entering the space.

2.6.2.1. Passive technologies

Passive technologies respond to external stimuli such as temperature and light; they do not require control by the Energy Management System, which makes them simpler to install and use but less flexible.

The main categories are:

- Photochromic: As the intensity of the light striking the glass increases, the organic or inorganic compounds present in the glass at the time of its manufacture undergo a change in their molecular structure, thereby reducing the glass's light transmittance. This change is temporary and reversible; the compounds return to their natural state once the incident radiation is reduced.
- Thermochromic: In this category, the stimulus is the temperature of the active layer; once the critical temperature (Tc) is reached, the active molecules change their structure, thereby continuously altering the transmittance as the temperature rises. There are two main types of thermochromic materials: the first is always transparent to visible radiation and can selectively alter the absorption coefficient for infrared radiation, whilst the second alters both infrared and visible radiation.
- Phase change materials: PCMs can be integrated into glazing technologies; thanks to their ability to absorb and release large amounts of latent heat, they can help maintain a constant indoor temperature. Furthermore, the difference

in the visible light transmittance coefficient between the liquid and solid states (a characteristic of paraffins) also enables control of incoming solar radiation.

2.6.2.2. Active technologies

Active technologies are characterised by their independence of environmental conditions; their optical properties are usually controlled by adjusting the applied voltage to the active layer. The most widely used technologies are liquid crystal (LC) and electrochromic (EC) technologies [29].

- Liquid crystal: consisting of two conductive layers with a polymer matrix in between, in which spherical crystals are dispersed; normally, these are randomly scattered, making the layer opaque and causing light to scatter. When a voltage is applied to the two conductive layers, the liquid crystals align with the electric field, drastically reducing light scattering and making the layer transparent in a very short time.
- Electrochromic: the layers consist of two types of molecules: the organic ones change colour as a result of reversible oxidation or reduction reactions. The inorganic molecules include metal oxides, and the operating principle involves the migration of lithium ions from one electrochromic layer to another, thereby altering the layer's transparency. The transition from the clearest to the darkest state can occur in several stages, depending on the applied voltage, which normally does not exceed 5V.

2.6.2.3. Focus on electrochromic glazing

Among all active technologies, the electrochromic smart window has become the focus of researchers due to its characteristics such as active regulation, low energy consumption, short response time and rich colour [30]. Unlike liquid crystal glazing, which is mainly used to control privacy and daylight [31], electrochromic glazing can be used to control solar heat gains, which directly impact the building's thermal balance and HVAC energy demand. The properties of EC windows are especially well-suited for building energy flexibility applications in which solar gains can be manipulated to lower peak loads, thereby enabling demand response strategies. In contrast, passive smart glazing technologies, such as thermochromic and photochromic windows, are inherently dependent on environmental stimuli and cannot be controlled according to user preferences or grid requirements. For these reasons, electrochromic glazing was selected as the reference smart glazing technology in this study.

This technology was developed to control the amount of light entering through a window; however, an analysis of the solar emission spectrum reveals that approximately 46% of solar energy is distributed in the near-infrared (NIR) range, spanning 780–2500 nm. To achieve complete regulation of energy entering through the transparent opening, in terms of both visibility and thermal control, more sophisticated electrochromic glass models have been developed. These are known as dual-band EC, as they can independently control visible light and NIR; this makes it possible to limit the amount of incoming energy whilst continuing to utilise natural light, or to limit potential glare effects whilst still allowing a portion of EM radiation to enter the space [30].

Figure 13, taken from the study by Riganti et al. [29], compares visible light transmittance with the SHGC (g-value) for three types of static glazing: one electrochromic and one dual-band electrochromic, each with eight different states. The points with the highest Tvis and SHGC values indicate the most transparent states. It shows that the first four states of the dual-band type significantly reduce the SHGC factor whilst causing only a modest decrease in the Tvis factor, demonstrating the ability to control the NIR radiation portion separately from the visible portion.

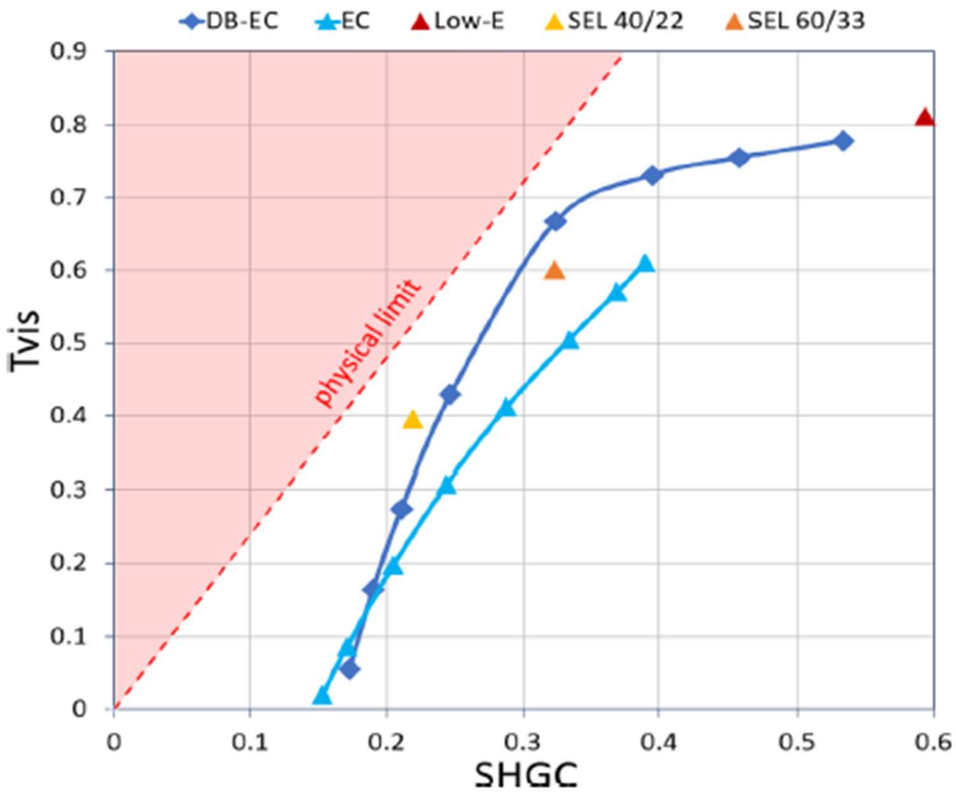

Figure 13: Relationship between the Visible Transmittance (Tvis) and the Solar Heat Gain Coefficient (SHGC) of electrochromic and static technologies from [29]

In the same paper, the energy savings achievable with this technology are assessed, and it is emphasised that they depend heavily on the control method applied to the glass.

- Rule-based control algorithm: this type of control is based on fixed if-then rules; it takes certain parameters as input and, following a series of logical steps, produces an output. In this case, the parameters considered are the indoor air temperature and the solar radiation incident on the window, which are used to determine the optimal electrochromic glass state among the eight possible states.
- Model-based control algorithm: This type of control does not operate on fixed rules but uses mathematical models to predict certain parameters – such as energy consumption for air conditioning and lighting – based on the possible choices within the controlled parameter, in this case, the state of the electrochromic glass. In this way, the best option is selected to minimise the objective function – often defined as the total energy consumed – whilst still maintaining the comfort parameters specified by the users.

3 METHODOLOGY

This chapter will outline the methodology adopted in the study. Given the lack of similar studies in the literature, no pre-validated procedure was applied; each step was assessed and developed specifically to ensure the best conditions for a sound and balanced study. The following will therefore describe the choices made to establish the boundary conditions, such as the distribution of flexibility events, climate data, and the metrics used to evaluate the results.

3.1. DISTRIBUTION OF FLEXIBILITY EVENTS

The studies analysed cover a wide range of flexibility events, some very short, lasting around 15 minutes, and others lasting up to 3–4 hours [22]. For this study, following several preliminary simulations, it was decided to consider 1-hour events. The method used to identify the time slots for considering flexibility events is described below.

As described in the first chapter, flexibility events can be driven by various factors: maximising the use of renewable energy sources, minimising CO_2 emissions, alleviating strain on the electricity grid, and economic considerations. The choice of which factor to focus on can vary greatly depending on the building in question, its characteristics, the electricity grid serving it, and the occupants' requirements. For this study, the economic factor was selected, as data on electricity costs are publicly available, up-to-date and easy to obtain. Furthermore, as a result of the European Emissions Trading System (EU ETS), energy costs are partly linked to CO_2 emissions and the use of renewable energy sources (RES); it is therefore possible, at least in part, to pursue more than one objective.

The national monthly electricity consumption figures for 2024 were obtained from TERNA's website [32], the organisation that manages Italy's electricity transmission grid. This was the most recent year for which full reports had been published at the time of the research, and the figures are as follows:

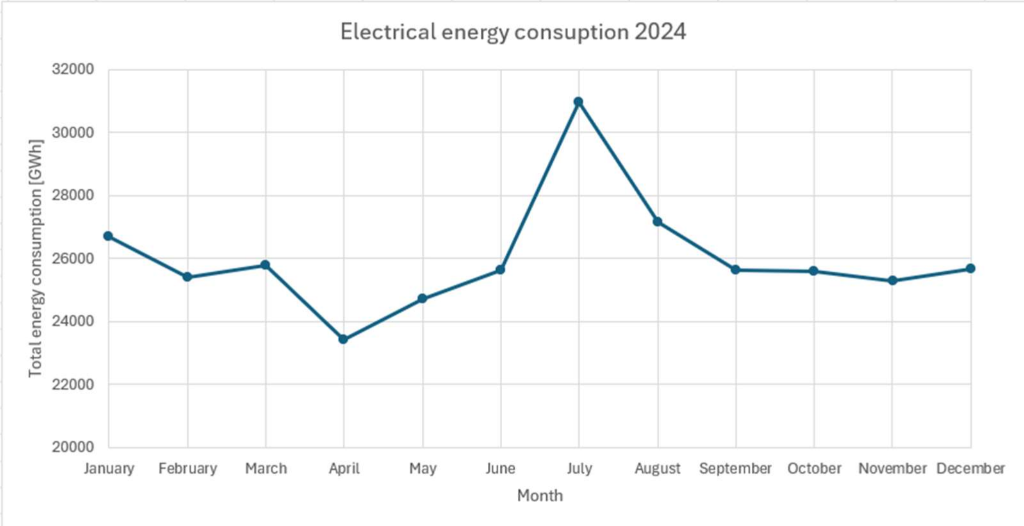

Figure 14: Monthly electrical energy consumption 2024

The highest consumption figures are recorded in July and August, possibly due to high temperatures and the intensive use of air-conditioning systems, with December following.

The hourly values of the Prezzo Unico Nazionale (PUN) – the reference price for electricity purchased on the Italian power exchange – were derived from the website of the Gestore dei Mercati Energetici (GME) [33], the state-owned company responsible for organising and managing the wholesale electricity and natural gas markets in Italy. Considering total consumption data and the periods historically associated with the highest air-conditioning consumption due to weather conditions, two periods were selected for the following analysis: the winter period, comprising November and December 2024 and January 2025, and the summer period, comprising June, July and August 2025.

3.1.1. The SAX reduction technique

The hourly datasets obtained from GME for the respective periods outlined contain a significant amount of data; in order to analyse them in a comprehensible manner, maintain the daily breakdown and identify recurring patterns, the SAX reduction technique was employed.

The SAX (Symbolic Aggregate Approximation) technique is a method for reducing and transforming time series. Whilst this technique results in a loss of detail in the historical data, it makes the data easier to analyse and allows individual periods to be categorised. The technique consists of two stages:

- **Data aggregation (PAA – Piecewise Aggregate Approximation)**: The dataset is divided into broader, regular time intervals; for each interval, the mean value of the variable is calculated and assigned.
- **Symbolic encoding**: The range comprising all the values of the variable within the time series is divided into intervals defined by thresholds (breakpoints); each interval is assigned a symbolic category denoted by a letter. Subsequently, the mean value calculated in the previous step is replaced with the symbolic category corresponding to the interval to which it belongs.

Once the analysis is complete, each day in the time series will be represented by a sequence of symbols—which can be interpreted as words—whose length equals the number of time intervals into which each day has been divided; at this point, it will be easy to identify the days with similar profiles.

To reduce the size of the dataset whilst minimising the loss of detail, 3-hour intervals were used, resulting in an 8-letter code for each day and four symbols to represent the average price for that interval.

The analysis continues to identify frequent price patterns ("motifs") and infrequent ones ("discords"); the latter are discarded as atypical. The days identified as motifs are further divided into three clusters using the Ward method, which aims to merge groups in a way that minimises the increase in a measure of heterogeneity for the entire dataset, known as "intra-cluster variance". Finally, for each group, a centroid profile has been calculated and will serve as the representative profile for that cluster.

3.1.2. Choice of time slots

The following are the three representative clusters for the winter and summer seasons, respectively:

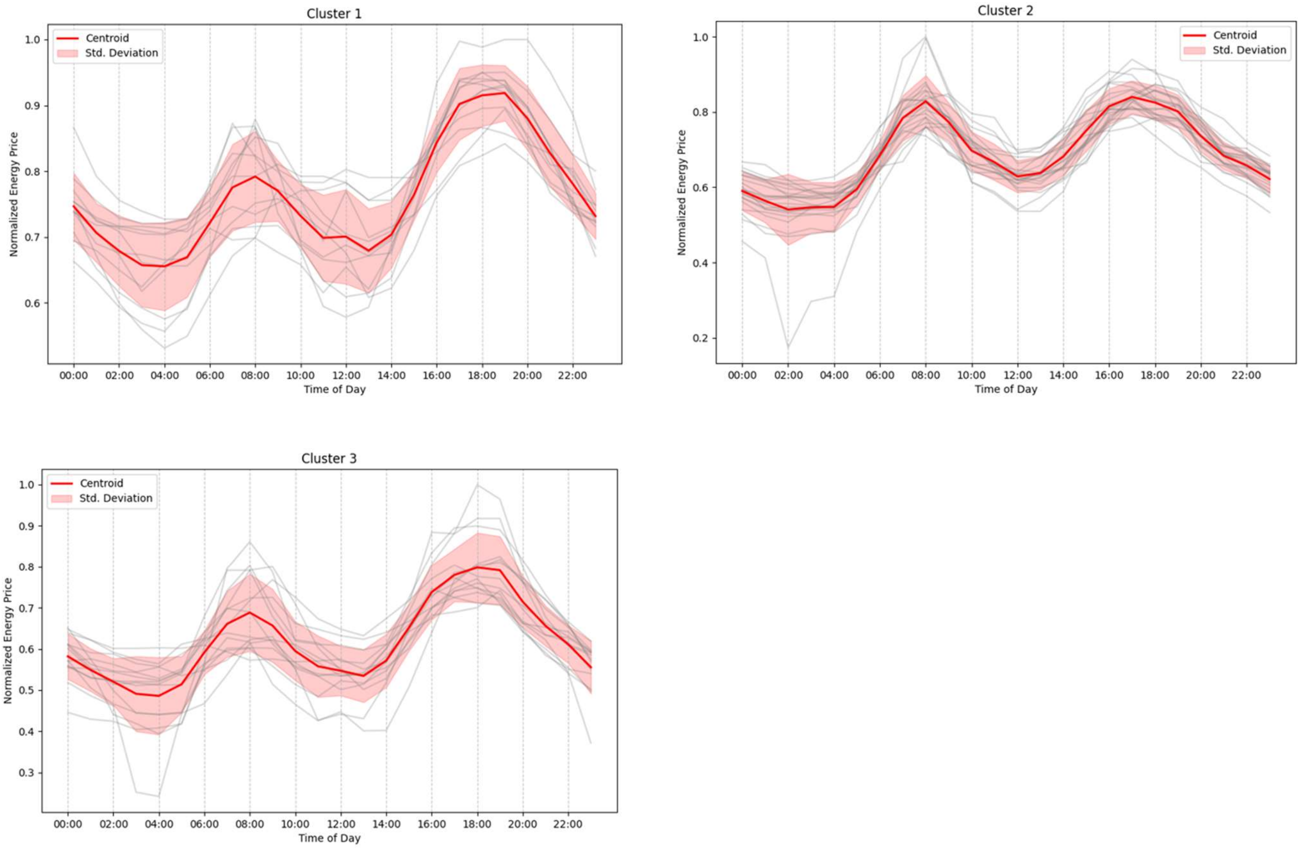

Figure 15: Representative cluster November, December, January

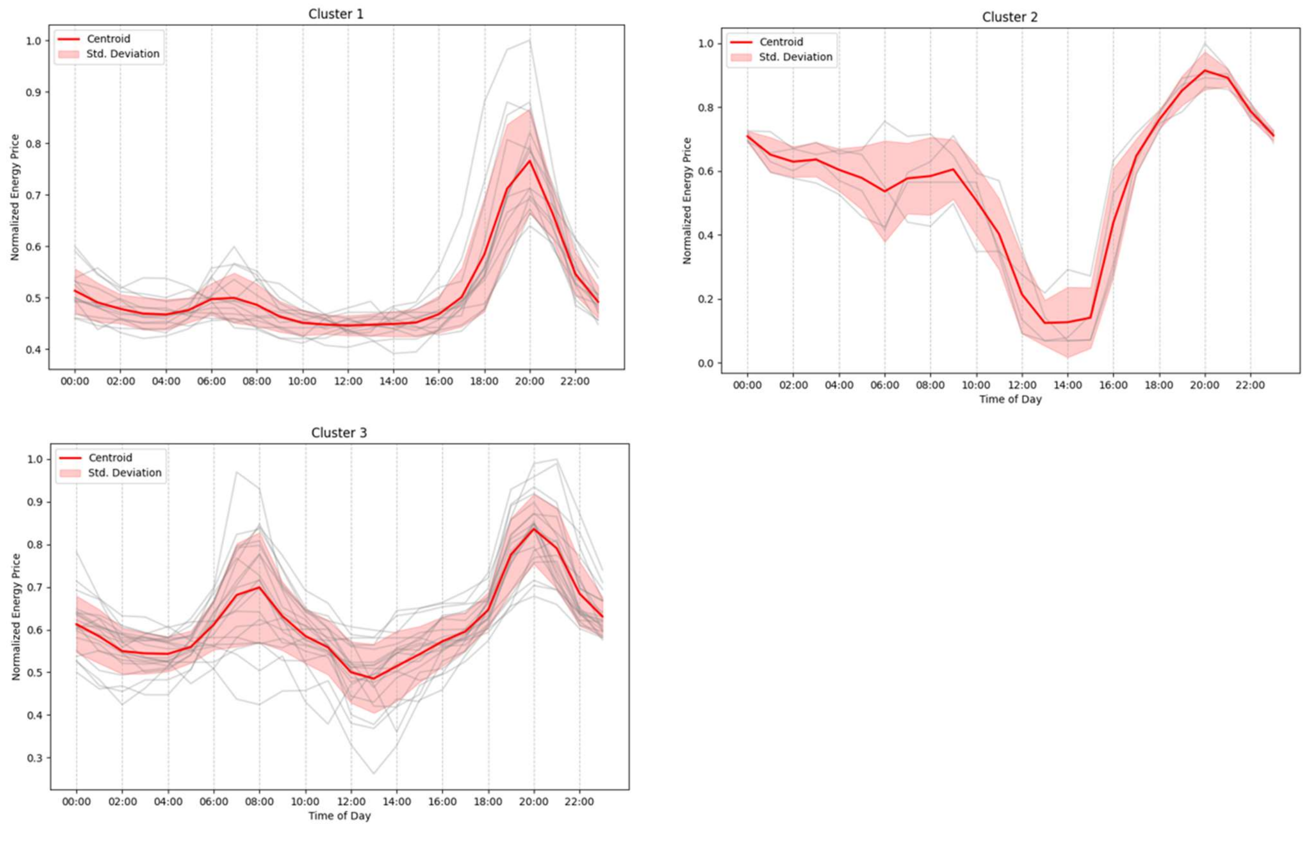

Figure 16: Representative cluster June, July, August

Considering the results of the analysis carried out, the differences between the profiles and timings of the two seasons, and the possible times of sunset and sunrise, two time slots lasting 1 hour were selected for use throughout the study:

- **Morning event:** 8 – 9
- **Evening event:** 17 – 18

3.2. WEATHER CONDITIONS

The selection of weather conditions was another important step in the study's development, as it is the main driver of air-conditioning energy consumption. The first objective was to identify several locations representative of different climates, so that the building envelope elements under analysis could be subjected to a wide range of conditions and their behaviour could be assessed comprehensively.

3.2.1. Initial procedure

Following the analysis conducted to identify the time slots for flexibility events (FE), three Italian cities were initially selected: Turin, Florence, and Messina. A preliminary assessment of the climates was carried out by calculating the values of the Heating Degree Days (HDD) and Cooling Degree Days (CDD) parameters using Typical Meteorological Year (TMY) files based on the period 2005–2023, obtained from the European Union's Photovoltaic Geographical Information System (PVGIS) website [34].

$$HDD = \sum \max(0, T_{base} - T_{mean})$$

$$CDD = \sum \max(0, T_{mean} - T_{base})$$

The base temperature used in the **HDD** calculation is the outdoor temperature **below** which buildings require heating to maintain a comfortable environment.

The base temperature used in the **CDD** calculation is the outdoor temperature **above** which buildings require cooling to maintain a comfortable environment

The mean temperature is the average outdoor temperature for the day, calculated

as $T_{mean} = \frac{T_{max}+T_{min}}{2}$

The results of the calculation are strongly influenced by the building's base temperature. The same base temperature was used for all three locations.

Consequently, although the absolute values of the HDD and CDD parameters may not fully represent the selected cities, the differences among the results demonstrate climatic variations.

Table 1: HDD and CDD values for the selected Italian cities

Location	HDD	CDD
Turin	2447,5	297,1
Florence	1936,5	455,8
Messina	736,4	1243,8

Given Italy's topography, the identified locations can serve as good examples of different climates; however, compared with many European countries, Italy has a warmer climate. For this reason, the Norwegian city of Trondheim has been added to the study as a reference point for a particularly cold climate.

3.2.2. Selection of simulation days

Once the reference climates had been identified, the next step was selecting the simulation days. A number of selection criteria were initially considered but were subsequently ruled out as insufficiently relevant to the study or overly restrictive for a broad-based analysis.

From now on, all climate data files used have been obtained from the Climate One Building website [35]. For each identified city, data files covering the years 2009 – 2023 have been used.

3.2.2.1. Maximum average power

For the first criterion, a basic model of the case study (described in detail in the next chapter) was used, to which no advanced building-envelope elements were added. For each of the four identified sites, one-year simulations were conducted; subsequently, the days with the highest average heating and cooling loads were identified.

This selection method was rejected because it focuses on the most critical days, which account for only a small percentage of the year; furthermore, the choice is heavily dependent on the building’s characteristics and past history, thereby diverting attention from climatic conditions to some extent.

3.2.2.2. Italian legislation

The second approach uses the Italian standard UNI 10349 [36], which provides climate data on temperature and solar radiation for the main Italian municipalities; for each municipality, it also defines values of these parameters' representative of a peak day and an average day for both the winter and summer seasons. Once this data had been obtained, the climate files for the various cities were searched for days whose temperature and solar irradiance characteristics were as similar as possible to those specified in the standard.

This method, as well as not being applicable to the city of Trondheim, is difficult to implement as it is hard to find days that accurately represent the values reported in the standard; the main risk also lies in limiting the simulations, and therefore the case study, to a single day with a very specific climate, thereby straying from the ultimate objective of the work, which is to identify a generic comparison method applicable even to elements and scenarios beyond those analysed.

3.2.3. Standardised method for selecting climate parameters

To move away from a specific day and location, the final decision was to manually set the parameters for temperature and solar radiation on a horizontal plane. To best generalise the simulated conditions, the two curves were modelled as perfect sine waves. This made it possible to recreate well-controlled conditions that could be adapted to any climate by adjusting just a few parameters.

The equation of a sine curve is: $y(t) = Asin(\omega t + \phi) + V_0$

Where:

- $\boldsymbol{y(t)}$: Value of the parameter at time t.
- $\boldsymbol{A}$ **(Amplitude)**: Indicates the maximum value reached by the sinusoid relative to the parameter V_0.
- $\boldsymbol{\omega}$ **(Angular frequency)**: ω = $2\pi f$ is the frequency. It determines the oscillation speed.
- $\boldsymbol{\phi}$ **(Initial phase)**: Determine the value of the equation for $t = 0$
- $\boldsymbol{V_0}$ **(Offset)**: It is the vertical translation. It indicates the value around which the sinusoid oscillates (the mean value or vertical centre).

3.2.3.1. Weather file analysis

To identify realistic parameter values for generating the sinusoidal curves, the climate data files for the four selected locations were analysed using a Python program.

Initially, three different periods were identified for the analysis:

- **Winter**: December, January, February, March
- **Mid-season**: April, May, September, October, November
- **Summer**: June, July, August

Secondly, the days were categorised by the degree of cloud cover using the 'total sky cover' parameter, which ranges from 0 (completely clear sky) to 10 (maximum cloud cover). The daily average of this parameter was calculated, resulting in the following categories:

- **Clear**: Total sky cover <=2
- **Mixed**: 2 < Total sky cover < 8
- **Cloudy**: Total sky cover >= 8

To ensure more consistent conditions, in line with the aim of modelling perfect sine waves, the days marked as **Mixed** have been excluded.

For the remaining days, now categorised by season and cloud cover, the following were calculated:

- **Mean temperature**: calculated as the median of the daily average temperature values, calculated as $T_{mean,daily} = \frac{T_{max}+T_{min}}{2}$
- **Temperature amplitude**: calculated as the median of the daily maximum temperature variation, calculated as $T_{ampl,daily} = T_{max} - T_{min}$
- **Solar radiation amplitude**: calculated as the median of the maximum variation in solar radiation on the horizontal plane $I_{ampl,daily} = I_{max} - I_{min}$

The mean temperature is needed to determine the value around which the curve will fluctuate; however, for solar radiation, this parameter is not required because the curve is always centred on 0. Furthermore, any value less than 0 obtained from the equation will be set to 0 for obvious reasons.

The final missing parameter is the initial phase; for the temperature curve, this has been set to 6 hours to centre the curve on the full length of the day and ensure that the temperature peak coincides with 12 noon.

The curve for solar radiation was modelled differently: the following dates were used as reference days for the three identified seasons:

- Winter: 15 January
- Mid-season: 15 April
- Summer: 15 July

For each reference day at the selected locations, sunrise and sunset times were identified, and the angular frequency and initial phase parameters were adjusted to accurately reflect them.

3.2.3.2. Selection of reference days

During the course of the study, a reference case classified as 'Cloudy' and one as 'Clear' had originally been selected for each season; however, following some preliminary simulations, it was found that applying the conditions identified as 'Mid-season' meant that the required air-conditioning loads and the timing of flexibility events were not compatible with the choices made. Therefore, carrying out analyses for these simulations, as were subsequently run for the other cases, would have been complicated and unproductive. For these reasons, from now on, only the winter and summer periods will be considered.

The following tables present solar radiation and temperature values, derived from EnergyPlus simulations and plotted for different climates and day types. It should be noted that the solar radiation values refer to the radiation incident on a vertical south-facing wall, since, as described in the next chapter, the reference building's main façade also features glazed openings facing this direction. Finally, for ease of evaluation, the curves are centred on 12 noon, as are the temperature curves, with sunrise and sunset times not considered for the time being.

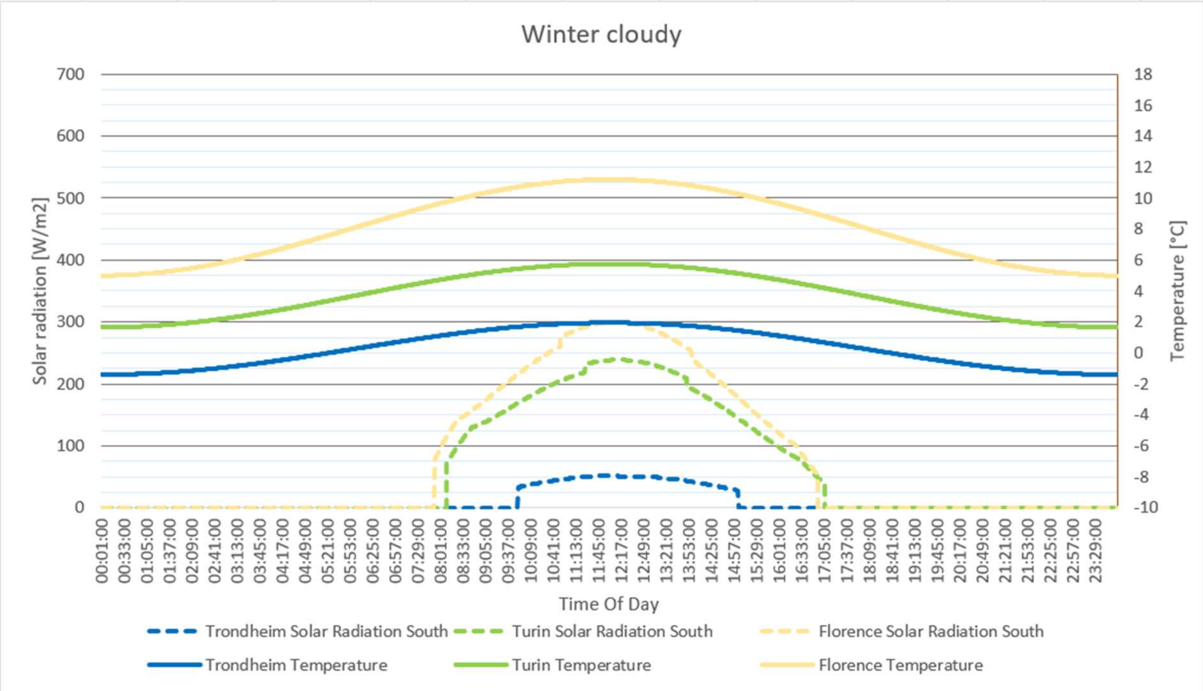

Figure 17: Winter cloudy temperature-solar radiation reference values

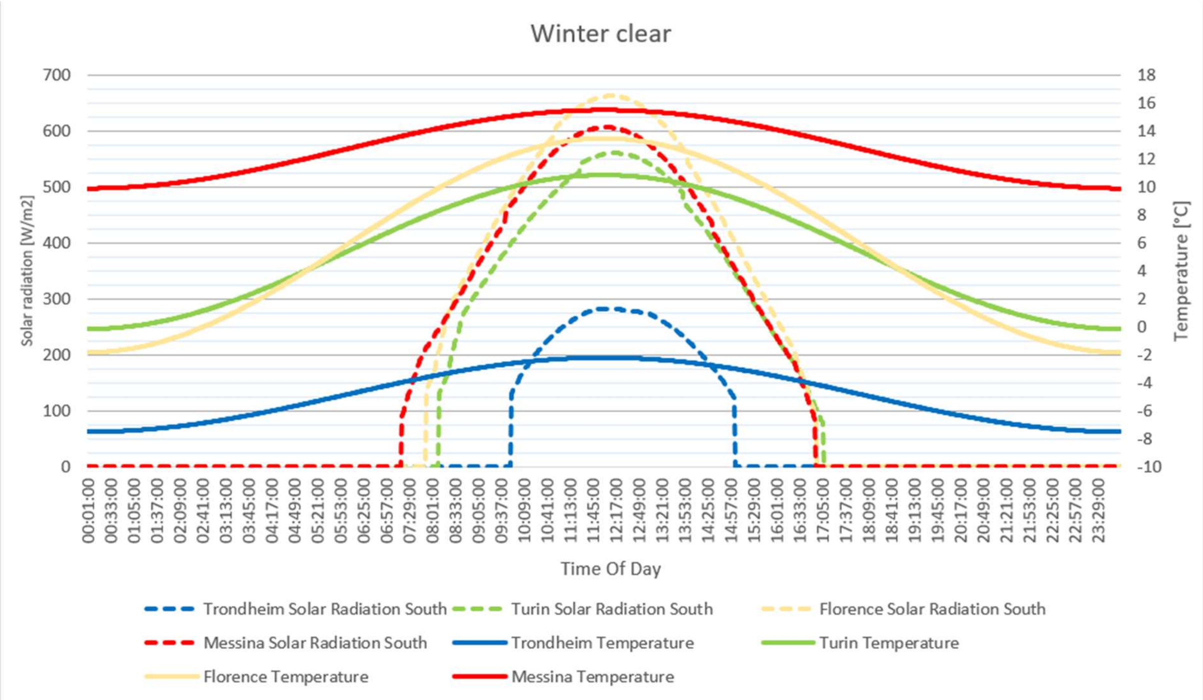

Figure 18: Winter clear temperature-solar radiation reference values

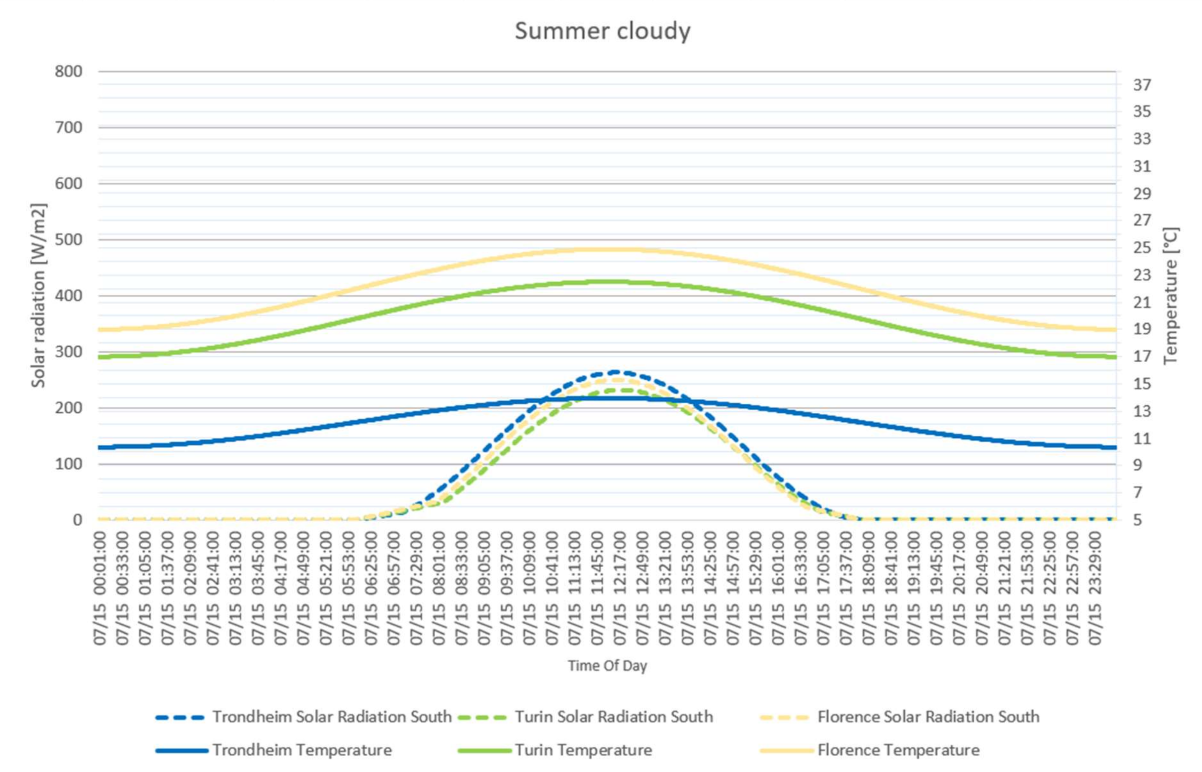

Figure 19: Summer cloudy temperature-solar radiation reference values

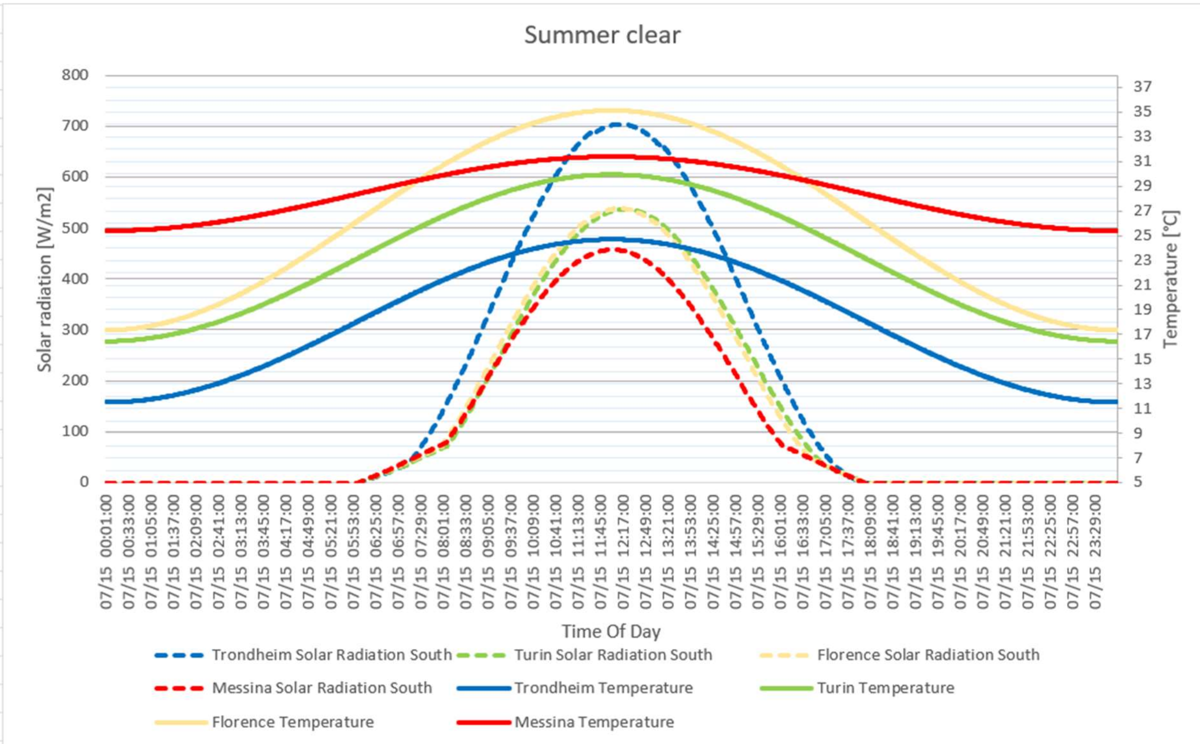

Figure 20: Summer clear temperature-solar radiation reference values

The trends for the city of Messina are not included in the graphs showing cloudy days since the datasets did not contain enough days that met the minimum requirement for classification, making the results unreliable.

After analysing the graphs, a reference case was selected for each scenario:

- **Winter cloudy: Trondheim**. This case was chosen to provide a reference scenario focused on heating, with almost no solar radiation and relatively low temperatures.
- **Winter clear: Turin.** This case was chosen to consider a scenario with low temperatures and consistent solar radiation. It was preferred over the Florence case due to slightly lower peak temperatures and solar radiation.
- **Summer cloudy: Florence.** The three cases show almost identical solar radiation trends, and this case was chosen for its higher average temperature.
- **Summer clear: Florence.** The combination of strong solar radiation, a wide range and a high peak in the temperature curve makes this case a good reference for the most severe summer conditions.

The following table shows the mean and range values used to construct the selected sine curves and lists the sunrise and sunset times used in the simulations.

Table 2: final values for the climatic parameters

Season	Sky type	T mean [°C]	T range [°C]	I range $[W/m^2]$	Sunrise [h]	Sunset [h]
Winter	Cloudy	0,275	1,675	28	9:30	15:15
Winter	Clear	5,35	5,5	439	8:00	17:00
Summer	Cloudy	21,95	2,95	403	5:45	21:00
Summer	Clear	26,25	8,9	891,5	5:45	21:00

The complete temperature and solar radiation curves for the south-facing wall in the four final cases are shown in the following graphs.

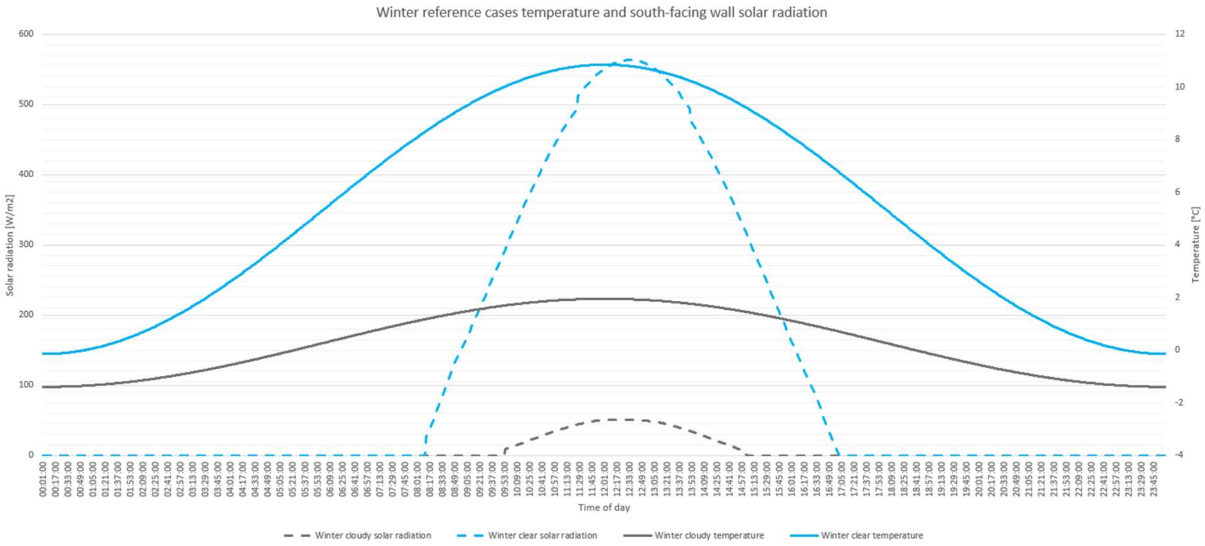

Figure 21: Winter weather conditions

Figure 22: Summer weather conditions

The procedure carried out made it possible to obtain the parameters set out above, which are necessary for constructing sinusoidal curves and, above all, to move away from a specific location and date, enabling one to refer solely to a type of climate, taking another step towards a general method that can be applied, with only minor adjustments, to a wide variety of cases and situations.

However, when applying this method to the simulations carried out using EnergyPlus, it proved necessary to specify the date and location corresponding to those previously associated with each climate, as certain parameters—such as humidity, which will prove to be of fundamental importance, and the solar angle for calculating solar radiation on vertical walls—are required and can only be obtained from a climate file. Although this was not envisaged during this study, it is theoretically possible, as has already been done for temperature and solar radiation, to artificially construct variations in the other necessary parameters, thereby eliminating the need to refer to a specific location.

3.3. ASSESSMENT METHODOLOGY

Given the absence of detailed comparative studies in the scientific literature involving fundamentally different building envelope technologies applied to flexibility events, it was necessary to develop and assess a suitable comparison methodology. Due to the different nature of the advanced envelope elements investigated and their influence on various energy flows within the building, a fair and representative comparison can only be achieved by focusing on the aspects common to all the analysed cases, namely the HVAC system and its associated energy consumption. This approach enables the quantification and comparison of the impact of each technology under the different operating conditions considered.

In the simulations carried out at the start of the flexibility event, two internal setpoints are modified:

- **Winter**: lowering of temperature and minimum relative humidity
- **Summer**: raising of temperature and maximum relative humidity

These will be returned to their nominal values at the end of the event.

The case in which PCM material is used within the building envelope also involves pre-charging strategies for the material, carried out prior to the flexibility event, which consist of increasing the indoor temperature setpoint in winter (and reducing it in summer) in order to facilitate the accumulation of thermal energy within the PCM. The setpoints used and the pre-charging strategies will be analysed in detail in the next chapter

3.3.1. Reference case

Comparing cases involving very different technologies can yield misleading, difficult-to-interpret results; for this reason, a reference case has been defined in which no advanced building envelope elements are applied. This makes it possible to quantify the energy performance of the analysed room under standard conditions and during flexibility events, thereby enabling a clearer assessment of the impact of the applied technology and the associated control method.

For each climate type assessed, during the modelling of the reference case, the environment, the building envelope, the internal loads and the ventilation remain unchanged for all cases. The only exception is the insulation level of the external walls and ceiling, which will be adjusted to comply with the regulatory limits for the reference locations from which the climate parameters were derived by varying the insulation layer thickness.

Given the significant impact of glazing components on energy exchange with the external environment, two distinct reference cases were considered: for the first, double glazing was used, a component with good thermal performance that is already widely used in the commercial market; for the second, triple glazing was considered, a component with excellent thermal performance that is commercially available but less commonly used due to its higher costs.

All the characteristics of the room under consideration and the building envelope components used will be described in detail in the next chapter.

3.3.2. Key Performance Indicator

The main indicators used to measure the thermal performance of the cases analysed are described below. It should be noted that all metrics based on energy or power differences are evaluated by comparing the case in which the flexibility event is applied with the identical case in which the event is not applied. In both cases, the same building technologies are employed, ensuring that the measured differences are solely attributable to the flexibility strategy.

- **Autonomy [min]**: measures the duration during which the system load is zero, and the internal conditions remain within acceptable limits
    - In most cases, it measures the time from the start of the flexibility event until the new indoor conditions set by the new setpoints are reached and the system resumes normal operation. When climatic conditions result in a thermal equilibrium such that the air-conditioning system's contribution is not required, even after the conditions set by the new setpoints are met, this metric also includes this period.

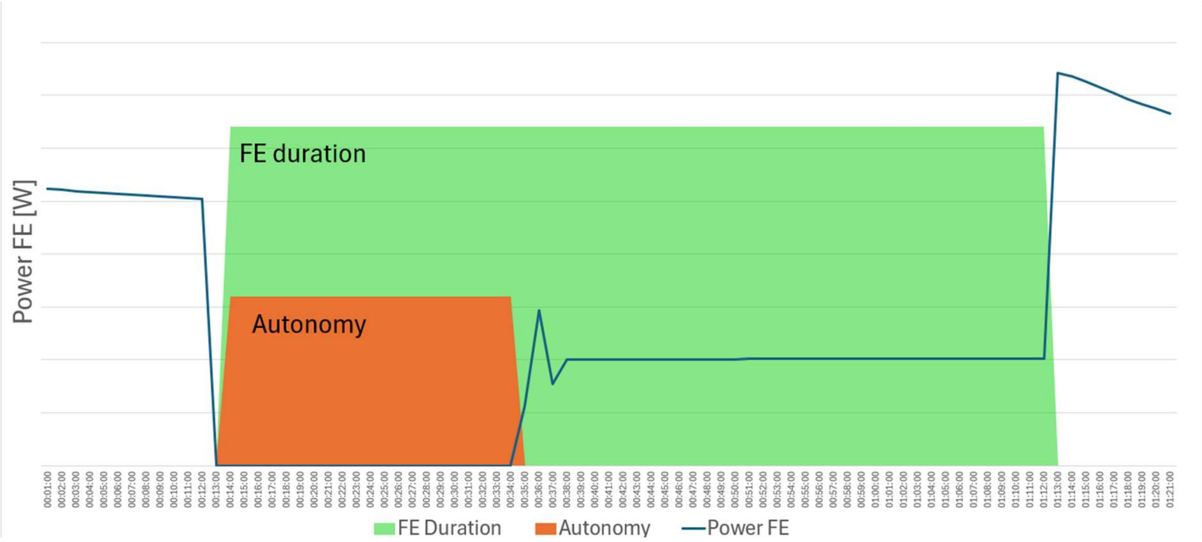

Figure 23: Autonomy example graph

- **Degree of partialisation [%]**: measures the average power required by the system during the event compared with the average power consumed in the scenario where no changes were made to its operation.
  - $Partialisation = \frac{\int_{t_{start}}^{t_{end}}[P_{ref}(t) - P_{FE}(t)]dt}{\int_{t_{start}}^{t_{end}} P_{ref}(t)dt}$

Simply stating a percentage may not fully describe the effect that the building envelope component has on the entire system during a flexibility event; this is because the technologies analysed may, even during periods of normal operation, result in a reduction or increase in energy consumption compared with the reference cases and those involving other technologies, and these variations cannot be accurately expressed as a percentage. For this reason, the following metric is introduced:

- **Peak shaving capacity [Wh] [37]**: represents the difference in energy between the case where the flexibility event is considered and the case where there are no changes to the system's operation.
  - $E_{PS} = \int_{end}^{t_{start}}(P_{ref}(t) - P_{FE}(t))\,dt$

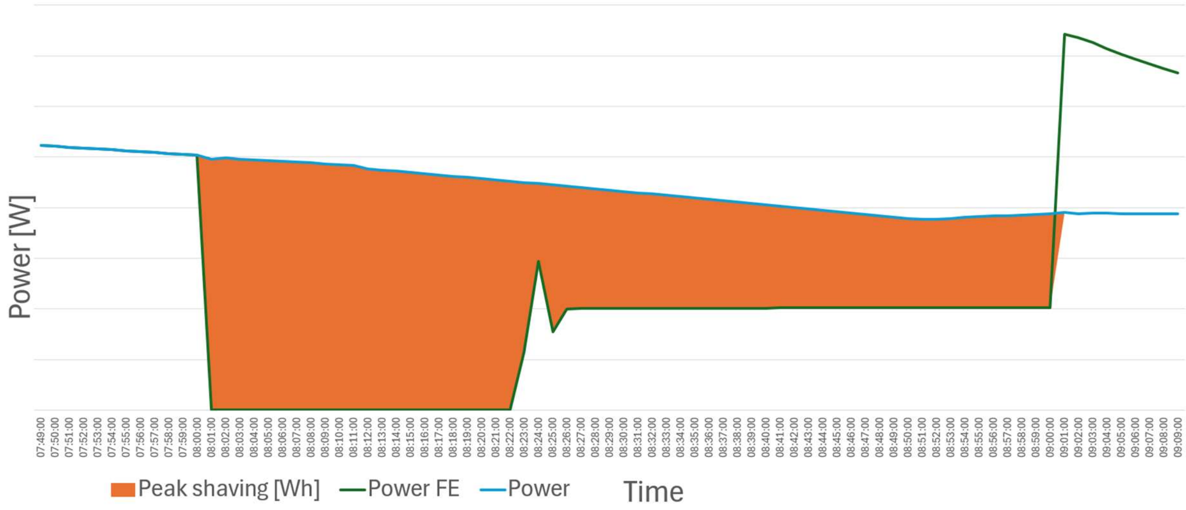

Figure 24: Peak shaving capacity example graph

- **Rebound energy [Wh] [9]**: Once the flexibility event has ended, the air-conditioning system must return the room to normal conditions; to do so, it will need to use more power than in the base case; this metric quantifies the additional energy used during the recovery phase. The duration of this phase depends on external and internal conditions and the system's maximum power; ideally, it ends once internal conditions have been restored, but to ensure that the entire energy demand is accounted for, it will be measured over a one-hour period following the end of the event.

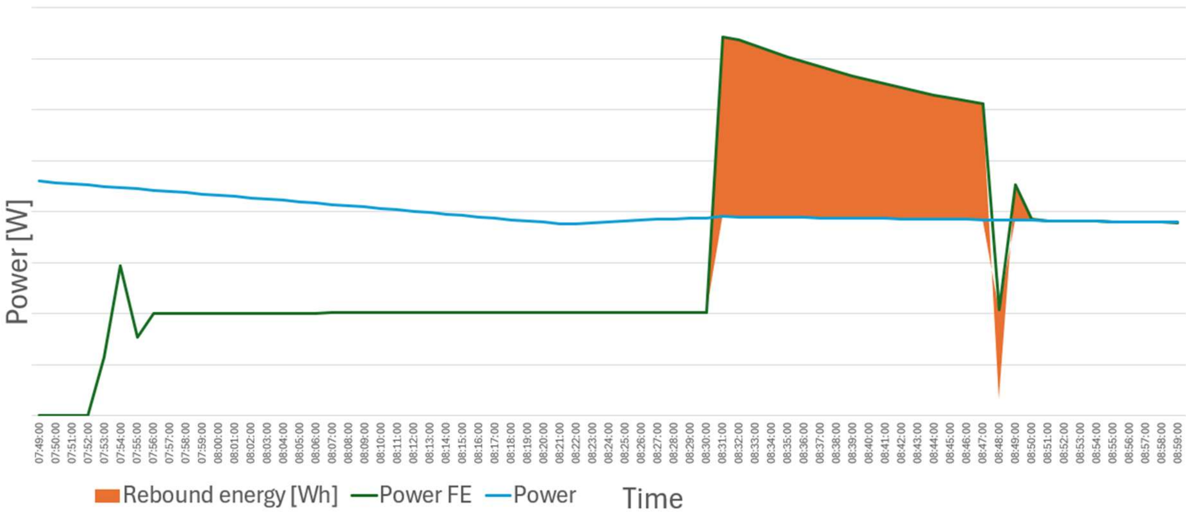

Figure 25: Rebound energy example graph

- **Precharge energy [Wh] [22]**: When phase-change material is used, the pre-heating phase involves a change in the temperature setpoint, which consequently leads to higher energy consumption, partly due to heat accumulation within the material and partly due to greater heat loss to the external environment. This metric measures the additional energy used during this phase.
- **DR energy balance [Wh]**: The metric measures the difference in energy consumption between the scenario involving the flexibility event and the standard scenario, considering the entire duration of the event, the recovery phase and, where needed, the pre-charge phase.

4 SIMULATION METHODOLOGY

This chapter describes the simulation environment used, the characteristics of the building under consideration, and the application of the previously described building envelope technologies.

The study was conducted using EnergyPlus, a leading dynamic energy simulation tool. It is an open-source software developed by the United States Department of Energy (DOE) based on the BLAST and DOE-2 codes that " implements detailed building physics for air, moisture, and heat transfer including treating radiative and convective heat-transfer separately to support modelling of radiant systems and calculation of thermal comfort metrics; calculates lighting, shading, and visual comfort metrics; supports flexible component-level configuration of HVAC, plant, and refrigeration systems; includes a large set of HVAC and plant component models; simulates sub-hourly time steps to handle fast system dynamics and control strategies" [38]

4.1. PREMISE DESCRIPTION

The simulations were carried out using a single office space with characteristics similar to those used in the BESTEST diagnostic method.

- Single thermal zone

Internal dimensions:

- Plan 8 x 6 m
- Height 2,7 m

Windows:

- Two glazing elements located on the south-facing wall, 3 x 2 m (WWR=0,55)

Exposures:

- The south and west façades are exposed to the outdoor environment and are therefore subjected to wind and solar radiation.
- The ceiling is exposed to the outdoor environment, including wind, but not to solar radiation.
- Floor, north and west-facing walls are all considered adiabatic.

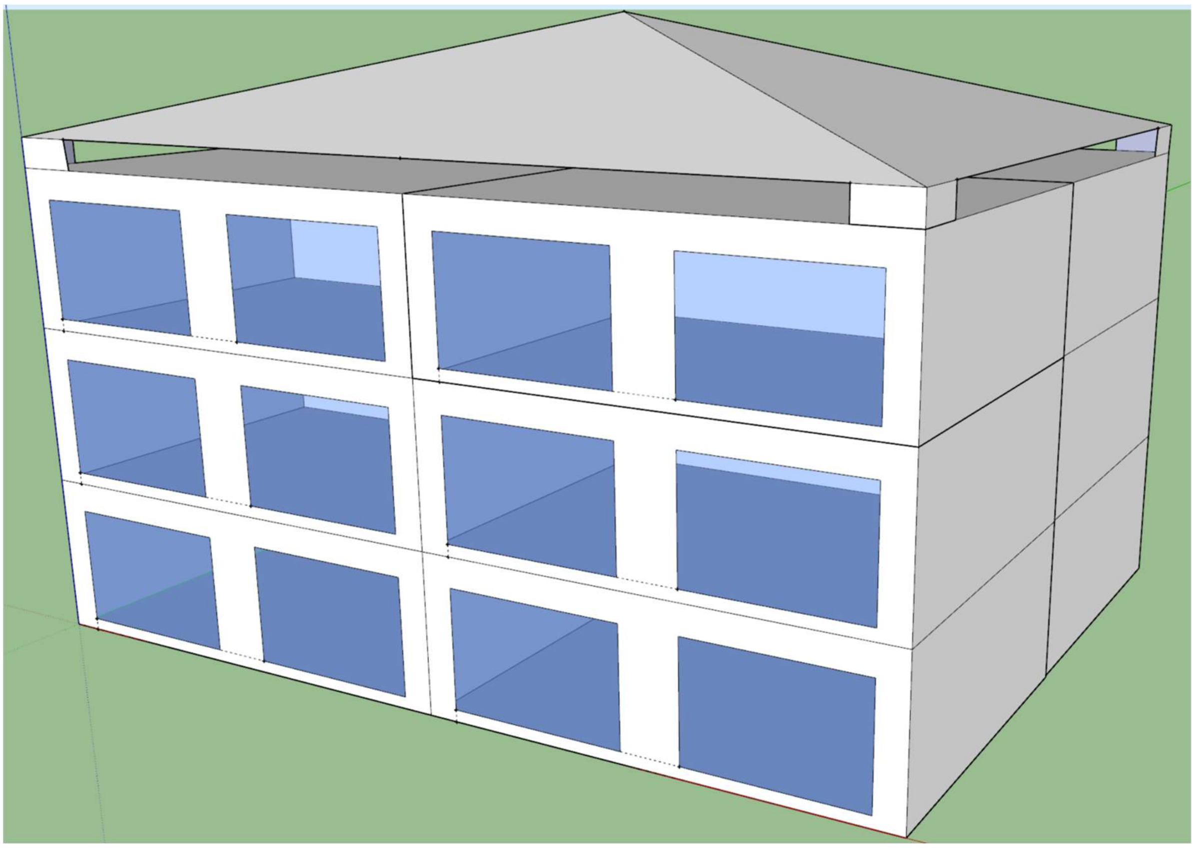

Figure 26: South-facing view of the whole building

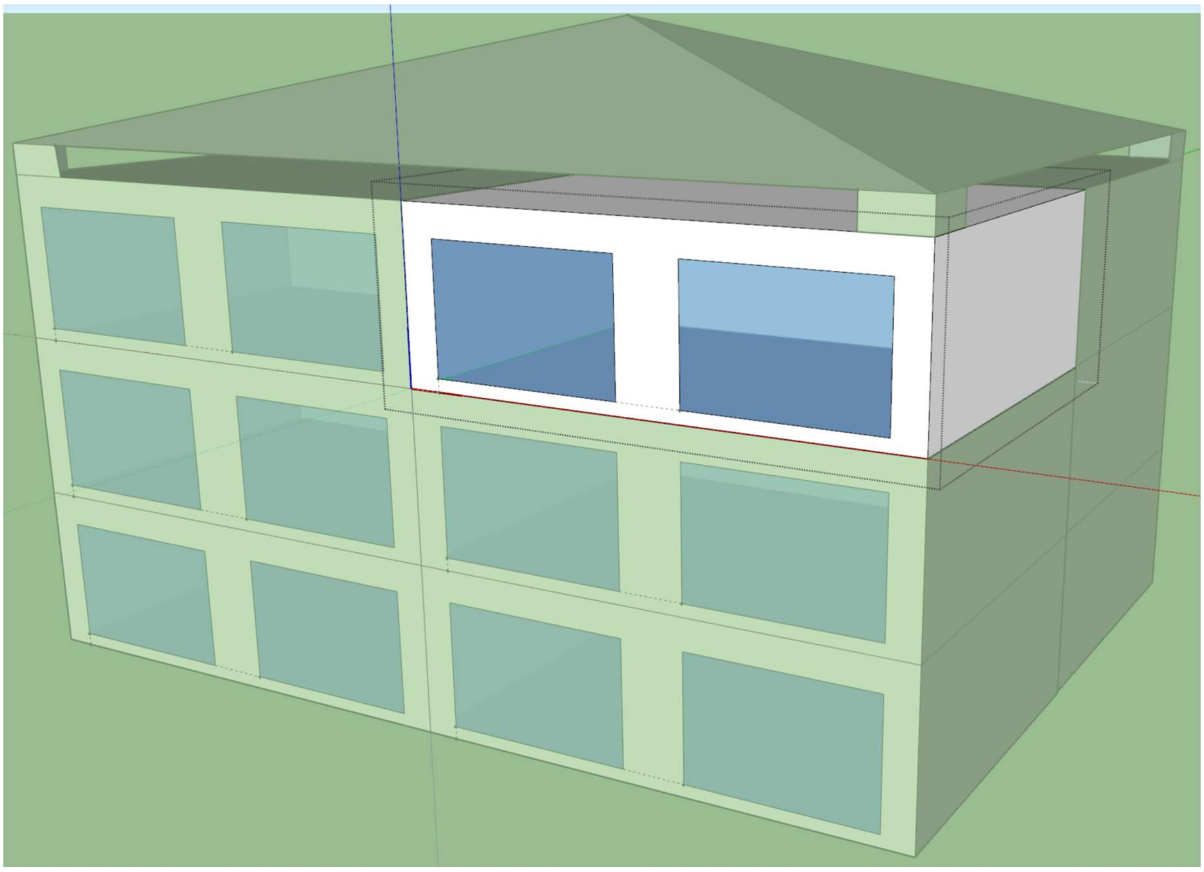

Figure 27: Simulated environment

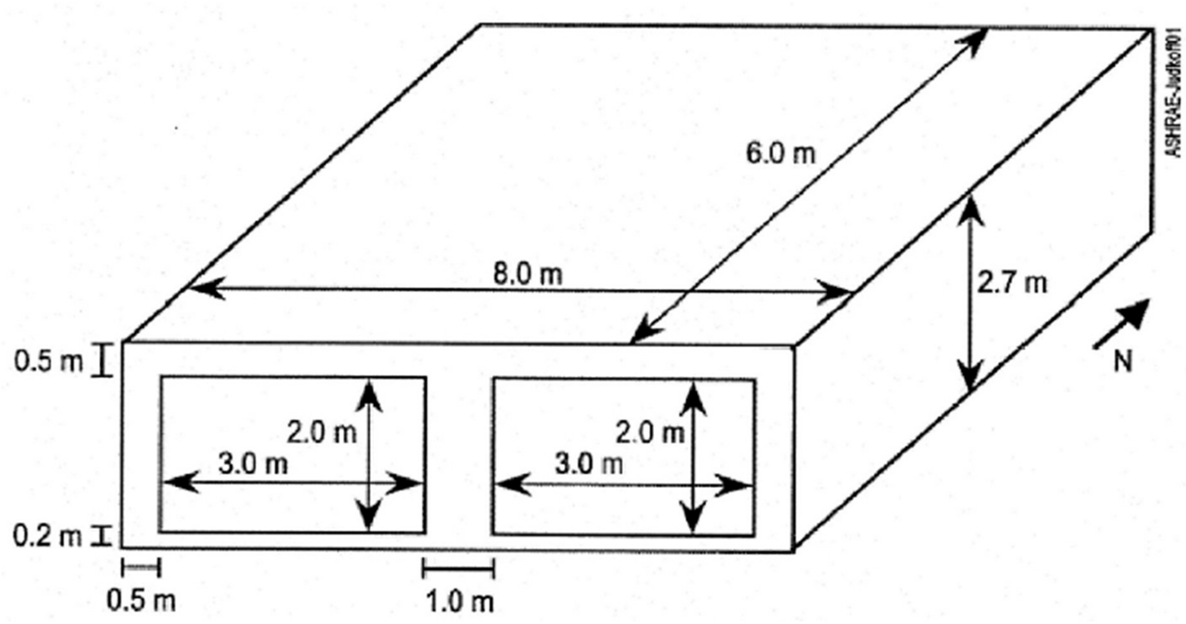

Figure 28: Building geometry based on BESTEST Case 600

4.2. OPAQUE ENVELOPE

For each case analysed, the same stratigraphy of the opaque envelope was used, varying only the insulation thickness to meet the minimum U-value $\left[{W}/{m^2K}\right]$ requirements for each location from which the climate data were extracted.

The relevant regulations used were the "Minimum Requirements Decree 2025" [39] for Italian cities and "Tek 17" [40] for the Norwegian case.

Table 3: Maximum U-value opaque envelope

	U-Value vertical envelope $\left[{W}/{m^2K}\right]$	U-Value horizontal envelope $\left[{W}/{m^2K}\right]$
Trondheim	0,18	0,13
Turin	0,26	0,22
Florence	0,29	0,26

The following table lists the layers that make up the opaque envelope and their properties, starting from the inner layer. The stratigraphy used in the Turin case study will be provided for reference.

Table 4: Opaque envelope characteristics

Layer	k [W/mK]	Thickness [m]	R-value [m^2K/W]	Density [kg/m^3]	Cp [J/(kgK)]
Exterior Wall					
Plaster	0,4	0,02	0,05	1120	960
Polystyrene insulation	0,035	0,125	3,57	23	1470
Concrete	1,046	0,3	0,29	2300	657
Plaster	0,4	0,02	0,05	1120	960
Floor					
Ceramic tile	1,2	0,01	0,01	2000	850
Tile bedding	1,4	0,03	0,02	2100	650
Polystyrene insulation	0,035	0,07	2	23	1470
Concrete	1,046	0,15	0,14	2300	657
Plaster	0,4	0,02	0,05	1120	960
Ceiling					
Ceramic tile	1,2	0,01	0,01	2000	850
Tile bedding	1,4	0,03	0,02	2100	650
Polystyrene insulation	0,035	0,15	4,29	23	1470
Concrete	1,046	0,15	0,14	2300	657
Plaster	0,4	0,02	0,05	1120	960
Internal wall					
Plaster	0,4	0,02	0,05	1120	960
Gypsum board	0,65	0,02	0,03	1100	840
Rock wool insulation	0,034	0,06	1,76	200	710

To meet the minimum insulation requirements at the three locations analysed, the following thicknesses of thermal insulation were used in the external walls and ceilings:

Table 5: Insulation thickness

	External wall insulation thickness [m]	Ceiling insulation thickness [m]
Trondheim	0,185	0,26
Turin	0,125	0,15
Florence	0,11	0,125

4.2.1. PCM characteristics

As described in Chapter 2, to facilitate interaction between the indoor air and the PCM, the latter was incorporated as one of the innermost layers of the inner walls, between the plaster and the gypsum board. One of the key characteristics of the material is the temperature—or temperature range—at which the phase change occurs. Since the transformation is driven by indoor air temperature, it is necessary to ensure that the transition temperature is compatible with comfort values, taking into account the hysteresis process analysed in the second chapter.

To identify the optimal transition temperature, the base model of the analysed room was considered, in which the interior walls were integrated with a layer of macro-encapsulated PCM, each time with a different peak melting temperature. The indoor temperature was set to 40 °C and the outdoor temperature to -5 °C; the air conditioning system was off until the indoor temperature reached 10 °C to evaluate its natural evolution, as shown in *Figure 29* below.

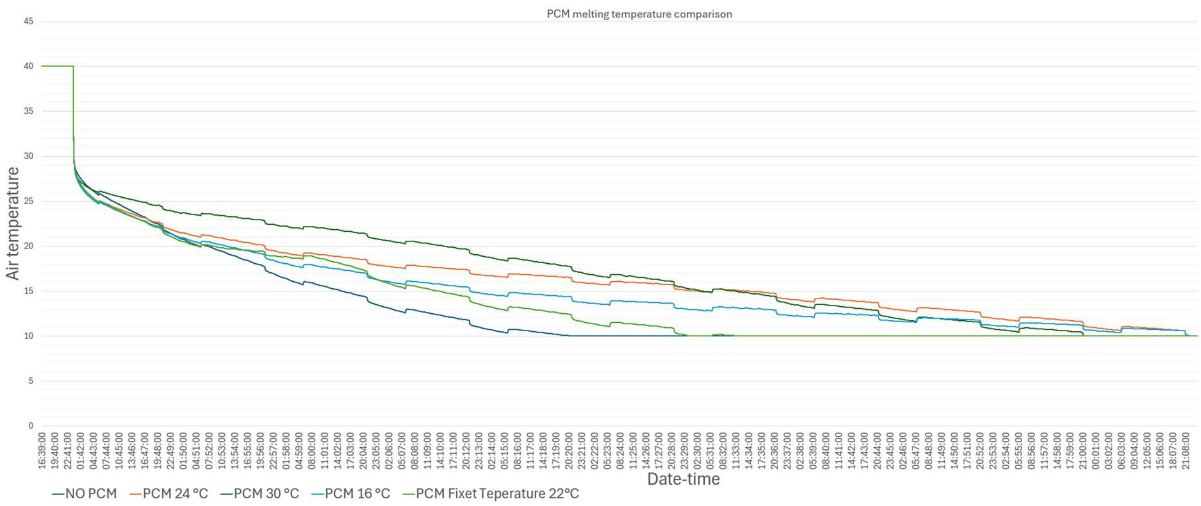

Figure 29: PCM melting temperature comparison

The case without PCM showed the fastest temperature drop due to its lower thermal mass. In the other cases, a higher peak melting temperature results in a higher average temperature during the initial period and a faster decline as the temperature approaches the lower limit. This occurs because most of the latent heat accumulated by the material is released into the air when the material is near its melting temperature, thereby slowing the drop in air temperature; once solidification is complete, the PCM can no longer make a significant contribution. For this reason, a material with a phase-change range centred around 24 °C was selected from the Rubitherm manufacturer's website [23]; the technical data sheet with the specifications is provided below.

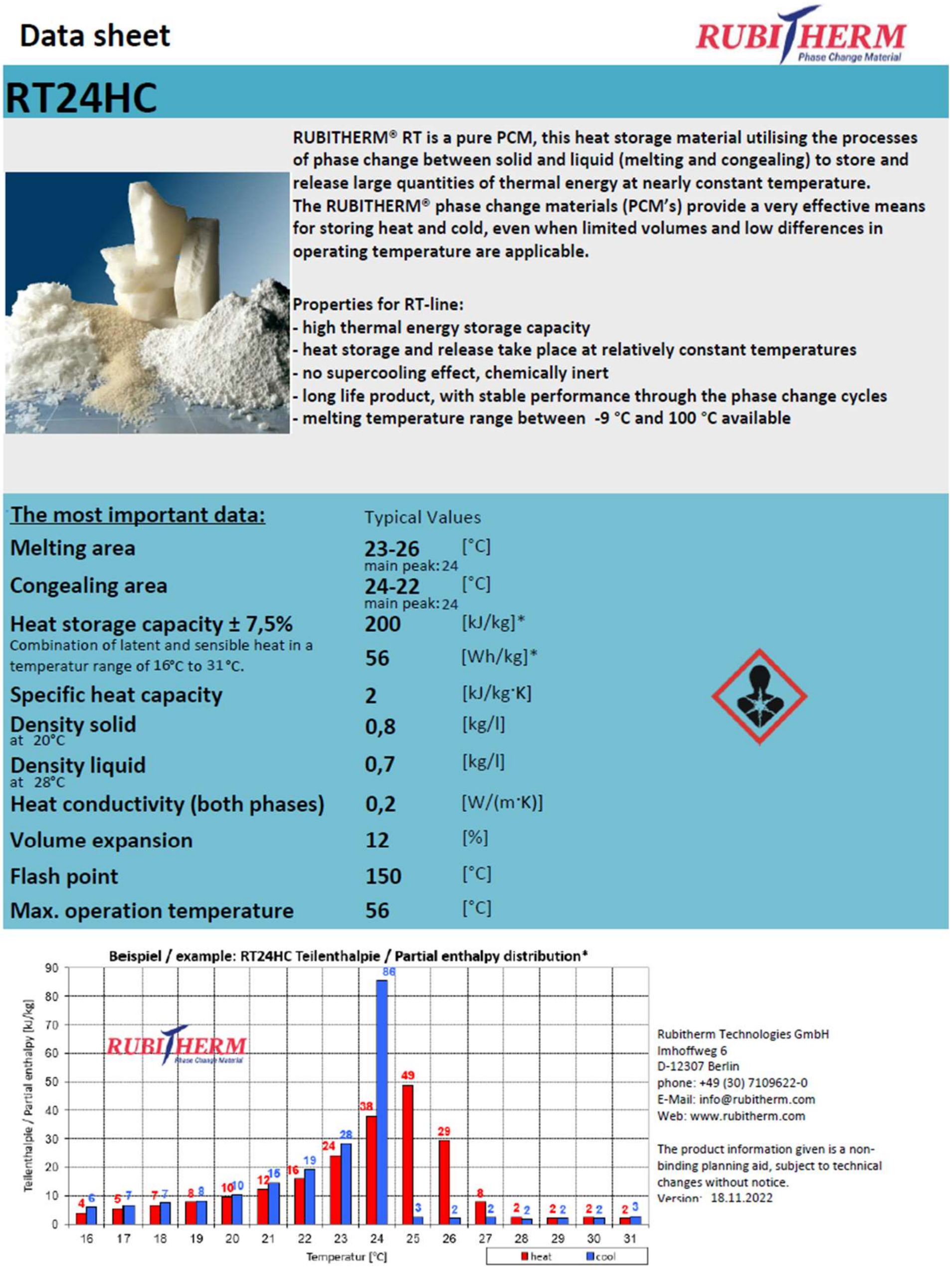

Data sheet

RUBITHERM Phase Change Material

RT24HC

RUBITHERM® RT is a pure PCM, this heat storage material utilising the processes of phase change between solid and liquid (melting and congealing) to store and release large quantities of thermal energy at nearly constant temperature.
The RUBITHERM® phase change materials (PCM's) provide a very effective means for storing heat and cold, even when limited volumes and low differences in operating temperature are applicable.

Properties for RT-line:
- high thermal energy storage capacity
- heat storage and release take place at relatively constant temperatures
- no supercooling effect, chemically inert
- long life product, with stable performance through the phase change cycles
- melting temperature range between -9 °C and 100 °C available

The most important data:	Typical Values	
Melting area	23-26 main peak: 24	[°C]
Congealing area	24-22 main peak: 24	[°C]
Heat storage capacity ± 7,5% Combination of latent and sensible heat in a temperatur range of 16°C to 31°C.	200 56	[kJ/kg]* [Wh/kg]*
Specific heat capacity	2	[kJ/kg·K]
Density solid at 20°C	0,8	[kg/l]
Density liquid at 28°C	0,7	[kg/l]
Heat conductivity (both phases)	0,2	[W/(m·K)]
Volume expansion	12	[%]
Flash point	150	[°C]
Max. operation temperature	56	[°C]

Rubitherm Technologies GmbH
Imhoffweg 6
D-12307 Berlin
phone: +49 (30) 7109622-0
E-Mail: info@rubitherm.com
Web: www.rubitherm.com

The product information given is a non-binding planning aid, subject to technical changes without notice.
Version: 18.11.2022

Figure 30: PCM data sheet

4.3. GLAZING COMPONENTS

As described above, two reference cases were designed: one featuring a double-pane glazing system and the other a triple-pane glazing system. In addition, the following advanced technologies were used: a double-skin model, traditional electrochromic glass (EC), and the more advanced dual-band electrochromic type (DB-EC).

The performance characteristics of the two types of traditional glazing and the double-skin system were evaluated using the Window program, developed by the Lawrence Berkeley National Laboratory (LBNL) [41], while the data regarding the traditional and dual-band electrochromic units were extracted from the work by Riganti et al. [29].

The DGU unit was designed to match the thermal transmittance of the EC and DB-EC components, which also feature double-pane technology with an argon-air-filled cavity. For the DSF, on the other hand, the goal was to determine parameters similar to those of the TGU, which was achieved using the same type of glass. The following table lists the parameters for the glazing units used. The two electrochromic glass panels are listed from the clearest state (State 1) to the darkest (State 8).

Unit	State	Layout	T_{VIS} [-]	T_{SOL} [-]	SHGC [-]	U-value [W/m²k]
DGU		ECLAZ 6mm Argon 90% air 10% 16mm Planiclear 6mm	0,823	0,587	0,632	1,21
TGU		ECLAZ 6mm Argon 90% air 10% 16mm CL XTREME 61-29 6mm Argon 90% air 10% 16mm Planiclear 6mm	0,555	0,202	0,328	0,877
DSF		ECLAZ 6mm Air 30mm CL XTREME 61-29 6mm Argon 90% air 10% 16mm Planiclear 6mm	0,555	0,202	0,326	1,088
EC	State 1	EC laminate 14mm Argon 90% air 10% 16mm Clear glass + Low-E 4,8mm	0,6	0,29	0,39	1,2
	State 2		0,57	0,26	0,37	
	State 3		0,51	0,22	0,33	
	State 4		0,41	0,16	0,29	
	State 5		0,31	0,11	0,24	
	State 6		0,20	0,07	0,21	
	State 7		0,09	0,03	0,17	
	State 8		0,02	0,01	0,15	
DB-EC	State 1	DB-EC laminate 9,8mm Argon 90% air 10% 16mm Clear glass + Low-E 4,8mm	0,78	0,45	0,53	1,2
	State 2		0,76	0,36	0,46	
	State 3		0,73	0,28	0,40	
	State 4		0,67	0,20	0,32	
	State 5		0,43	0,11	0,25	
	State 6		0,27	0,06	0,21	
	State 7		0,16	0,04	0,19	
	State 8		0,06	0,02	0,17	

Table 6: Glazing components characteristics

Finally, it should be noted that within EnergyPlus, the DSF is modelled using the "WindowProperty:AirflowControl" element; in this way, together with the construction type of the element described above, the DSF is simulated as an additional layer with dimensions identical to those of the window and therefore does not cover the entire façade of the building.

4.3.1. Shading devices

To provide a more comprehensive analysis, the introduction of a high-reflectivity external venetian blind system was assessed; in the case of the DSF, this was installed within the ventilated cavity, with the following main features:

- **Slat width:** 0,025 m
- **Slat conductivity:** 0,9 $W/_{mK}$
- **Slat beam solar reflectance:** 0,8
- **Slat diffuse solar reflectance:** 0,8

Shading elements were used only in the summer simulations; however, this item will not appear in the 'Summer Cloudy' scenario, as the solar radiation falling on the windows never reaches the minimum value set for activation. To assess their impact, the DGU and TGU reference simulations in the "Summer Clear" event were conducted both with and without blinds. Furthermore, the blinds were not used in the simulations that implemented EC glazing to better isolate the contribution of this technology.

When the blinds are installed, they are automatically activated when the total solar radiation incident on the window exceeds **350 W/m²**. The orientation of the slats is also continuously monitored via the **"BlockBeamSolar"** input, ensuring they remain at a right angle to direct sunlight.

4.4. VENTILATION

The premises will be mechanically ventilated, except in winter, when double-skin technology is used in SA mode; in this case, the analysed element will directly supply the required airflow. The required airflow has been calculated in accordance with the values specified in the standard UNI EN 16798-5-1:2018/NA:2025, which adopts the European standard on comfort and ventilation values for premises. The analysed building has been classified as Category II, "Low Polluting Building", The following two tables, extracted from the referenced standard, contain the parameters used.

Table B.6 — Design ventilation rates for sedentary, adults, non-adapted persons for diluting emissions (bio effluents) from people for different categories

Category	Expected Percentage Dissatisfied	Airflow per non-adapted person l/(s per person)
I	15	10
II	20	7
III	30	4
IV	40	2,5

Figure 31: Design ventilation rates for sedentary adults from UNI EN 16798-5-1:2018/NA:2025

FprEN 16798-1:2016 (E)

Table B.7 — Design ventilation rates for diluting emissions from different type of buildings

Category	Very low polluting building, LPB-1 l/(s m²)	Low polluting building, LPB-2 l/(s m²)	Non low-polluting building, LPB-3 l/(s m²)
I	0,5	1,0	2,0
II	0,35	0,7	1,4
III	**0,2**	**0,4**	**0,8**
IV	0,15	0,3	0,6

Figure 32: Design ventilation rates for different types of buildings from UNI EN 16798-5-1:2018/NA:2025

To determine the airflow values, the following parameters were considered:

- Surface area: 48 m^2
- Volume: 129,6 m^3
- Maximum occupancy: 3 persons

The contribution to the infiltrations was also considered and was valued at:

- 0.5 air changes per hour (ACH)

Table 7: airflow rates

	$^{l}/_{s}$	$^{m^3}/_{h}$	ACH
Mechanical ventilation	54,6	196,56	1,52
Infiltration	18	64,8	0,5
Total	72,6	261,36	2,02

4.5. INTERNAL GAINS

The presence of persons, lighting, and electrical loads within the room constitutes a heat input. To quantify this, constant parameters were selected for all cases under analysis to accurately represent a real-world situation.

- Lighting load: 7 $^{W}/_{m^2}$
- Electrical load: 12 $^{W}/_{m^2}$
- Constant metabolic activity: 100 $^{W}/_{pers}$

Table 8: internal gains

Heat source	Total load [W]	Radiant fraction [-]	Schedule
Lighting	336	0,42	Constant
Electric	576	0,50	Constant
Persons	300	0,30	6:00 AM - 9:00 PM

4.6. AIR CONDITIONING SYSTEM

There are many technologies for cooling and heating spaces, such as air-handling systems, radiators, underfloor heating, chilled ceilings, and fan coils. The most significant difference among the various systems in terms of energy flexibility is their thermal inertia. The study conducted by Aterconi et al. [8] addresses this issue by distinguishing between radiant systems with medium/high thermal inertia—such as underfloor heating and chilled ceilings—and those with low thermal inertia, such as fan coil units. The study demonstrates that systems with greater thermal inertia contribute significantly to maintaining indoor conditions within acceptable ranges for a longer period following a flexibility event.

Given this study's focus on building envelope components—to exclude the dependence of indoor conditions on the HVAC system—the latter was modelled in EnergyPlus as an ideal system, described in the Input-Output Reference manual as: "This component can be thought of as an ideal unit that mixes air at the zone exhaust condition … with the specified amount of outdoor air and then adds or removes heat and moisture at 100% efficiency in order to produce a supply air stream at the specified conditions”. [42] In the various simulations, the system was designed to ensure the necessary energy supply under all conditions, without, however, drawing excessive power during recovery phases at the end of the FE.

The building does not utilise a heat recovery system because the large volume of ventilation air imposes a significant energy load relative to the energy associated with heat loss through the opaque and transparent building envelope. For this reason, as demonstrated during the study, the addition of a heat recovery system would substantially reduce the total thermal loads, making it impossible to compare the different scenarios during the events under investigation.

4.6.1. Indoor air parameters and flexibility strategies

Control of indoor conditions is based on air temperature and humidity. Given the assumed sedentary activity of the occupants, the temperature setpoints were set at:

- 21°C heating
- 26°C cooling

The air conditioning system also controls relative humidity, with setpoints established at:

- 50 % during the winter season
- 60 % during the summer season

These values have been set as the lower and upper limits, respectively. During the summer, when the relative humidity falls below the set value, the system will not humidify the air; conversely, during the winter, if the relative humidity exceeds 50%, the system will not dehumidify the air. This decision was made to account for humidity-related energy loads without simulating a complex HVAC system and incurring simultaneous heating and cooling loads due to differing energy demands, for example, between summer cooling and the potential need of heat for humidification.

To reduce energy demand during FE events, the setpoints for the two parameters described are modified.

As described by Saffari [22], the maximum variation in indoor temperature depends on the duration for which this variation is maintained; as shown in *Figure 33*, for events lasting one hour, the maximum acceptable variation is 2.2 °C. The temperature setpoints for the entire duration of the events will therefore be:

- 19°C heating
- 28°C cooling

Time period	0.25 h	0.5 h	1 h	2 h	4 h
Max. operative temperature change allowed	1.1 °C	1.7 °C	2.2 °C	2.8 °C	3.3 °C

Figure 33: Allowed operative temperature change

During events, the target relative humidity level is also adjusted; this is generally considered acceptable when it falls between 30% and 70%. Consequently, it was decided to set a maximum deviation of 10% from the normal value, resulting in the following new limits applicable during events:

- 40 % during the winter season
- 70 % during the summer season

4.7. SIMULATION CONTROL

The building's energy performance is strongly influenced by past events and conditions due to thermal storage effects; experiments on the model revealed that the choice of the simulation start date had a significant impact on the results.

In both winter and summer cases, the day of interest is the 15th; in both cases, the simulations were started on the 14th, with climate parameters for temperature and solar radiation dictated by the sinusoidal curves described above, with no flexibility events. This method allows the use of EnergyPlus's default warm-up mechanism to apply cyclic and constant conditions to the simulation environment, bringing the room to a stable thermal state.

As described in the EnergyPlus documentation [42], the warm-up system simulates the first day set by the user (in this case, the 14th) repeatedly until stable temperature conditions are reached or the maximum number of days set by the user is reached. Once one or both conditions are met, the simulation is run for the entire set period.

4.8. CONTROL STRATEGIES

As described in Chapter 2, the most interesting aspect of advanced building envelope technologies—and the one that best meets the requirements of a building subject to flexible conditions—is the ability to dynamically control and modify certain parameters and characteristics. The control methods applied to each technology studied are described below.

4.8.1. DSF control strategies

The 4-opening DSFs can be used in four different modes. To fully assess the potential of this component, all modes were tested, each during the appropriate season.

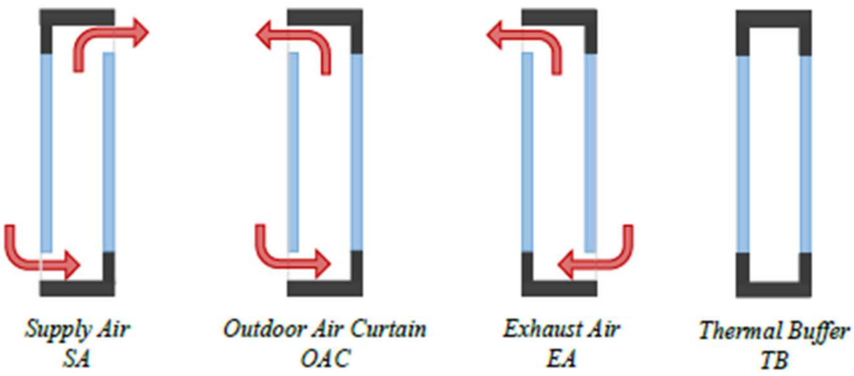

Figure 34: DSF ventilation modes

Table 9: Operating mode and flow rates of the DSF system

Season	Mode	Air source	Air destination	Flow rate [m³/h]
Winter	SA	Outdoor	Indoor	196,56
	TB	-	-	-
Summer	OAC_Low	Outdoor	Outdoor	98,28
	OAC_High	Outdoor	Outdoor	393,12
	EX	Indoor	Outdoor	196,56

The flow rates shown in the table represent the total flow rate processed by the DSF systems in each configuration. As the model comprises two separate windows, each associated with its own DSF, the flow rate for a single window corresponds to 50% of the value shown.

In SA and EX modes, the air flow rate is necessarily equal to the ventilation flow rate; in OAC mode, as demonstrated by a number of studies, including [15], an increase in the airflow rate can help to remove heat from the cavity more efficiently, resulting in lower loads within the room. For this reason, two scenarios have been evaluated in which the airflow rate is half and twice the ventilation flow rate, respectively.

4.8.2. PCM control strategies

To assess the PCM's ability to mitigate changes in indoor conditions, three scenarios were evaluated: one without room preconditioning and two with it, to evaluate the effectiveness of this technique and identify its strengths and weaknesses.

When preconditioning is carried out, the temperature is adjusted by 2 °C from the normal setpoint; in winter, it is increased to preheat the room by melting part of the material, whilst in summer, it is lowered to partially solidify the material in anticipation of the flexibility event. In the two cases evaluated, preconditioning lasts 60 and 30 minutes before the start of the event, respectively. The table below shows the setpoints applied for the three cases during the morning winter flexibility event (8–9 am); the nomenclature used here and in the following is:

- **PCM**: Case without preconditioning
- **PCM 1H**: Case with 1-hour preconditioning
- **PCM 05H**: Case with 30 minutes preconditioning

Table 10: Temperature setpoint during winter morning FE with PCM preheating strategies

Case	Temperature setpoint [°C]			
	7:00	7:30	8:00	9:00
PCM	21	21	19	21
PCM 1H	23	23	19	21
PCM 05H	21	23	19	21

4.8.3. Electrochromic glazing control strategies

To control both types of electrochromic glass studied, the Rule-Based control (RBC)—developed by Riganti et al. [29]— was used, as it requires only knowledge of the indoor temperature, the solar radiation incident on the glass, and the presence of people, all of which are variables provided by EnergyPlus. It should be noted that this control method was not developed specifically for integration with energy flexibility events, but rather to ensure energy savings in both heating, ventilation and air conditioning (HVAC) and lighting systems.

The image below illustrates the control method used; the only modification made concerns the nomenclature of the glass states:

- FullClear → State 1
- Int 1 → State 2
- Int 2 → State 3
- Int 3 → State 4

- Int 4 → State 5
- Int 5 → State 6
- Int 6 → State 7
- FullDark → State 8

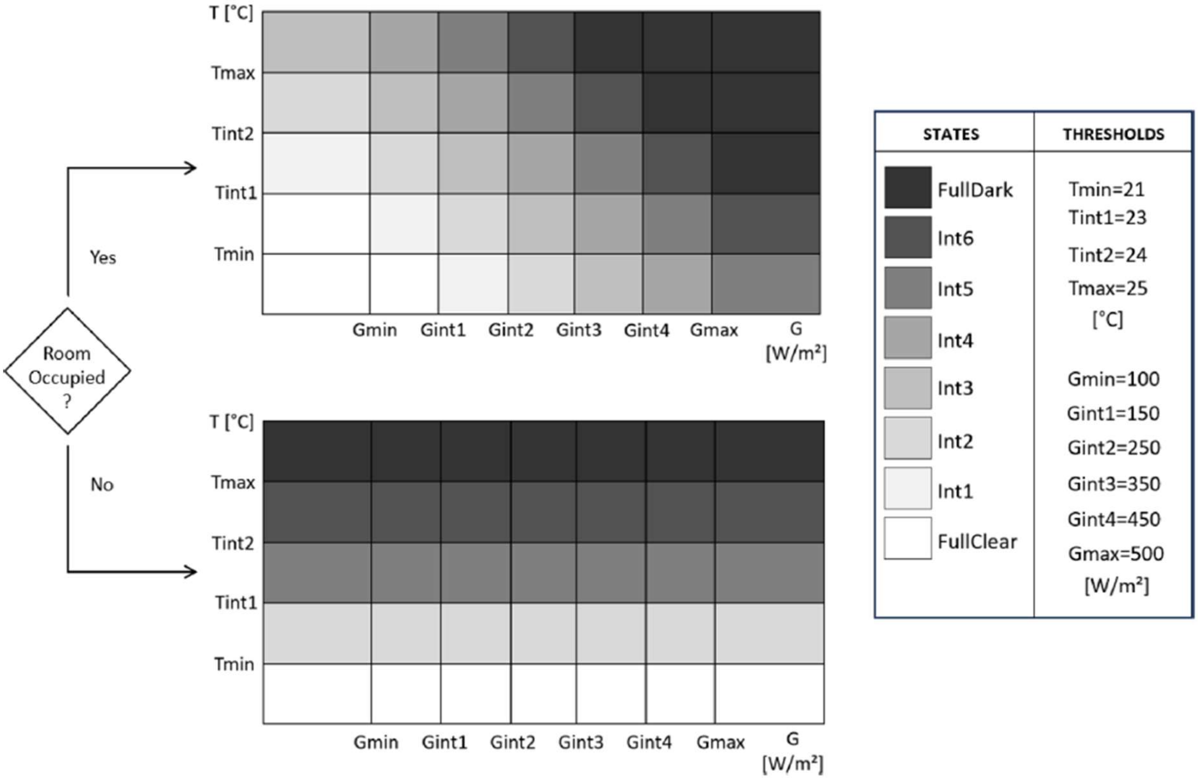

Figure 35: Diagram representing the logic of the RBC algorithm controlling the EC windows

The control logic has been implemented in EnergyPlus using the Energy Management System (EMS), the integrated programming environment that allows for implementing custom control logic, monitoring simulation variables, and modifying the behaviour of building systems and components in real time via user-defined algorithms.

4.9. PCM ALGORITHMS

EnergyPlus calculates transient heat conduction through opaque and multi-layer elements using the **Conduction Transfer Function (CTF)**: "this has all the usual restrictions of a transformation-based solution: constant properties, fixed value of some parameters, and do not produce results for the interior of the surface" [42].

To simulate materials with more complex behaviour, such as PCMs and variable thermal conductivities, the programme uses the **Conduction Finite Difference (CondFD)** solution algorithm; the user can choose between a semi-implicit and a fully implicit model. The algorithm directly solves the heat conduction equation within a wall by discretising it into a series of spatial nodes and computing the temporal evolution of temperature at each node; this method allows for the simulation of more complex conditions and non-linear phenomena, at the expense of greater computational effort and possible numerical instability.

These types of models, integrated into EnergyPlus, have often been used without a thorough review of all available results; the work by Zhilyaev et al.[43] has recently shown that a careful validation of the results obtained has revealed various inconsistencies in simulations representing PCMs subject to hysteresis, in which partial solidification/melting of the material occurs, mainly due to "the fact that the hysteresis model in EnergyPlus is based on a simplified curve-switch theory and by the impossibility of taking supercooling effects into account".

4.9.1. Errors found

The graph below shows the results of a 15-day simulation in which the internal temperature is maintained at a constant 21°C, whilst the external conditions are those previously classified as 'Winter Clear'. In this simulation, a PCM layer was incorporated as the innermost layer of the external walls and ceiling; the curves shown below depict the temperature of the outermost PCM node of the south-facing wall and the ceiling, which, within the stratigraphy, is in direct contact with the insulating layer.

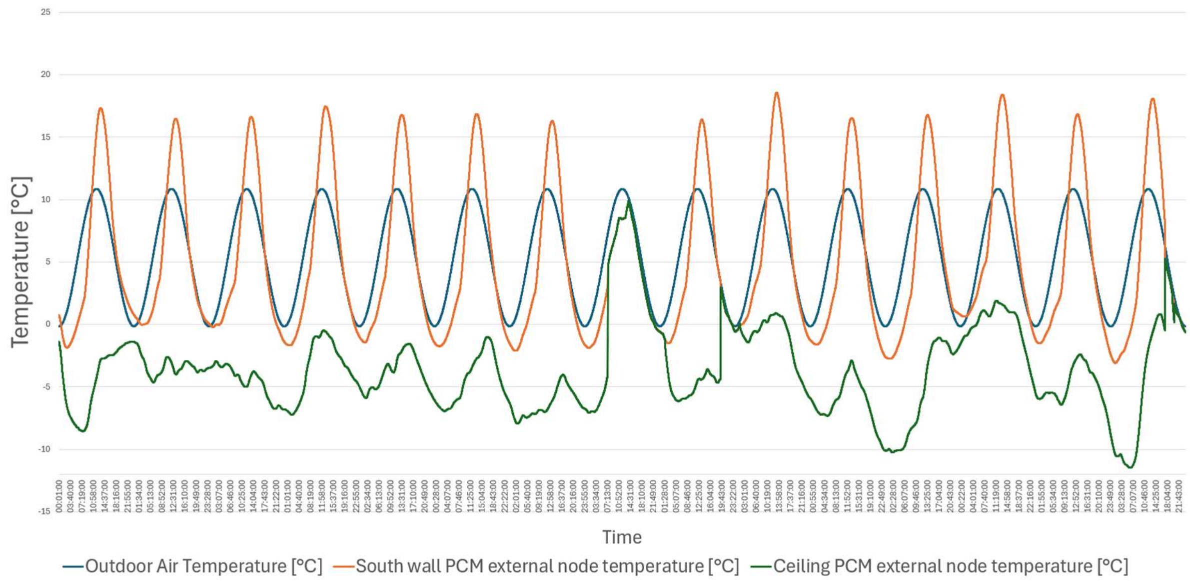

The orange and green curves were seen to show anomalous values that are inconsistent with the expected physical behaviour; indeed, the temperatures at these two nodes located within the envelope should be consistently higher than the external temperature, given the temperature difference between the external and internal environments. In particular, the curve for the PCM in the ceiling shows very low values and significant fluctuations, attributable to simulation errors or numerical instability.

In an attempt to mitigate this problem, the EnergyPlus version modified by Zhilyaev et al. [43] was used, in which the simulation algorithm for hysteresis-exhibiting PCMs was corrected to accurately track the melting and solidification curves. This attempt did not yield the desired results; whilst the temperatures of the external nodes showed slight changes, the results, particularly for the ceiling, remained confusing and unacceptable.

The temperature values of the external nodes of the PCM embedded in the internal walls were then analysed. The values obtained for the material embedded in the north and west walls and in the floor are shown below (the blue line representing the north face is difficult to see as it almost always coincides with the orange line representing the west face); in each case, the node shown is the one facing the exterior of the room under study and therefore towards a hypothetical adiabatic layer.

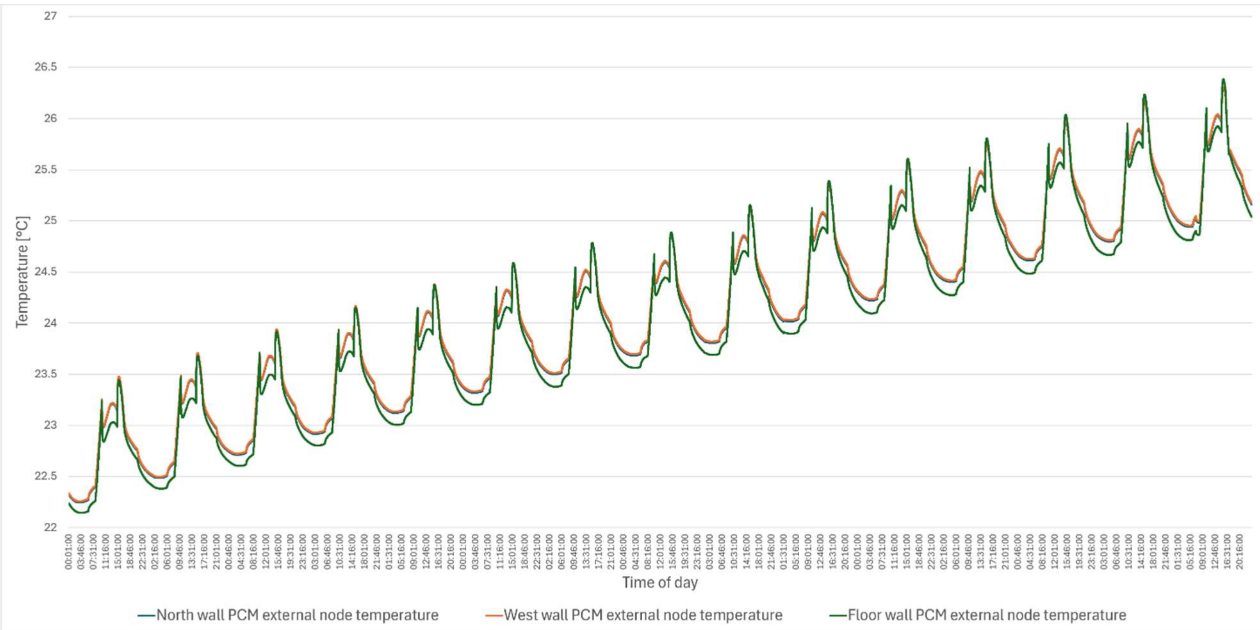

The results above are no longer characterised by extremely anomalous trends, as was the case for the external walls, with temperature values below the physically possible range. However, as the simulation progresses, the node temperatures rise gradually, even though the room's internal temperature remains at 21 °C.

In both cases, the temperature of the PCM nodes facing the interior – which was not shown in the previous graphs – varies minimally, whether for the material in the external or internal walls, and these variations are perfectly consistent with the environmental conditions

4.9.2. Limitations of the simulation model

In view of the results obtained, it was decided to entirely remove the PCM from the externally exposed surfaces, retaining it only in the floor and on the north and west walls; this was done to minimise the main issues. Furthermore, given the limited benefits of implementing the modified hysteresis simulation code, the simulations were carried out using the original EnergyPlus version 25.2.0.

The causes of these errors remain unknown to the author and could be attributed either to an incorrect implementation of the PCM, which could cause numerical instability, or to simulation errors arising from the algorithm integrated into EnergyPlus.

Bearing in mind the points outlined in this paragraph, the results presented in the next chapter cannot be considered entirely accurate or representative of the actual behaviour of this technology; they have nevertheless been retained so as not to exclude a highly significant ABE from the present study.

4.10. SIMULATION MATRIX

The following section lists all the simulations carried out, broken down by season, and defines the terminology used throughout this document for the technologies and control methods.

Winter:

- **DGU Ref:** Reference case using no ABEs and a Double-Glazing Unit
- **TGU Ref:** Reference case using no ABEs and a Triple-Glazing Unit
- **DSF SA:** Double skin façade system in Supply Air mode
- **DSF TB:** Double skin façade system in Thermal buffer mode, with normal ventilation
- **PCM:** Enhanced internal walls without preconditioning
- **PCM 1H:** Enhanced internal walls with 1 hour preconditioning
- **PCM 05H:** Enhanced internal walls with 30 minutes preconditioning

- **EC:** Electrochromic glazing
- **DB-EC:** Dual-band electrochromic glazing

Summer:

- **DGU Ref:** Reference case using no ABEs and a Double-Glazing Unit
- **DGU Ref No blind:** Reference case using no ABEs and a Double-Glazing Unit, blind control not active
- **TGU Ref:** Reference case using no ABEs and a Triple-Glazing Unit
- **TGU Ref No blind:** Reference case using no ABEs and a Triple-Glazing Unit, blind control not active
- **DSF OAC Low:** Double skin façade system in Outdoor Air Curtain low airflow
- **DSF OAC High:** Double skin façade system in Outdoor Air Curtain high airflow
- **DSF EA:** Double skin façade system in Exhaust Air mode
- **PCM:** Enhanced internal walls without preconditioning
- **PCM 1H:** Enhanced internal walls with 1 hour preconditioning
- **PCM 05H:** Enhanced internal walls with 30 minutes preconditioning
- **EC:** Electrochromic glazing
- **DB-EC:** Dual-band electrochromic glazing

5 RESULTS ANALYSIS

This chapter is devoted to analysing the results of the simulations, with the aim of quantifying, using the appropriate KPIs, the effect of the technologies and their associated control methods. The technologies will be compared using simulation results under the same reference climate.

To fully assess the results, the KPIs should not be interpreted independently, as each one describes a different phase or effect of the flexibility event. Autonomy and degree of partialisation mainly quantify the system's ability to reduce or interrupt the load while maintaining acceptable indoor conditions. However, these two indicators do not fully capture overall flexibility performance, since greater autonomy may be associated with higher rebound energy after the event. For this reason, peak-shaving capacity quantifies the absolute amount of energy shifted or avoided during the event, while rebound energy quantifies the additional energy required to restore the initial operating conditions. In cases involving PCM, the precharge energy must also be considered, as the improved flexibility achieved during the event is partly enabled by energy stored during precharging.

5.1. COMPARISON OF TECHNOLOGIES FOR EACH CLIMATE

Changes in indoor conditions, energy consumption and the results achieved are primarily determined by external conditions; to better understand the results, it is necessary to carefully assess the temperature and solar irradiance values at the times when energy flexibility events occur. Given the substantial volume of ventilation air, attention must also be paid to the humidity levels of the outside air, as humidification and dehumidification can result in considerable energy loads. The two winter scenarios are characterised by fairly constant humidity levels in the outside air, whilst during the summer months, this value fluctuates significantly, which will affect energy consumption. These figures will be presented at the start of each paragraph to provide a clearer understanding of the reasons behind the results.

5.1.1. Winter cloudy

Figures 36 and 37 show the temperature, the incident solar radiation on the south-facing façade and humidity over the analysed day. The two time slots during which the flexibility events occur are also shown using the green line, ranging from 8:00 – 9:00 AM and 5:00 – 6:00 PM.

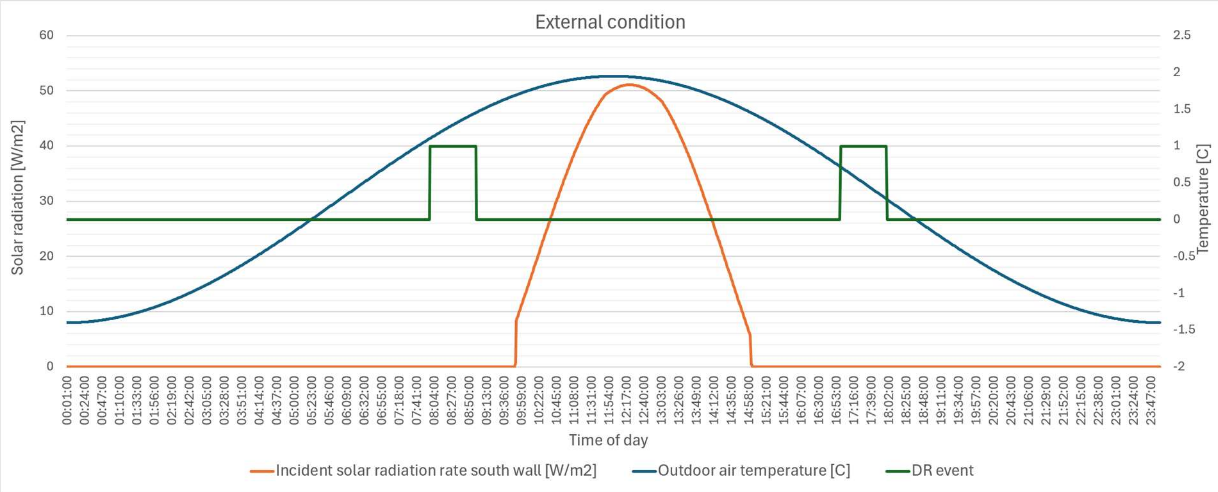

Figure 36: Winter cloudy external temperature and solar radiation

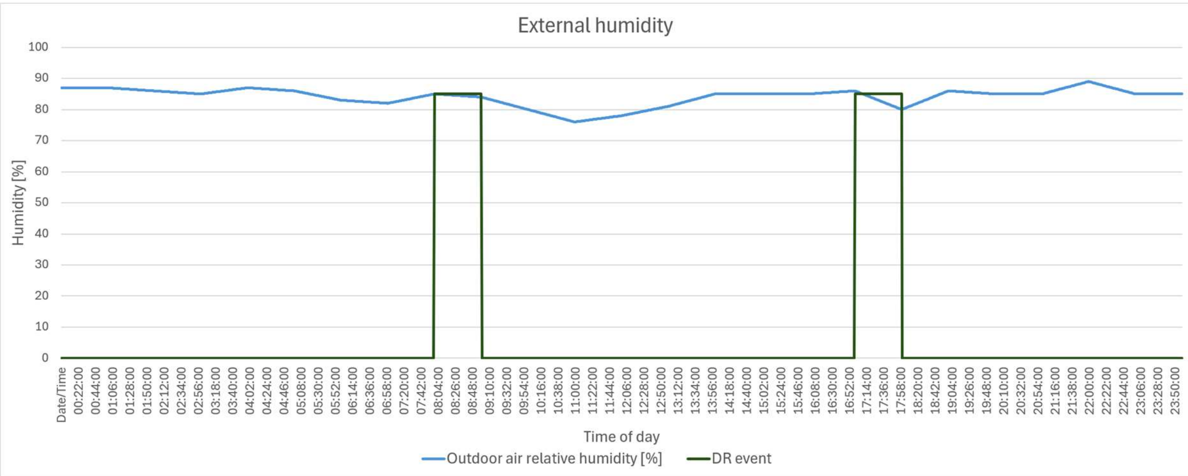

Figure 37: Winter cloudy external humidity

The flexibility events were observed to occur before dawn and after sunset; as a result, no solar radiation strikes the building during these events.

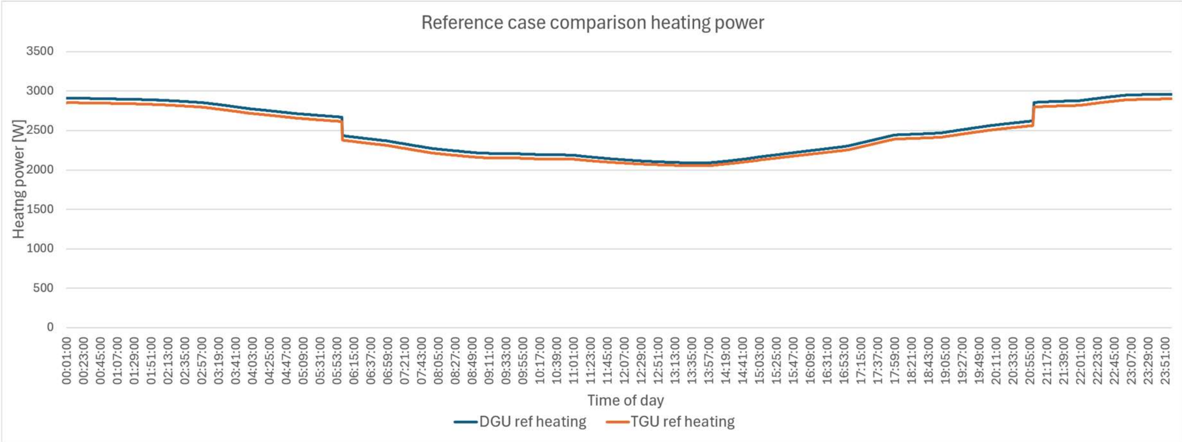

Figure 38: Winter cloudy reference case power comparison

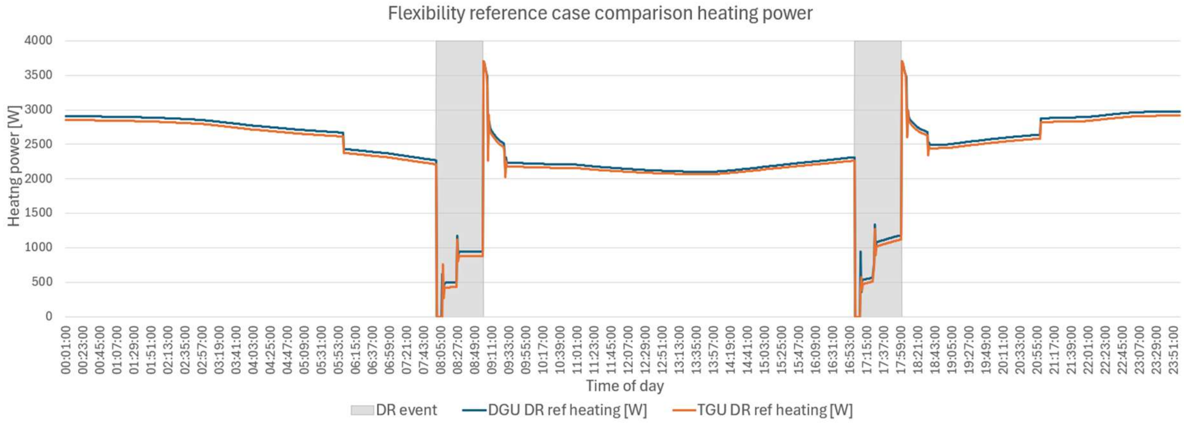

Figure 39: Winter cloudy reference case DR power comparison

The graphs in *Figures 38 and 39* show the trend in heating power for the TGU and DGU reference cases, as required by the system during normal operation and on a day characterised by demand response (DR) events, respectively. In the first case, the use of TGU glazing systems reduces energy demand by an average of 100–150 W.

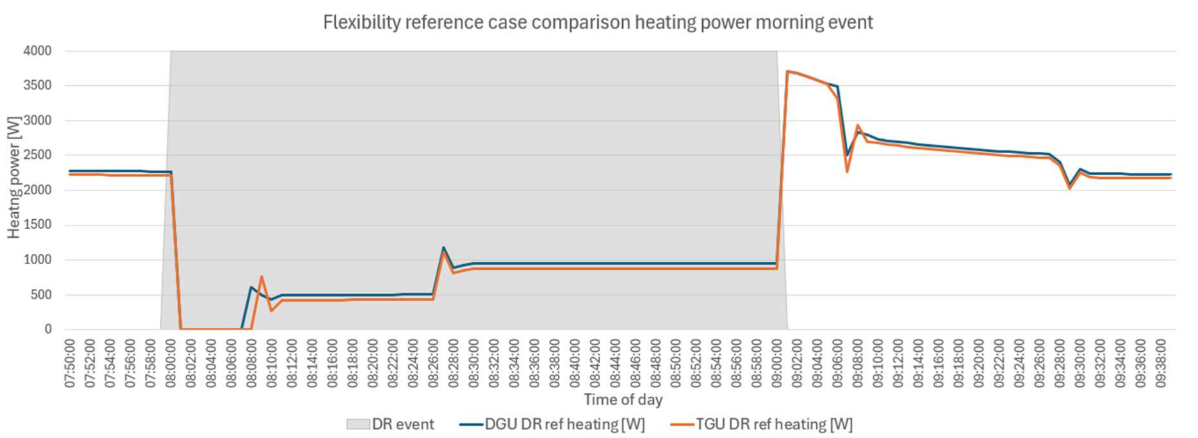

Figure 40: Reference case morning DR event heating power

A closer look at the power trends for the two reference cases during the morning event reveals certain recurring characteristics throughout the analysis. Starting at the beginning of the event (8:00 am), the heating load drops suddenly to zero due to changes in the temperature and humidity setpoints, followed by two power increases during the event and a recovery phase at the end, characterised by above-average power for a few minutes.

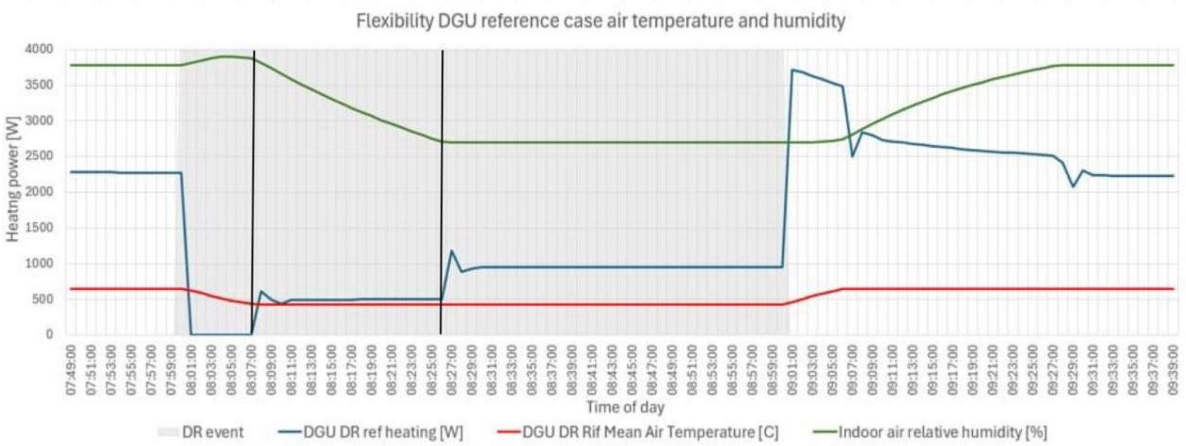

Figure 41: DGU reference case morning DR event, heating power, air temperature and humidity trends

The graph in Figure 41 shows the power (referring to the left axis), temperature and humidity (both referring to the right axis) trends for the DGU reference case during the morning event; the two power steps, indicated by the two vertical black lines, coincide with the moments when the new temperature threshold (19°C) and humidity setpoint (40%) are reached. In this case, the factor limiting autonomy is the drop in temperature, which reaches its threshold before humidity does. However, the limiting factor is not always the same: depending on the climatic conditions and the envelope technology adopted, humidity or another performance variable may reach its prescribed limit first, thereby determining the end of the autonomy period.

Having analysed the load profiles for the reference cases, we can now interpret the results more clearly. *Tables 11 and 12* present the results for the 'Winter cloudy' scenario, broken down into morning and afternoon events. For each scenario, the values obtained for the various KPIs used have been colour-coded on a scale from green to red; as a general rule, results characterised by a greenish hue indicate a positive outcome, whilst red results indicate critical issues. With regard to the Degree of partialisation, the ideal target, which would allow for the complete shutdown of the heating system, is 100%. High values for 'Autonomy' and 'Peak shaving capacity' indicate the system's good ability to adapt to flexibility events, whilst high values for 'Rebound energy' and 'DR energy balance' are to be regarded as negative.

Table 11: Winter cloudy morning DR event KPI results

WINTER CLOUDY						
8:00-9:00						
CASE	**Autonomy [min]**	**Degree of partialisation [%]**	**Peak shaving capacity [Wh]**	**Precharge energy [Wh]**	**Rebound energy [Wh]**	**DR energy balance [Wh]**
DGU Ref	7	69%	1540.7	-	299.3	-1241.4
TGU Ref	8	71%	1551.7	-	303.4	-1248.3
DSF SA	4	52%	1132.0	-	258.8	-873.2
DSF TB	8	74%	1593.5	-	315.1	-1278.4
PCM	10	77%	1602.2	-	373.4	-1228.9
PCM 1H	14	81%	1690.7	1059.9	364.3	-266.6
PCM 05H	14	81%	1684.5	633.4	368.0	-683.2
DB-EC	7	69%	1540.9	-	299.5	-1241.4
EC	7	68%	1534.8	-	298.1	-1236.7

The reference configurations (DGU Ref, TGU Ref) show an autonomy of 7–8 minutes and a moderate degree of partialisation (69–71%), with a moderate peak shaving capacity (1540.7–1551.7 Wh) supported by a relatively low rebound energy (299.3–303.4 Wh) compared to the magnitude of the shifted load.

The DSF in SA mode exhibits the most critical behaviour in the entire dataset: an autonomy of just 4 minutes, a degree of partialisation of 52 per cent, and a peak-shaving capacity of 1132.0 Wh – the lowest values among all configurations. Rebound energy, on the other hand, is the lowest among all cases (258.8 Wh), but this is not in itself a positive sign: it is simply the consequence of a much shorter event window, during which a limited amount of energy is drawn off and therefore the required recovery is also proportionally lower. This result indicates that operation in 'Supply Air' mode – which is geared towards treating fresh air rather than storing heat within the cavity – does not provide a sufficient thermal reserve to meet heating demand during the event, forcing the system to resume operation prematurely.

The DSF in TB mode exhibits the opposite behaviour and proves to be the best-performing configuration among non-PCM technologies: an autonomy of 8 minutes, a degree of partialisation of 74%, and a peak-shaving capacity of 1593.5 Wh. This indicates that Thermal Buffer mode, by utilising the cavity in the façade as a storage mass, provides a heat reserve that extends the sustainable duration of the event and increases the margin for load reduction. Consequently, the rebound energy is the highest among the non-PCM cases (315.1 Wh), as the greater amount of energy removed during the event results in a proportionally higher recovery burden.

The non-precharged PCM achieves an autonomy of 10 minutes and a degree of partialisation of 77%, both higher than any non-precharged configuration, with a peak shaving capacity of 1602.2 Wh; however, the rebound energy is the highest among all non-precharged cases (373.4 Wh), indicating that the benefit gained during the event entails a significant recovery cost in this instance. The pre-charged variants, PCM 1H and PCM 05H, achieve the absolute best performance in terms of runtime (14 minutes) and degree of partialisation (81%), with the highest peak shaving capacity in the entire dataset (1,684.5–1,690.7 Wh); however, rebound energy remains high (364.3–368.0 Wh) and comparable to that of the non-precharged PCM, indicating that precharging does not produce a clear additional benefit in terms of rebound mitigation in this case, although it does result in a marked improvement in autonomy and partialisation; however, the longer pre-charge period and the resulting higher energy consumption do not bring about commensurate improvements

The electrochromic configurations (DB-EC, EC) faithfully replicate the behaviour of the reference cases across all parameters (autonomy: 7 minutes; degree of partialisation: 68–69 per cent; peak-shaving capacity: 1534.8–1540.9 Wh; rebound energy: 298.1–299.5 Wh), with no significant differences.

Table 12: Winter cloudy evening DR event KPI results

WINTER CLOUDY						
17:00-18:00						
CASE	Autonomy [min]	Degree of partialisation [%]	Peak shaving capacity [Wh]	Precharge energy [Wh]	Rebound energy [Wh]	DR energy balance [Wh]
DGU Ref	7	65%	1541.9	-	288.3	-1253.7
TGU Ref	7	67%	1548.7	-	292.6	-1256.1
DSF SA	3	49%	1137.2	-	275.6	-861.6
DSF TB	7	69%	1589.3	-	307.3	-1282.0
PCM	9	72%	1602.5	-	376.5	-1226.0
PCM 1H	13	76%	1704.0	1061.0	362.8	-280.2
PCM 05H	13	76%	1694.8	634.8	368.6	-691.4
DB-EC	7	65%	1540.9	-	288.2	-1252.7
EC	6	64%	1530.5	-	285.1	-1245.4

From comparing *Tables 11 and 12* it is immediately apparent that the results for the morning and evening events show only minimal differences; this is due to the similarity of the weather conditions during the two events. Indeed, in both cases, solar radiation is negligible, and the average outdoor air temperature differs by only 1 °C.

The reference configurations maintain an autonomy of 7 minutes and a degree of partialisation of 65–67%, with peak-shaving capacity and rebound energy remaining virtually unchanged compared with the morning (1541.9–1548.7 Wh and 288.3–292.6 Wh).

The DSF SA confirms its critical behaviour, with a further reduction in autonomy to 3 minutes, the lowest degree of partialisation in the entire dataset (49%) and the lowest peak shaving capacity (1137.2 Wh); rebound energy remains the lowest among the non-PCM cases (275.6 Wh), again as a direct consequence of the shorter event window. The DSF TB, by contrast, retains its position as the best-performing non-PCM configuration, with a runtime of 7 minutes, a degree of partialisation of 69% and a peak shaving capacity of 1589.3 Wh – figures virtually identical to those recorded in the morning, confirming the stability of the storage mechanism within the cavity even at the end of the day.

The non-precharged PCM shows a runtime of 9 minutes and a degree of partialisation of 72%, a slight decrease compared with the morning, with the highest rebound energy (376.5 Wh). The precharged variants, PCM 1H and PCM 05H, continue to lead in terms of autonomy (13 minutes), degree of partialisation (76%) and peak shaving capacity (1694.8–1704.0 Wh), with rebound energy still high (362.8–368.6 Wh) and essentially in line with the morning values. Once again, longer preheating does not yield any significant improvements.

The electrochromic configurations once again closely follow the reference cases in all KPIs, without standing out in either scenario.

The most significant finding to emerge from this scenario is the marked divergence between the two operating modes of the DSF, which remained consistent across both events: the SA mode consistently represents the worst-performing configuration in the entire dataset in terms of autonomy, degree of partialisation and peak shaving capacity, whilst the TB mode ranks as the best among non-PCM technologies for all three of these parameters. This indicates that the choice of the DSF's operating mode is the determining factor for its effectiveness as a flexibility tool during the heating season. Pre-charged PCMs remain the most effective technologies in terms of autonomy, degree of partialisation, and peak-shaving capacity in both scenarios, although they offer no clear advantage in rebound energy compared to non-pre-charged PCMs, contrary to what one might expect from the investment in pre-charging. Furthermore, both cases result in higher values for the DR energy balance; taking all aspects into account, therefore, the PCM 05 case emerges as the favourite

Following the analysis carried out, it should be noted that the results of the PCM simulations are subject to the calculation errors analysed in Chapter 4.9. In this regard, the difference between the PCM 1H and PCM 05H cases is of particular interest: there is a minimal difference in peak-shaving capacity between the two, favouring the case with the longer preheating phase by 10 Wh, at the expense of an additional 426.2 Wh consumed during the first phase; this result is consequently reflected in the DR energy balance. Such a small difference in results can be attributed to the previously discussed errors in chapter 4.9.2 "Limitations of the simulation model", which primarily involve an incorrect simulation of the PCM's phase change.

Figure 42 shows the PCM preheating power trends during the morning event; the different colours indicate the different pre-charging strategies: yellow for half an hour, red for a full hour. The power of the DGU reference case is also shown to make it easier to understand the changes brought about by the technology.

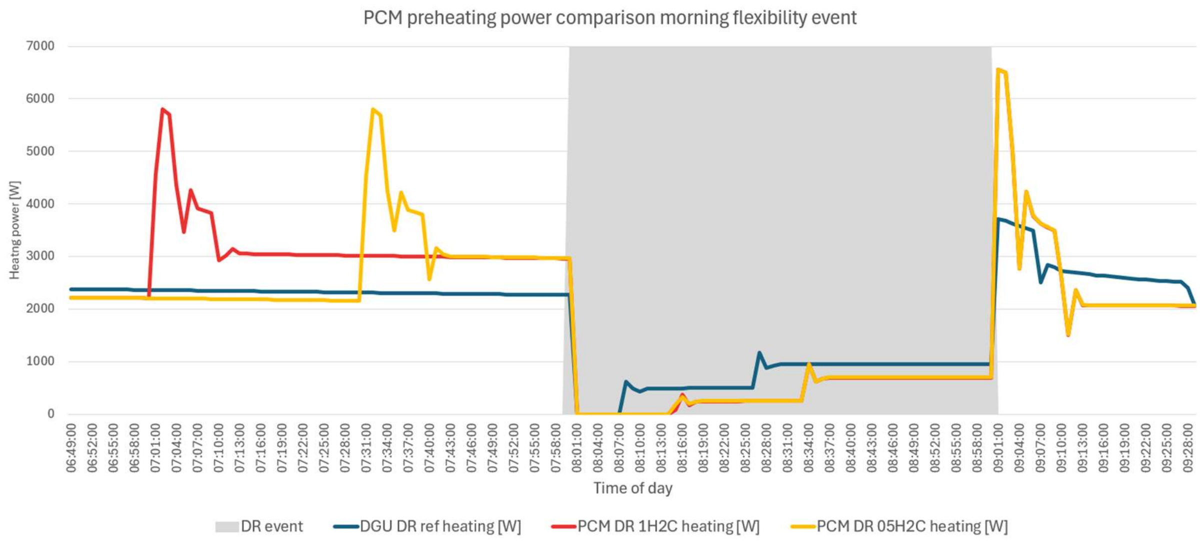

Figure 42: DGU and PCM 1H, 05H morning DR event heating power trends

A detailed examination of the power profiles reveals that during the event, the average power in the reference case is higher; for the other two, the only difference lies in the timing of the preheating phase, as indicated by the power peak that precedes the start of the event. The power profiles of the two cases remain consistently aligned throughout the event, demonstrating the minimal differences observed in the results.

However, when the entire period, including the preheating phase and the post-event rebound, is considered, a different picture emerges. As reported in *Table 11* through the rebound energy indicator, the PCM case requires significantly more rebound energy than the reference case. Therefore, although the PCM increases the duration of the flexibility event, this benefit is partially offset by the higher energy required to restore the indoor conditions after the event, making the overall trade-off less favourable.

Figure 43 shows the power profiles obtained for the 'Winter Cloudy Day' scenario using the DSF system, operating in 'Supply Air' and 'Thermal Buffer' modes. The differences in the results obtained depending on the system's operating strategy are noteworthy.

When operated in SA mode, the room's thermal performance is worse than in the DGU reference case, with Autonomy, Degree of Partialisation, and Peak Shaving Capacity all lower than in the other cases. Conversely, when the system is operated in TB mode, the results are slightly better than in the TGU reference case, consistent with the design choice to construct the DSF system with characteristics very similar to those of the TGU.

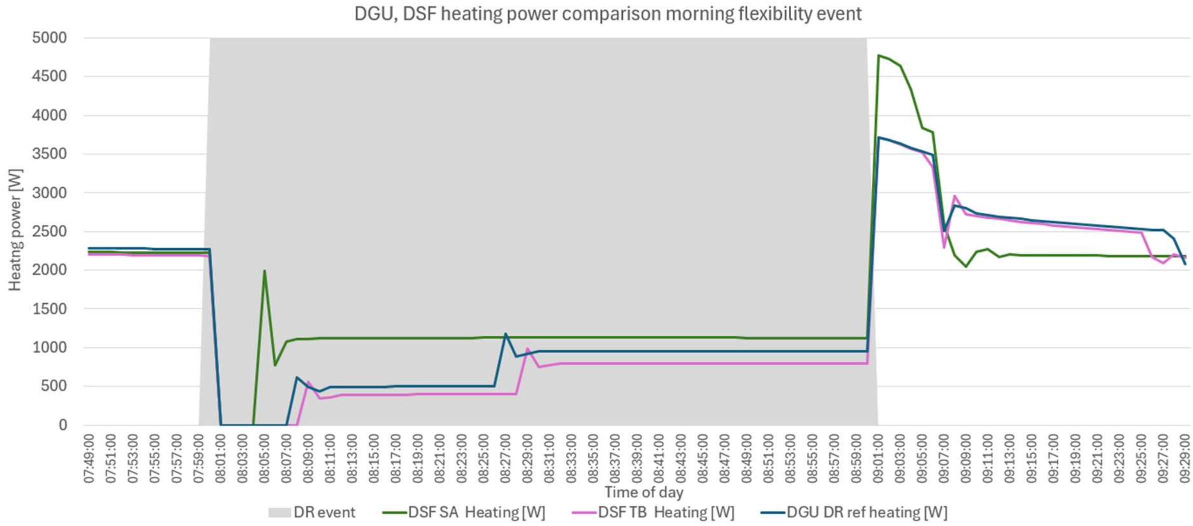

Figure 43: DGU and DSF SA, TB morning DR event heating power trends

The graphical representation of the power profiles for the DGU reference case and the two DSF operating modes during the morning event shows a significant difference between the results. The DSF SA case, represented by the green line, is characterised by higher consumption and a reduced range compared with DSF TB (in blue) and the reference case, DGU (in pink).

The reason for the poorer performance of the DSF system in SA mode is that, in the absence of solar radiation, the air forced through the cavity cannot extract heat from it, and the air is introduced into the room at a temperature almost identical to the outside temperature; however, this mode increases the heat exchange between the glass and the air itself, significantly increasing the heat lost through the glazing unit. TB mode, by contrast, maximises the thermal resistance of the transparent opening, bringing greater benefits to the entire system.

The final case concerns the two types of electrochromic glass; in this instance, the results obtained for the two systems are virtually identical to those of the DGU reference case. This is because the only variable the systems can control is the incoming solar radiation; however, throughout the day, the levels of solar radiation and internal temperature are such that, depending on the control system implemented, both systems are forced to operate in fully transparent mode; for this reason, the two systems behave like two conventional DGUs.

5.1.2. Winter clear

We will now analyse the results obtained for the Winter Clear reference day; *Figures 44 and 45* show the values of external temperature, solar radiation, and humidity, as well as the time intervals of the DR events.

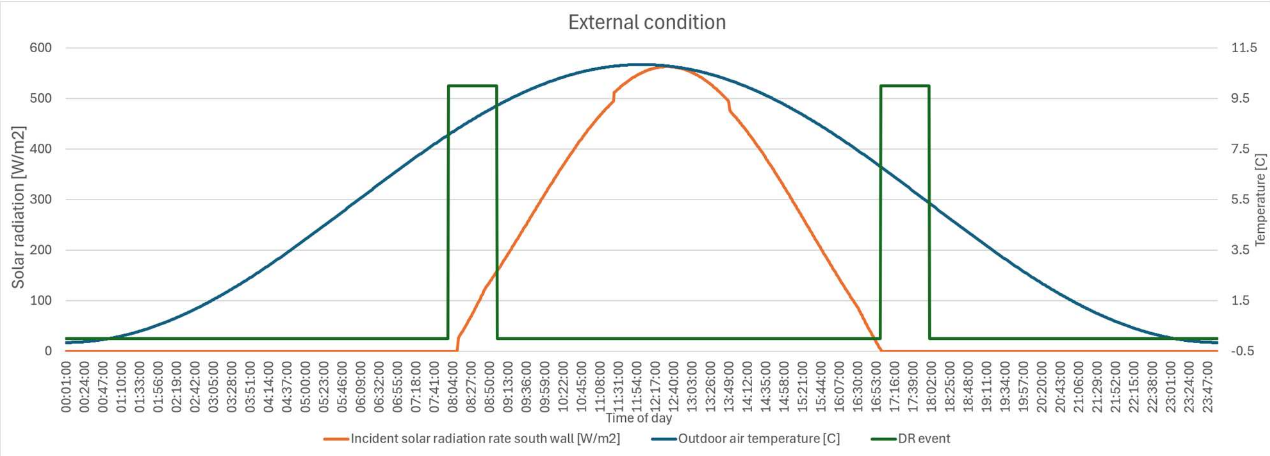

Figure 44: Winter clear external temperature and solar radiation

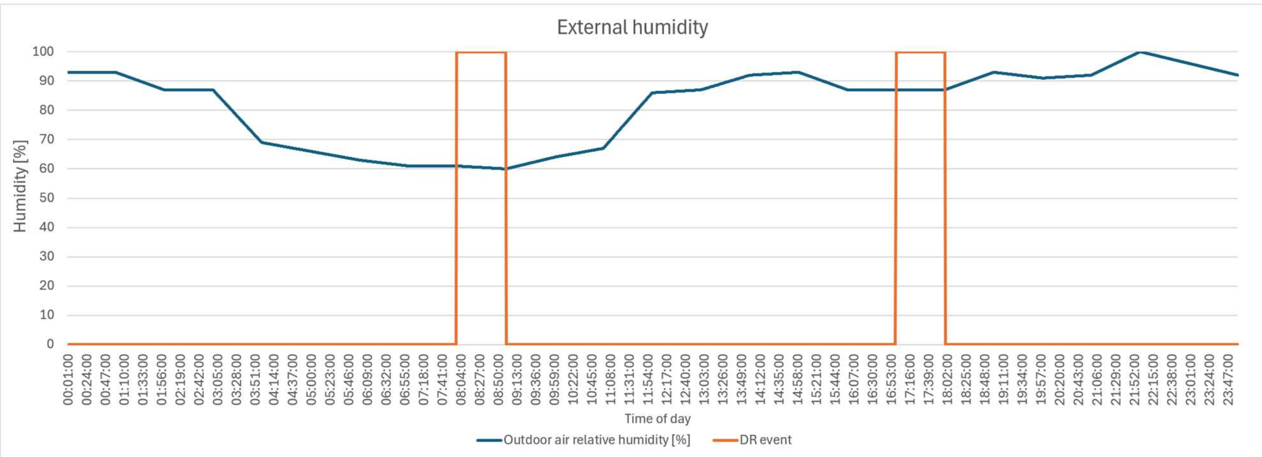

Figure 45: Winter clear external humidity

The morning event is characterised by an average temperature of around 8 °C and a humidity of 60%; solar radiation increases steadily throughout the event. The evening event has an outside temperature of 6 °C and a humidity of 90%, whilst there is no solar radiation.

The load profiles of the reference cases are analysed below:

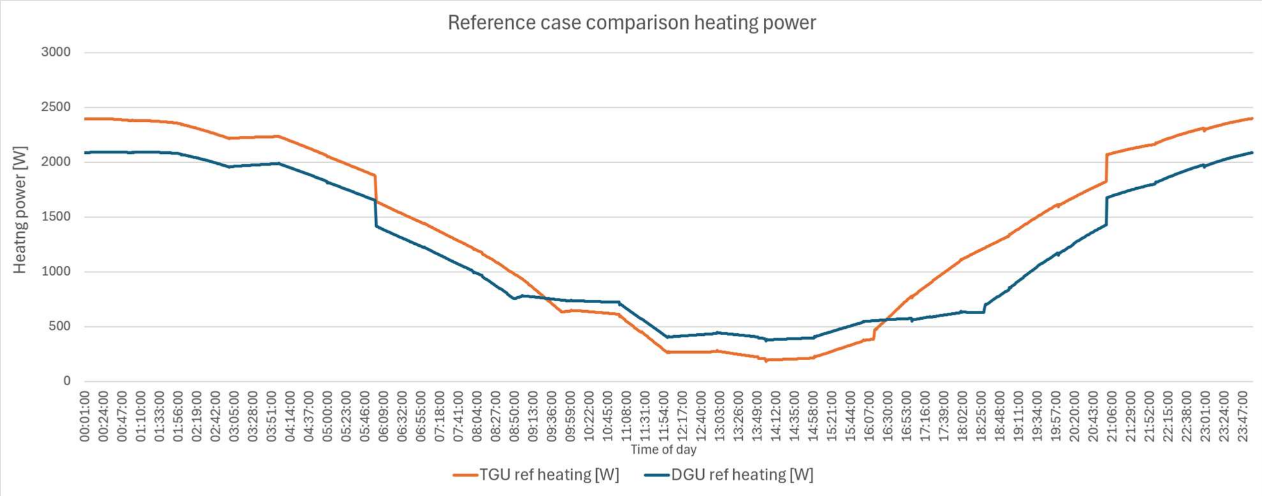

Figure 46: Winter clear reference case power comparison

The profiles in *Figure 46* show unusual characteristics: the TGU case, although it uses a glazing system with greater thermal insulation, results in higher energy consumption at night compared with the DGU case. During the middle of the day, this trend is reversed; consequently, a higher load is recorded in the DGU case.

To identify the causes of this seemingly anomalous behaviour, a number of variations on the two reference cases were evaluated; the first, shown below, involves the complete elimination of solar radiation, whilst keeping all other simulation parameters unchanged.

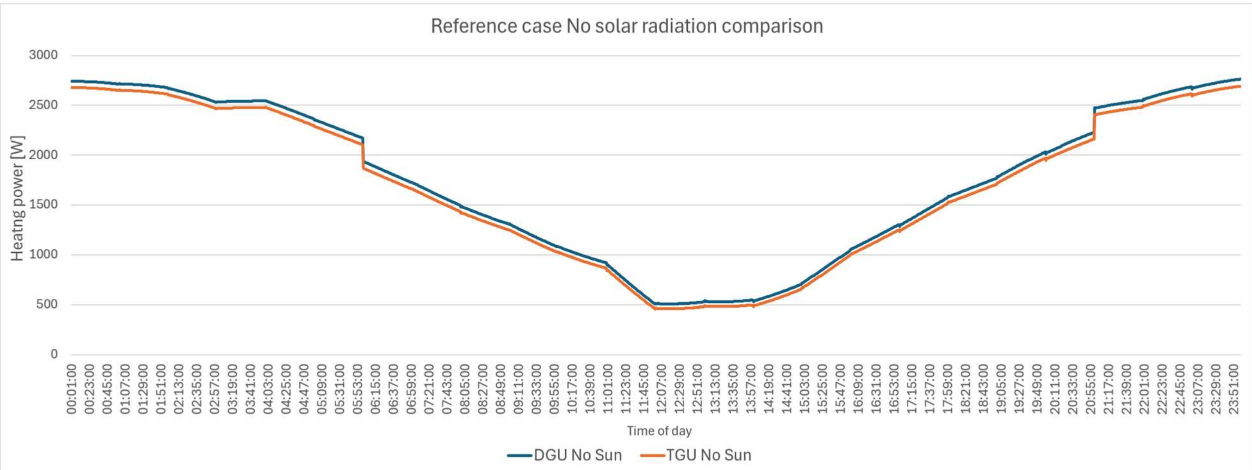

Figure 47: Winter clear reference case no solar radiation power comparison

As shown in *Figure 47*, the load profiles for the two reference cases are almost identical, differing by an average of 60 W, attributable to the greater insulation provided by the TGU system. This graph demonstrates that the previously observed differences are due to solar radiation and, more specifically, to its interaction with the glazing:

Referring to *Table 6*, an extract of which is shown below, labelled as *Table 13*, the DGU system has an SHGC that is almost double that of the TGU system.

Table 13: Extract from Table 6, characteristics of reference cases glazing components

Unit	State	Layout	T_{VIS} [-]	T_{SOL} [-]	SHGC [-]	U-value [W/m²k]
DGU		ECLAZ 6mm Argon 90% air 10% 16mm Planiclear 6mm	0,823	0,587	0,632	1,21
TGU		ECLAZ 6mm Argon 90% air 10% 16mm CL XTREME 61-29 6mm Argon 90% air 10% 16mm Planiclear 6mm	0,555	0,202	0,328	0,877

The DGU system, therefore, allows greater solar gain, enabling the space to accumulate heat during the day and release it at night, thereby reducing the thermal load on the air-conditioning system.

This analysis helped to explain the reason for the difference in thermal loads at night, but not why, during the middle of the day – when solar gain is at its peak – the trend is reversed. To understand this behaviour, two further simulations were carried out, restoring the solar radiation value to its original level but removing the humidity control.

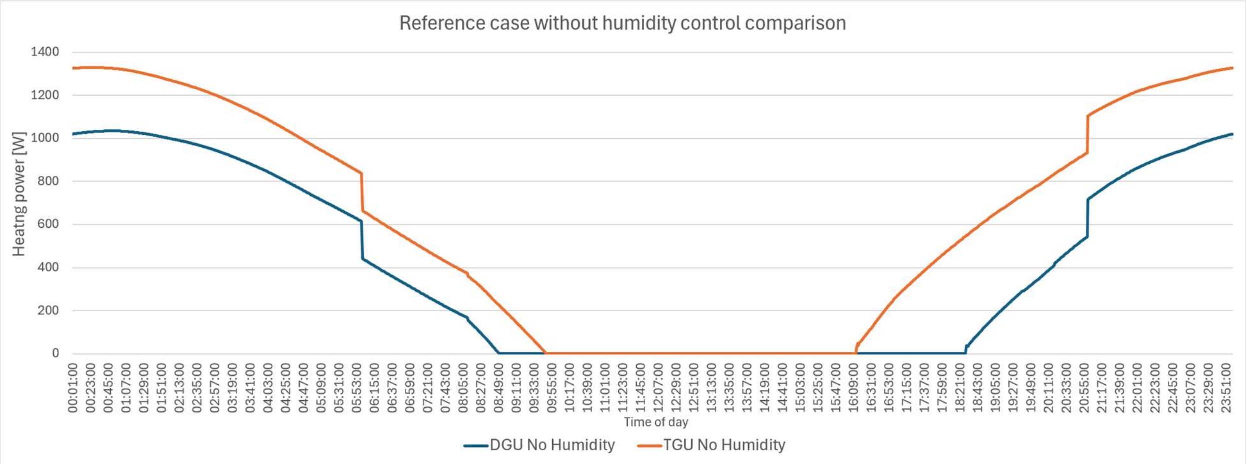

Figure 48: Winter clear reference case no humidity control power comparison

Figure 48 shows the heat load values when humidity control is not implemented. During the middle of the day, the load drops to zero because the sum of the internal loads and solar gains is sufficient to maintain the internal temperature above the setpoint of 21°C.

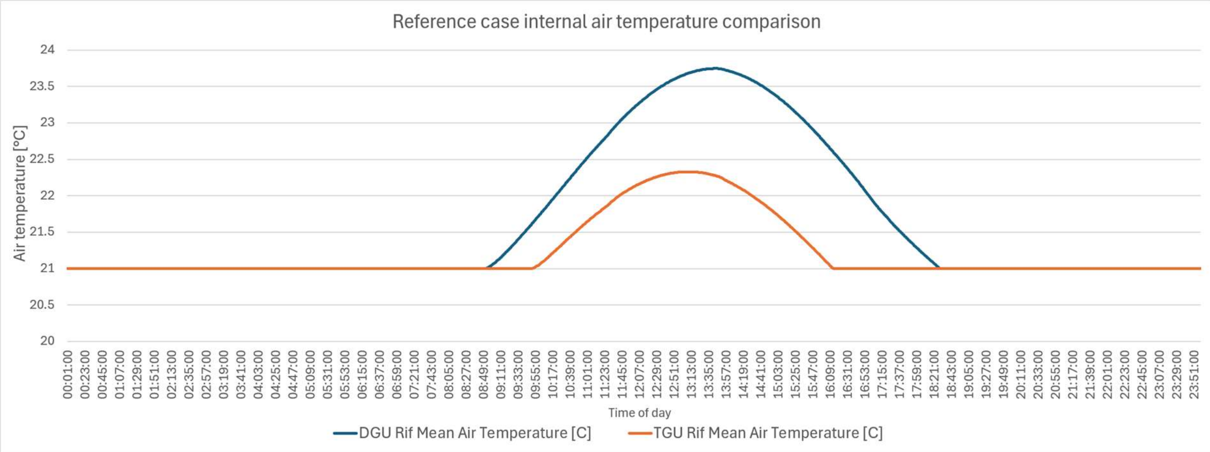

Figure 49: Winter clear reference case internal temperature comparison

Figure 49 shows the indoor air temperature values for the two reference cases. When the system load drops to zero, the temperature rises above 21 °C; this is more pronounced in the DGU case, given the greater solar gain of this glazing system.

The higher temperature in this case results in greater energy consumption by the system to reach the 50% humidity setpoint, thereby explaining the differences in heating load trends between the two reference cases analysed.

Now that we have gained a better understanding of the system's behaviour under these weather conditions, we can assess DR events and the impact of the technologies used.

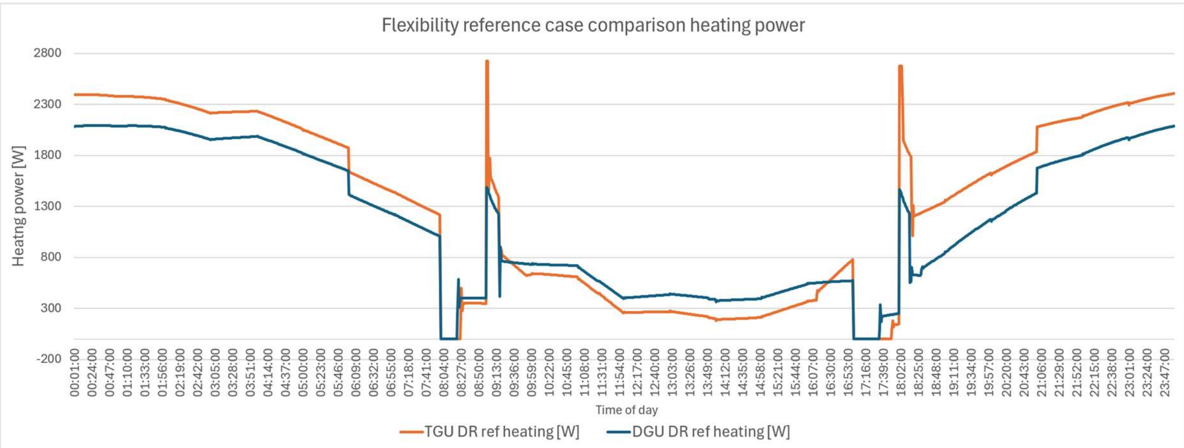

Figure 50: Winter clear reference case DR power comparison

Figure 50 shows the trend in heating power for the DGU and TGU reference cases on a day characterised by demand response (DR) events; the power peaks recorded in the TGU case at the end of both events are particularly evident.

Tables 14 and 15 present the results for the 'Winter clear' scenario, broken down into morning and afternoon events, using the same colour coding as before. Compared with the 'Winter Cloudy' scenario, the milder temperature and the greater contribution from solar radiation help to reduce the room's heating demand, thereby increasing its autonomy and the degree of partialisation.

Table 14: Winter clear morning DR event KPI results

WINTER CLEAR						
8:00-9:00						
CASE	Autonomy [min]	Degree of partialisation [%]	Peak shaving capacity [Wh]	Precharge energy [Wh]	Rebound energy [Wh]	DR energy balance [Wh]
DGU Ref	22	71%	611.1	-	156.7	-454.4
TGU Ref	26	82%	879.5	-	219.7	-659.8
DSF SA	45	99%	975.3	-	213.0	-762.4
DSF TB	30	86%	910.8	-	224.2	-686.5
PCM	22	72%	631.0	-	177.5	-453.4
PCM 1H	30	78%	682.4	1086.6	177.0	581.1
PCM 05H	30	78%	683.9	638.1	176.5	130.7
DB-EC	26	81%	848.9	-	208.0	-640.9
EC	28	85%	989.7	-	248.2	-741.5

The reference configurations show a marked difference between them: the DGU Ref achieves an autonomy of 22 minutes and a degree of partialisation of 71%, whilst the TGU Ref rises to 26 minutes and 82%, with a peak-shaving capacity that is almost double (879.5 Wh compared with 611.1 Wh). This difference means that heat during the event is better retained by the triple glazing, and therefore the load-reduction capacity is much higher than that of double glazing.

The DSF in SA mode has the best performance across the entire data set for three of the four parameters: autonomy of 45 minutes, degree of partialisation of 99 %, and peak-shaving capacity of 975.3 Wh, demonstrating its ability to make effective use of solar gains. The DSF in TB mode still gives a good result (30 minutes, 86 %, 910.8 Wh) but is still much less effective than SA during this time of the day, meaning that the storage in the cavity is not yet fully charged to provide an advantage similar to the direct use of incident radiation.

The non-precharged PCM offers no significant benefits, with performance similar to the worst-performing reference cases (22 minutes, 72%, 631.0 Wh). The pre-charged variants (PCM 1H and PCM 05H) both have an autonomy of 30 minutes and a degree of partialisation of 78 %, which is higher than the simple PCM and the DGU Ref, but lower than the TGU Ref, DSF SA and DSF TB; rebound energy is, moreover, the lowest among all configurations (176.5–177.0 Wh), meaning that the investment in pre-charging in this scenario reduces the recovery burden, but does not yield the best absolute result in terms of autonomy or partialisation.

The electrochromic configurations show very good performance: EC has a degree of partialisation of 85% and a peak-shaving capacity of 989.7 Wh, the highest value in the entire morning dataset, while DB-EC has intermediate performance (81%, 848.9 Wh).

Table 15: Winter clear evening DR event KPI results

WINTER CLEAR						
17:00-18:00						
CASE	Autonomy [min]	Degree of partialisation [%]	Peak shaving capacity [Wh]	Precharge energy [Wh]	Rebound energy [Wh]	DR energy balance [Wh]
DGU Ref	34	83%	492.8	-	166.1	-326.7
TGU Ref	50	98%	913.2	-	271.6	-641.6
DSF SA	10	75%	973.7	-	180.6	-793.1
DSF TB	60	100%	1054.8	-	295.4	-759.4
PCM	16	87%	600.2	-	224.0	-376.2
PCM 1H	49	95%	658.0	986.1	198.3	526.4
PCM 05H	50	95%	659.4	635.3	208.3	184.3
DB-EC	45	95%	795.5	-	250.9	-544.6
EC	56	99%	1053.4	-	298.7	-754.7

The reference configurations are much improved from the morning: the DGU Ref is up to 34 minutes and 83 %, and the TGU Ref is up to 50 minutes and 98 %, with the capacity to shave off nearly double (913.2 Wh).

The DSF SA doesn't perform as well as before, with an autonomy of only 10 minutes, but it still has a high peak shaving capacity (973.7 Wh) and a partialisation of 75 %.

This behaviour validates that the Supply Air mode is dependent on the presence of solar radiation at the same time as the event: when there is no solar radiation in the late afternoon, the system no longer has the real-time thermal gain that it had in the morning, and the indoor conditions quickly move out of the acceptable range, even though the power reduction is still substantial in the short term. The DSF TB, on the other hand, shows the opposite behaviour: the autonomy (60 minutes), the degree of partialisation (100%), and the peak-shaving capacity (1054.8 Wh) are the absolute maximum values across the data set. This result verifies that the Thermal Buffer mode can use the heat stored in the cavity during the sunny day and deliver a higher level of insulation.

The non-precharged PCM has an autonomy of only 16 minutes, which is less than that measured in the morning, although the degree of partialisation is higher (87%); the rebound energy is higher (224.0 Wh). The pre-charged variants PCM 1H and PCM 05H, on the other hand, have a much better performance than the morning, with an autonomy of 49-50 minutes and a degree of partialisation of 95 %, which is close to the DSF TB, while the rebound energy remains low (198.3-208.3 Wh) compared to the other parameters achieved. It is important to note, however, that although both configurations perform very well across all key parameters, the DR energy balance remains very large (526.4 Wh and 184.3 Wh), meaning that the investment in pre-charging remains too high relative to the benefit.

The electrochromic configurations confirm the good performance already observed in the morning, with a further improvement: EC achieves an autonomy of 56 minutes, a degree of partialisation of 99 % and a peak shaving capacity of 1053.4 Wh – values close to those of the DSF TB – whilst DB-EC still achieves high levels (45 minutes, 95%, 795.5 Wh). This shows that the dynamic modulation of transmittance remains effective after direct solar gain ceases, likely due to thermal energy stored during the day, as seen in the reference cases and the DSF TB.

The most important result in this scenario is the clear switch in the autonomy and degree of partialisation between the two DSF modes as a function of the time of day: the SA mode is best in the morning and worst in the evening, while the TB mode is best in the evening and worst in the morning. This pattern suggests that the effectiveness of the SA mode is related to the availability of solar radiation at the time of the event, whereas the TB mode is related to heat accumulated over the previous hours and is thus more effective the longer the time since the beginning of daily solar radiation; if used correctly, the system ensures almost total load shedding during both events; if used correctly, the system ensures almost total load shedding during both events.

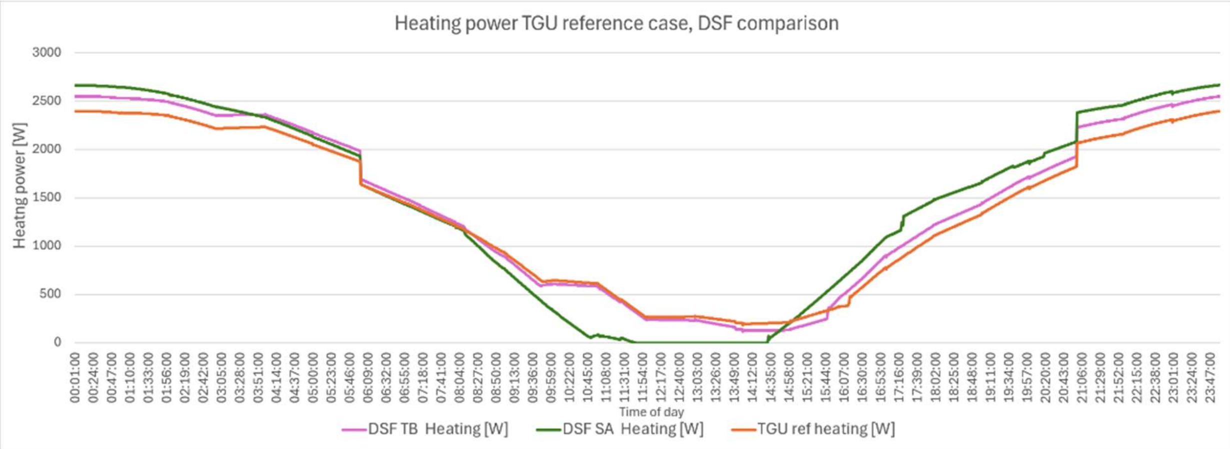

Figure 51: Heating power winter clear TGU, DSF SA and DSF TB

Figure 51 shows the load profiles for the TGU, DSF TB and DSF SA scenarios; as expected, the profiles for the first two are very similar; the DSF SA scenario differs mainly in the middle of the day, when the heating load drops to 0 due to the conditions achieved in this operating mode. *Figure 52* represents the same cases with DR events.

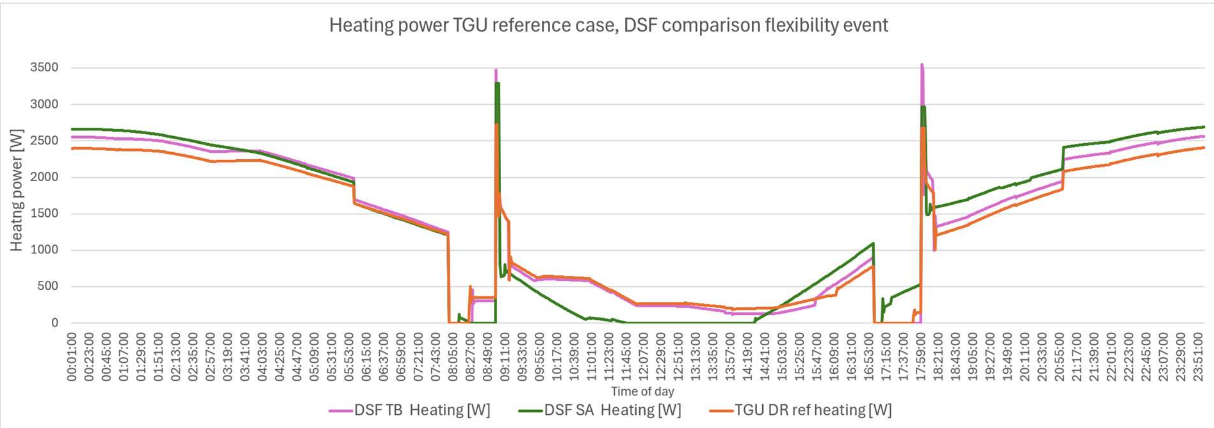

Figure 52: Heating power winter clear TGU, DSF SA and DSF TB during DR event

To better understand the thermal contribution of the DSF System and to motivate the thermal loads, the following graph shows indoor temperature values and the Facade Total Heat Transfer (FTHT) parameter described in section 2.4.2. for the DSF SA and DSF TB cases with DR events.

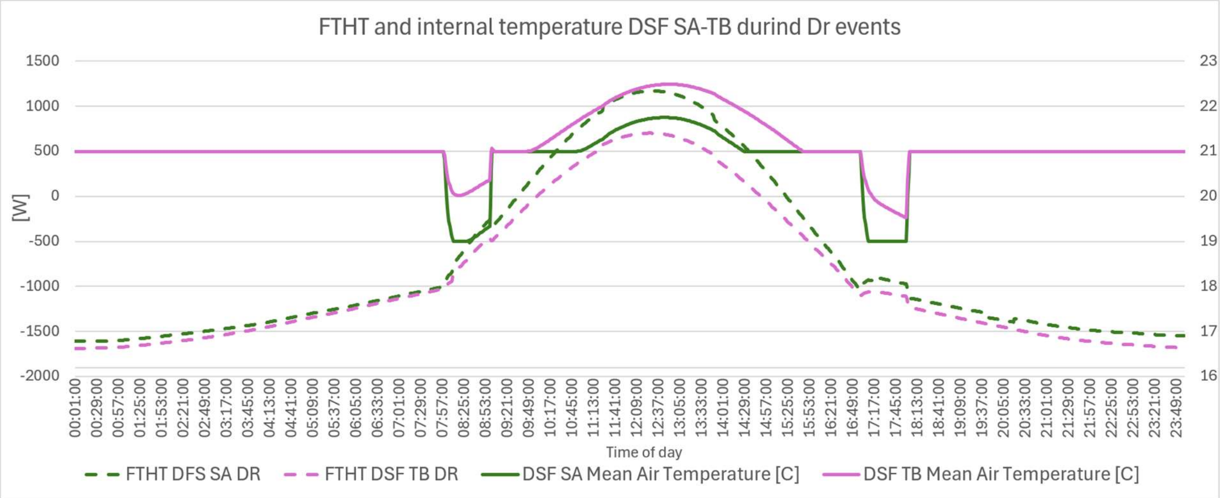

Figure 53: FTHT and air temperature in DSF SA-TB during DR events

The graph in *Figure 53* shows that the SA operating mode contributes most to the room's heat gain when solar radiation is at its peak; conversely, the TB mode allows the internal temperature to remain above the 19 °C threshold for longer during DR events. The difference in load, particularly for the morning event, is therefore due to the need for humidification, which is more demanding at higher indoor temperatures.

In line with the results obtained and the characteristics analysed, under the climatic conditions considered, the SA mode is preferable when the glazing is exposed to intense solar radiation; conversely, when solar gains decrease, as in the evening, the TB mode provides more stable indoor conditions.

We shall continue the discussion of the results by analysing the performance of electrochromic glazing. Given the high level of solar radiation incident on transparent surfaces – in contrast to the 'Winter Cloudy' scenario analysed previously – the control system described in section 4.8.3 applies gradual state changes during the simulations, thereby modifying the solar heat gains.

The load profiles for the reference cases and those using electrochromic glazing are shown below.

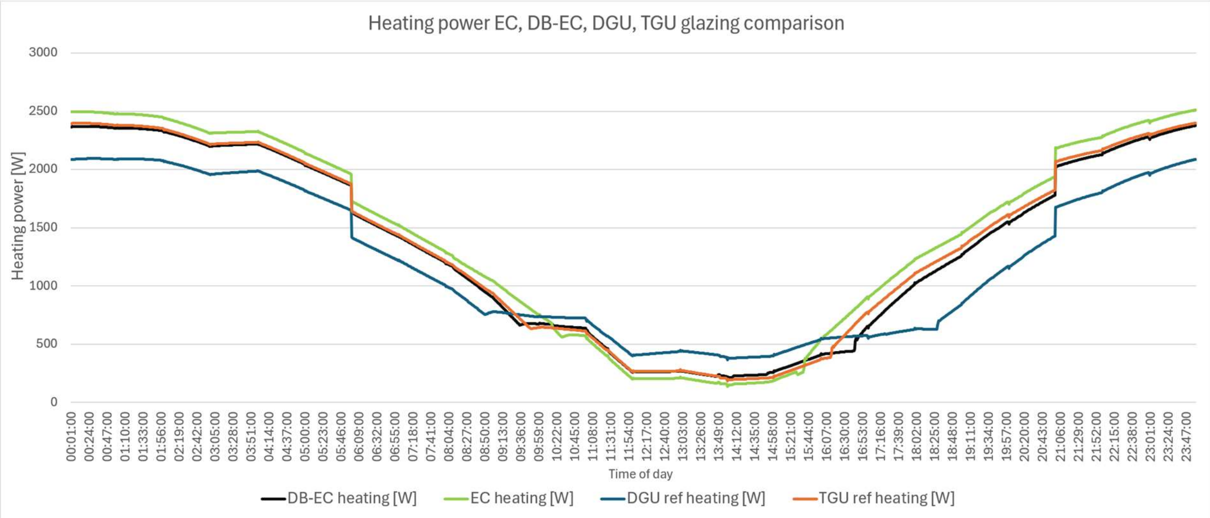

Figure 54: Heating power winter clear TGU, DGU, EC, DB-EC

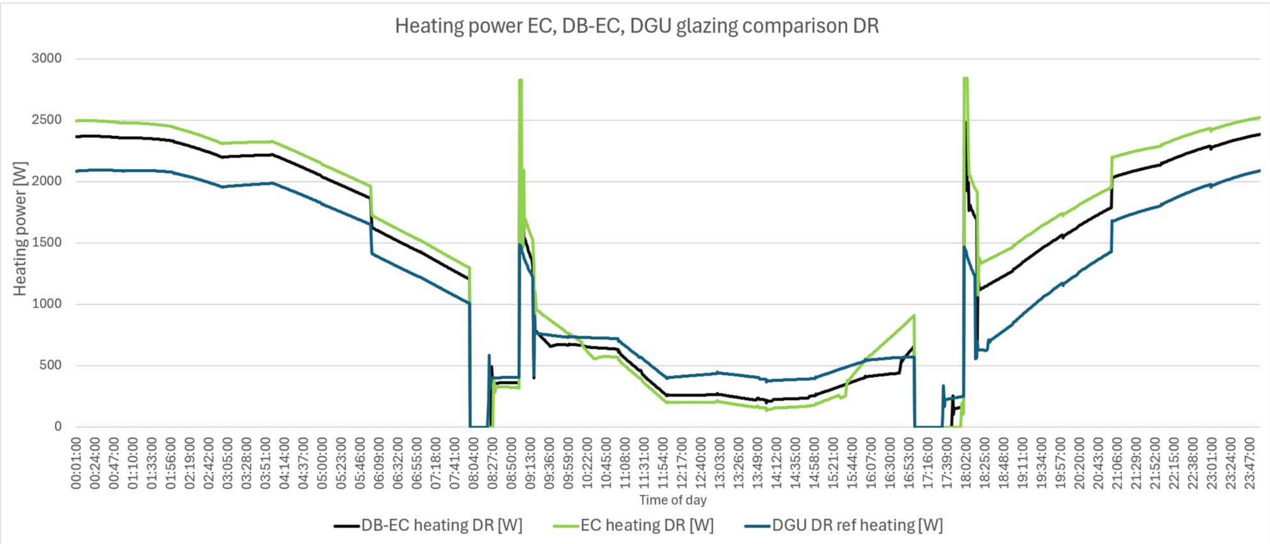

Figure 55: Heating power winter clear TGU, DGU, EC, DB-EC, DR event

In *Figure 55*, the data for the TGU system have not been included for reasons of representativeness; the line was, in fact, almost constantly superimposed on the black line representing the EC system.

The main difference between the two curves for the EC and DB-EC systems is the lower night-time load for the latter system; as previously noted in the comparison between DGU and TGU, this behaviour is linked to a different SHGC; the value of the latter, for each state of the two glazing systems analysed, is shown in the graph in *Figure 56.*

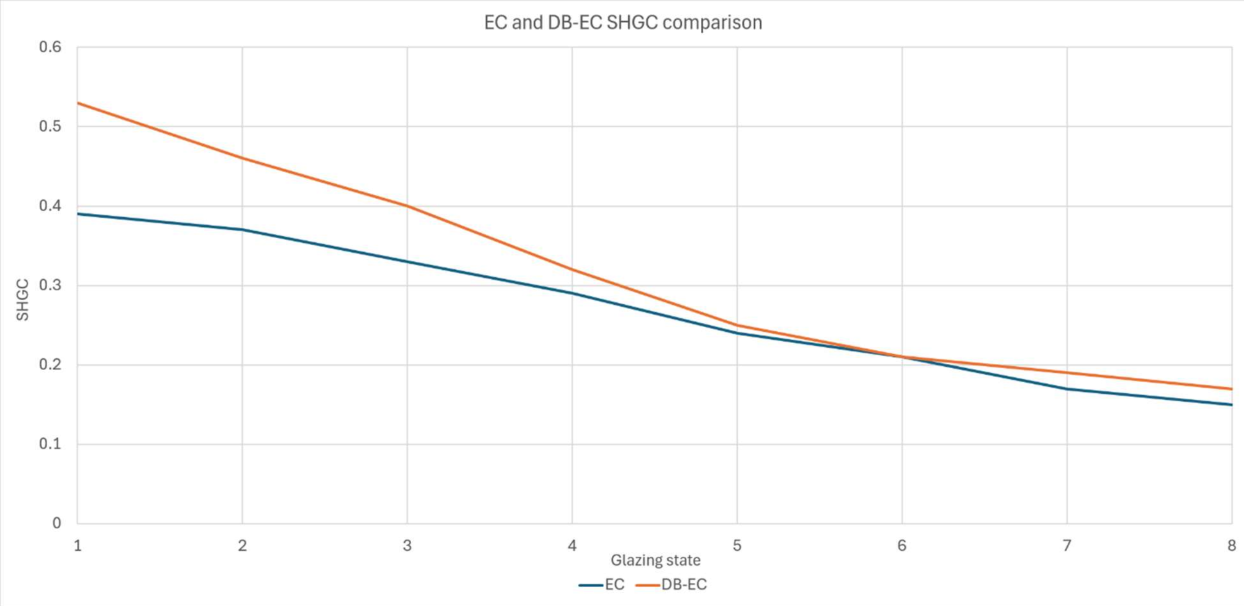

Figure 56: SHGC values for EC and DB-EC glazing

As was done previously for the reference cases, analysing the indoor temperature profiles from simulations of the two systems is useful for understanding the conditions; the states of the two glazing types are also shown below.

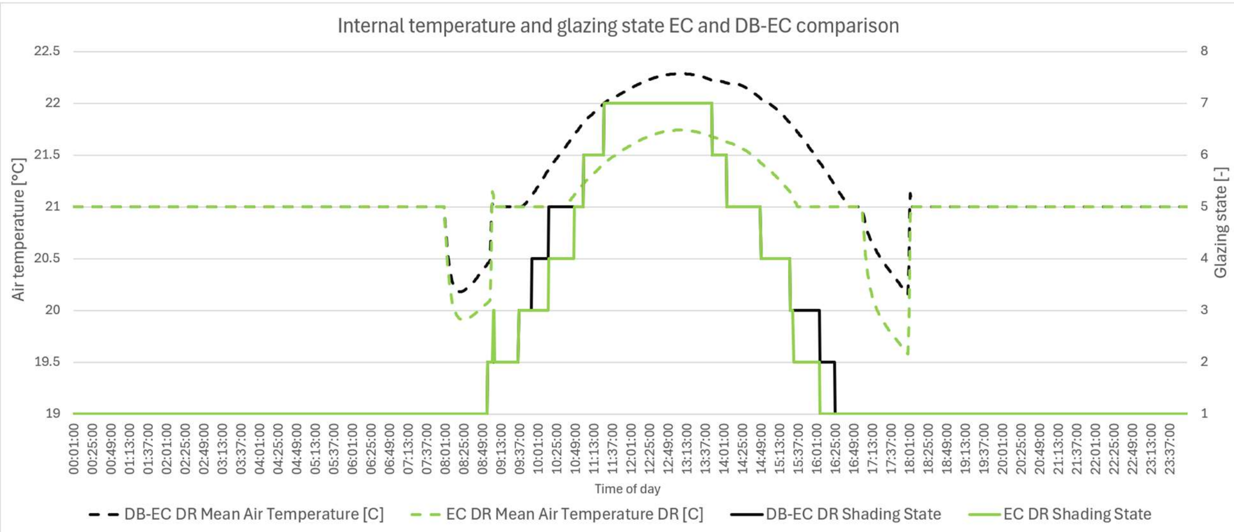

Figure 57: Temperature and glazing state in EC and DB-EC cases during DR

In line with the higher SHGC coefficient, the air temperature at midday rises more sharply in the EC-DB scenario due to the greater solar gain provided by this technology. As seen previously, this affects nighttime loads and the rate of temperature change during DR events, which, in the DB-EC scenario, declines more slowly.

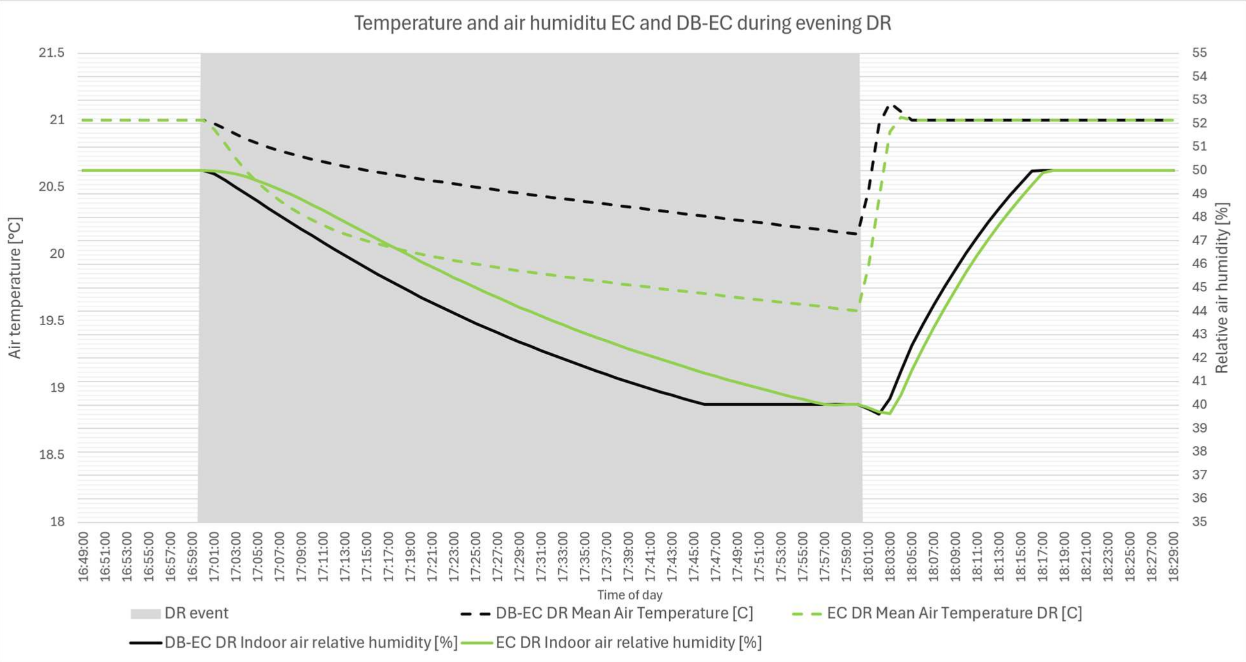

Figure 58: Temperature and humidity in EC and DB-EC cases during evening DR

By analysing the evening flexibility event shown in Figure 58, where the KPI values differ significantly among the cases, it can be observed that the lower peak-shaving capacity and reduced autonomy of the DB-EC case are mainly due to a faster decrease in indoor humidity. This behaviour is directly related to this configuration's greater ability to maintain higher indoor air temperatures, which in turn leads to lower relative humidity levels.

The analysis of these two components highlighted the importance of controlling all variables that may influence indoor conditions and the operation of the air-conditioning system. Based solely on the KPI values obtained, the scenario using conventional electrochromic glass appears to be more advantageous than the one using the advanced dual-band model; however, when analysing the trends of all indoor variables, it becomes apparent that DB-EC allows the room to accumulate significantly more heat, and that the limiting factor is relative humidity and the associated energy consumption.

Finally, the performance resulting from integrating PCM into the room was analysed. As shown in *Tables 14 and 15*, the technology did not yield any significant improvements and performed worse than the DSF and EC systems across all operating modes, particularly in peak-shaving capacity. Even with the preheating strategy, despite the substantial heat used, no clear improvements are observed, especially between the PCM 1H and PCM 05H cases.

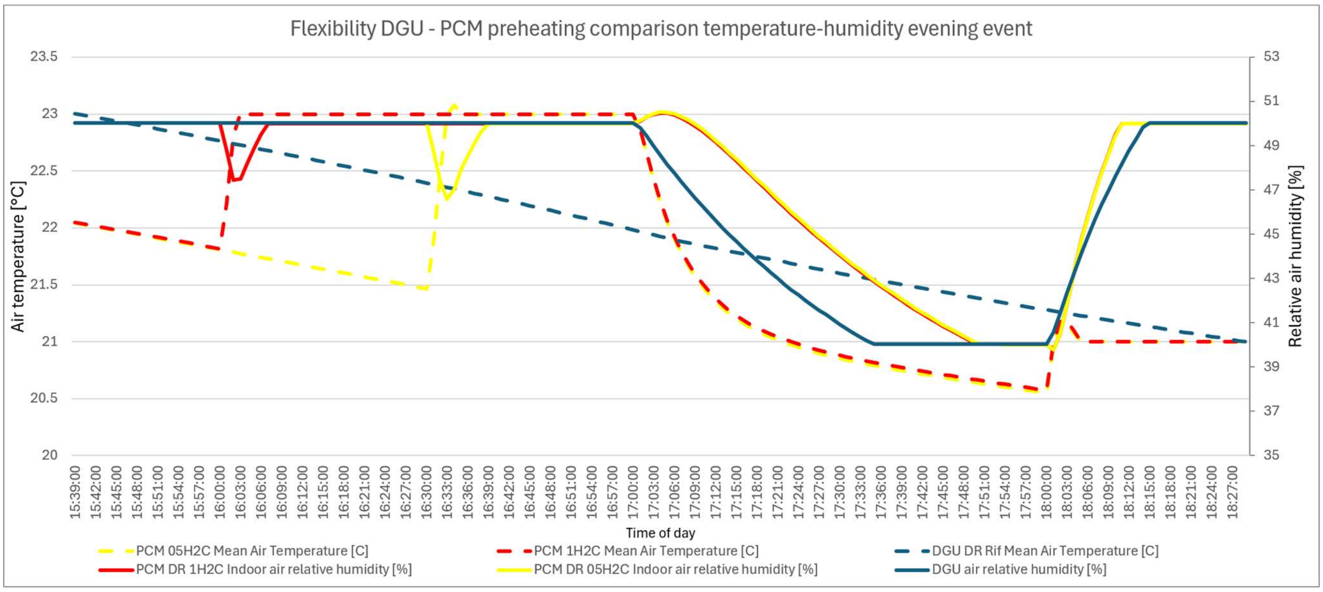

Figure 59: Temperature and relative humidity DGU, PCM 1H-05H evening DR comparison

Figure 59 compares the temperature and humidity values for the DGU and PCM cases with preheating during the evening DR event. In every case, the limiting factor is once again humidity; furthermore, both PCM cases, despite the difference in preheating time, exhibit almost identical temperature profiles, illustrating the material's inability to store or release heat. The temperature drop in these two cases is even more rapid than in the DGU case, despite all three cases reported using the same glazing system and, consequently, receiving the same solar gain. This behaviour may indicate numerical errors in the material simulation, as in the case of Winter Cloudy.

5.1.3. Summer cloudy

We continue our analysis of the results with the Summer Cloudy case; in this instance, the main objective is to cool the room and, when necessary, to dehumidify the air.

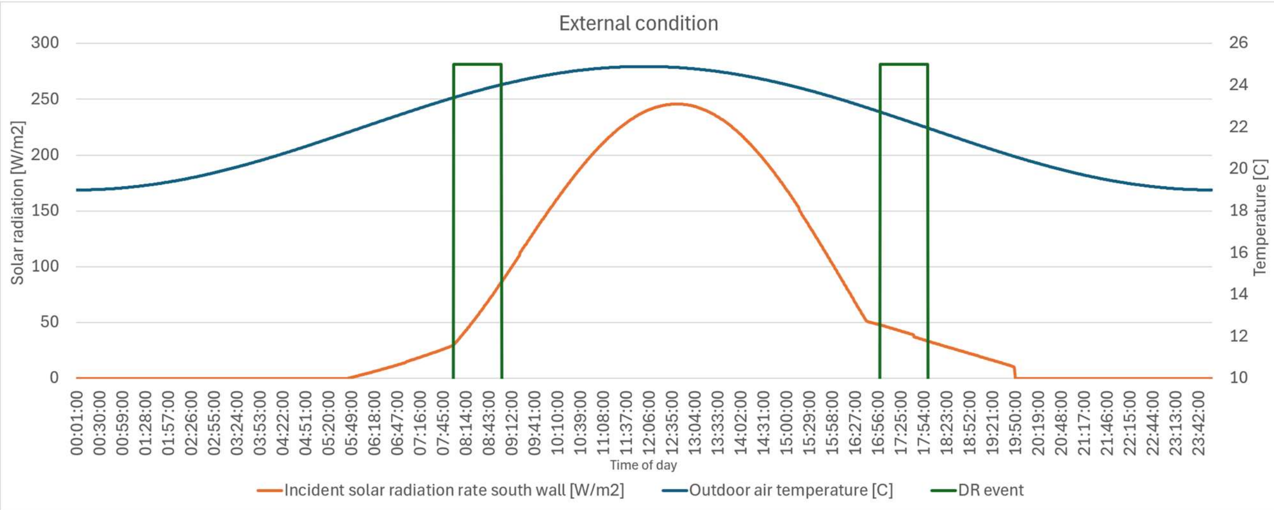

Figure 60: Summer cloudy external temperature and solar radiation

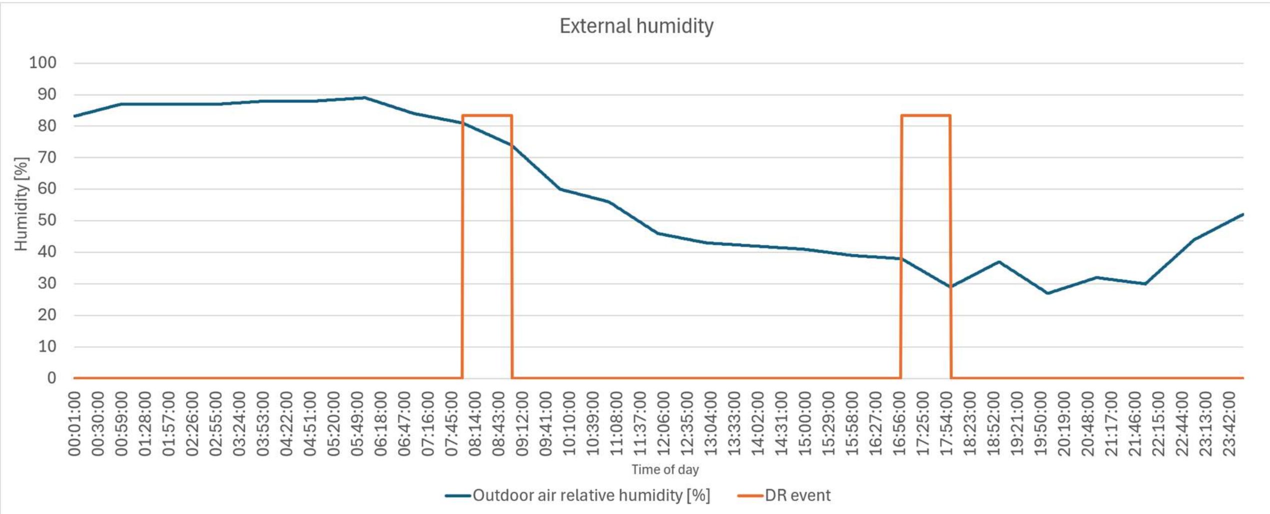

Figure 61: Summer cloudy external humidity

Both events are characterised by low solar radiation and an outside temperature of around 23–24 °C, the main difference lies in the outdoor humidity, averaging 70% during the morning event and 35% during the evening event; in the former case, this results in higher energy loads due to the need for dehumidification, as shown in the graphs in *Figures 62 and 63*, which show the cooling loads for the two reference cases.

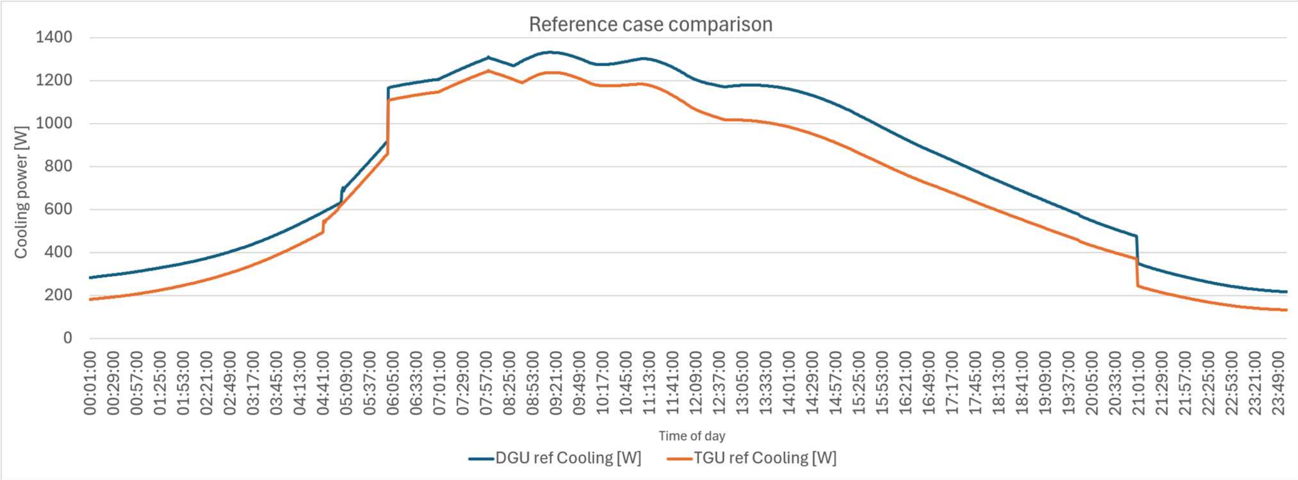

Figure 62: Summer cloudy reference case power comparison

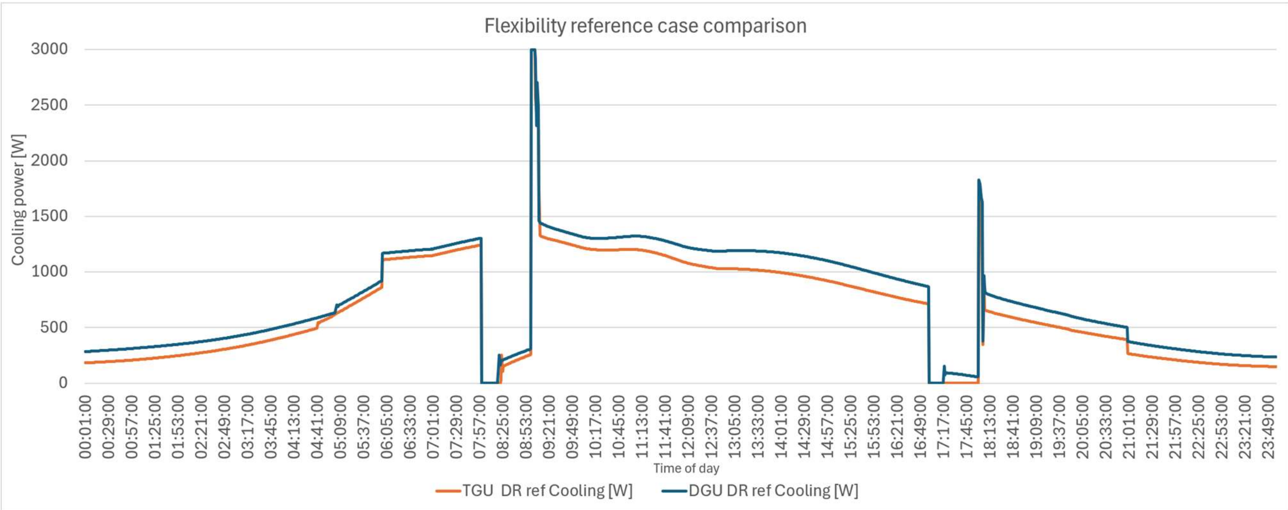

Figure 63: Summer cloudy reference case DR power comparison

The load profiles for the two scenarios in *Figure 62* follow similar trends, with a variable difference in load. During the morning event, the two reference cases in *Figure 63* have almost identical profiles; in the evening event, however, the TGU scenario shows complete autonomy.

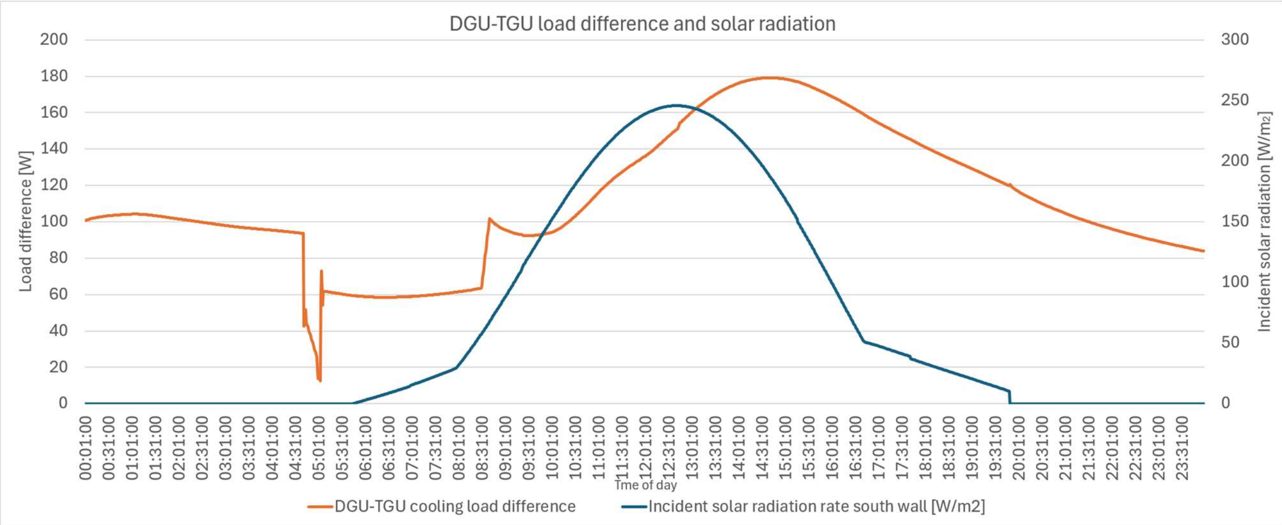

Figure 64: DGU-TGU load difference and incident solar radiation

The graph in *Figure 64* shows the trend in the load difference between the DGU and TGU cases, calculated as: $Load\ Difference = Load_{DGU} - Load_{TGU}$ and the incident solar radiation on the windows. It shows that the load difference increases during the afternoon, following a profile similar to that of solar radiation but with a 2-hour delay; this behaviour can be attributed to the difference in the SHGC factor between the two components, as discussed in section 5.1.2, thereby further motivating the differences during the evening event.

Looking at the results in *Tables 16 and 17 for the 'Summer Cloudy' case*, it is clear that, unlike the two winter scenarios discussed in the previous chapters, the differences in performance between the various technologies are minimal: as regards the morning event, when considering the Peak Shaving Capacity KPI, the difference between the worst performer and the best – PCM and DSF OAC High, respectively – is 78.9 Wh, whilst during the evening event almost all technologies manage to ensure total thermal load shedding.

Table 16: Summer cloudy morning DR event KPI results

SUMMER CLOUDY						
8:00-9:00						
CASE	Autonomy [min]	Degree of partialisation [%]	Peak shaving capacity [Wh]	Precharge energy [Wh]	Rebound energy [Wh]	DR energy balance [Wh]
DGU Ref	20	87%	1125.4	-	276.7	-848.6
TGU Ref	23	90%	1092.1	-	281.6	-810.5
DSF OAC Low	31	94%	1155.4	-	314.0	-841.4
DSF OAC High	34	96%	1164.6	-	317.3	-847.3
DSF EA	23	90%	1123.9	-	303.2	-820.7
PCM	24	90%	1085.7	-	263.2	-822.5
PCM 1H	32	94%	1124.4	1374.5	269.8	520.0
PCM 05H	31	93%	1115.6	818.1	280.1	-17.4
DB-EC	23	89%	1098.9	-	279.1	-819.9
EC	25	91%	1088.2	-	284.9	-803.3

The reference configurations (DGU Ref, TGU Ref) exhibit low autonomy (20–23 minutes) and moderate partialisation (87–90%), while their peak-shaving capacity ranges from 1092.1 to 1125.4 Wh and their rebound energy is relatively low (276.7–281.6 Wh). The DSF OAC Low and OAC High configurations give the best performance for three of the four parameters: autonomy of 31–34 minutes, degree of partialisation of 94–96% and peak shaving capacity of 1155.4–1164.6 Wh, all of which are the maximum values for the morning event. This result shows that the load reduction is greater and lasts longer when the cavity ventilation is increased (from Low to High) than in the reference cases. The rebound energy is always the largest in the data set (314.0–317.3 Wh), because the more energy that is removed during the event, the more energy is recovered.

The DSF EA configuration, however, has shorter autonomy, a lower degree of partialisation (23 minutes, 90%), and a lower peak-shaving capacity than the OAC configurations (1123.9 Wh), and a higher rebound energy than the reference cases (303.2 Wh).

The non-precharged PCM has the lowest peak-shaving capacity in the entire data set (1085.7 Wh) and the lowest rebound energy (263.2 Wh), as already observed in other scenarios, where the PCM reduces the recovery phase, irrespective of the load shift during the event. The pre-charged variants, PCM 1H and PCM 05H, have an autonomy (31–32 minutes) and a degree of partialisation (93–94 %) similar to the DSF OAC variants, with a peak shaving capacity of 1115.6–1124.4 Wh, but with significantly lower rebound energy (269.8–280.1 Wh) than the OAC Low and OAC High variants, meaning that a level of resilience similar to that of the DSF can be achieved with a lower recovery cost but with a substantial use of energy during the precooling phase.

No significant differences are observed between the electrochromic configurations (DB-EC, EC) and the reference cases across all parameters (autonomy: 23–25 minutes; degree of partialisation: 89–91%; peak shaving capacity: 1088.2–1098.9 Wh; rebound energy: 279.1–284.9 Wh).

Table 17: Summer cloudy evening DR event KPI results

SUMMER CLOUDY						
17:00-18:00						
CASE	Autonomy [min]	Degree of partialisation [%]	Peak shaving capacity [Wh]	Precharge energy [Wh]	Rebound energy [Wh]	DR energy balance [Wh]
DGU Ref	18	93%	753.1	-	124.3	-628.8
TGU Ref	60	100%	659.4	-	115.8	-543.6
DSF OAC Low	60	100%	573.6	-	99.7	-473.8
DSF OAC High	60	100%	554.9	-	95.2	-459.7
DSF EA	60	100%	612.1	-	110.8	-501.3
PCM	53	100%	683.6	-	101.1	-582.5
PCM 1H	60	100%	684.3	946.5	82.9	345.1
PCM 05H	60	100%	684.3	526.0	98.8	-59.5
DB-EC	35	99%	690.8	-	119.6	-571.3
EC	60	100%	648.9	-	114.2	-534.7

Most configurations reach maximum autonomy (equal to the duration of the entire event, 60 minutes) and have a partialisation close to or equal to 100% during the evening event. This saturation effect makes the two parameters less relevant for differentiation during this time slot and shifts the emphasis to peak-shaving capacity and rebound energy as differentiating indicators.

The opposite behaviour is observed for the reference configurations: the DGU Ref does not reach full autonomy (18 minutes, 93 %) but reaches the highest peak shaving capacity in the entire evening dataset (753.1 Wh), while the TGU Ref reaches full autonomy (60 minutes, 100 %) with a significantly lower peak shaving capacity (659.4 Wh) and lower rebound energy (115.8 Wh compared to 124.3 Wh). This indicates that the DGU Ref draws more power over a shorter period, causing internal conditions to exceed acceptable limits before the end of the event, whilst the TGU Ref, thanks to its characteristics, sustains conditions throughout the event.

All three configurations (DSF Low, OAC Low and EA) are fully autonomous (60 minutes, 100 %), but the capacity for peak shaving decreases with increasing solar control: EA 612.1 Wh, OAC Low 573.6 Wh, OAC High 554.9 Wh, the lowest value in the entire evening dataset. The order of rebound energy is the same: EA 110.8 Wh, Low 99.7 Wh, High 95.2 Wh (the lowest value of all).

The non-precharged PCM does not reach full autonomy (53 minutes), but it achieves 100% partialisation, most likely due to a really small power draw during the end of the event, and a high peak-shaving capacity among the non-precharged configurations (683.6 Wh), with a low rebound energy (101.1 Wh). The pre-charged variants, PCM 1H and PCM 05H, have the same peak shaving capacity as the non-precharged configuration, at 684.3 Wh, while the rebound energy of PCM 1H is the lowest of all (82.9 Wh), and PCM 05H is in an intermediate range (98.8 Wh). It should be noted that, although this is a very favourable performance across the four main parameters, PCM 1H still has a positive DR energy balance (345.1 Wh), meaning that the high pre-charge cost (946.5 Wh) is still disproportionate to the benefit gained.

The electrochromic configurations show different behaviour: EC is fully autonomous (60 minutes, 100%) with a peak shaving capacity of 648.9 Wh, while DB-EC is not (35 minutes, 99%) although it has a higher peak shaving capacity (690.8 Wh) and the highest rebound energy among the non-reference configurations (119.6 Wh), a behaviour similar to that observed for the DGU Ref.

By comparing the load profiles from simulations using the DSF system with those of the TGU reference case, which has the same layer configuration, it becomes clear why the OAC mode delivers better performance and why a higher airflow rate is beneficial.

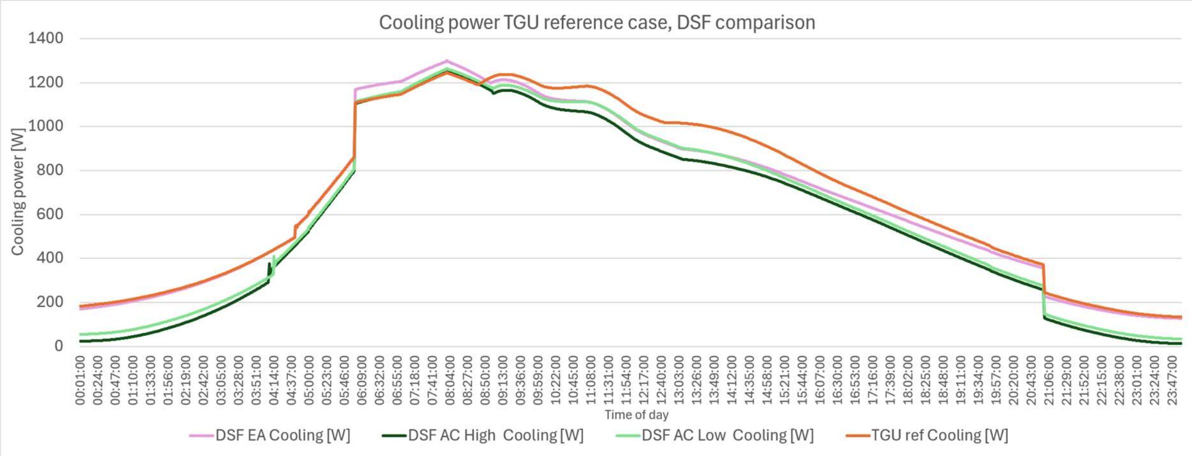

Figure 65: Cooling load TGU reference case, DSF comparison

As shown in *Figure 65*, the DSF OAC High system performs slightly better throughout the day compared with the other scenarios, consistently exhibiting a lower load; however, during the evening event, when all the technologies shown provide full load shedding, it delivers a lower Peak Shaving Capacity value due to its lower base consumption.

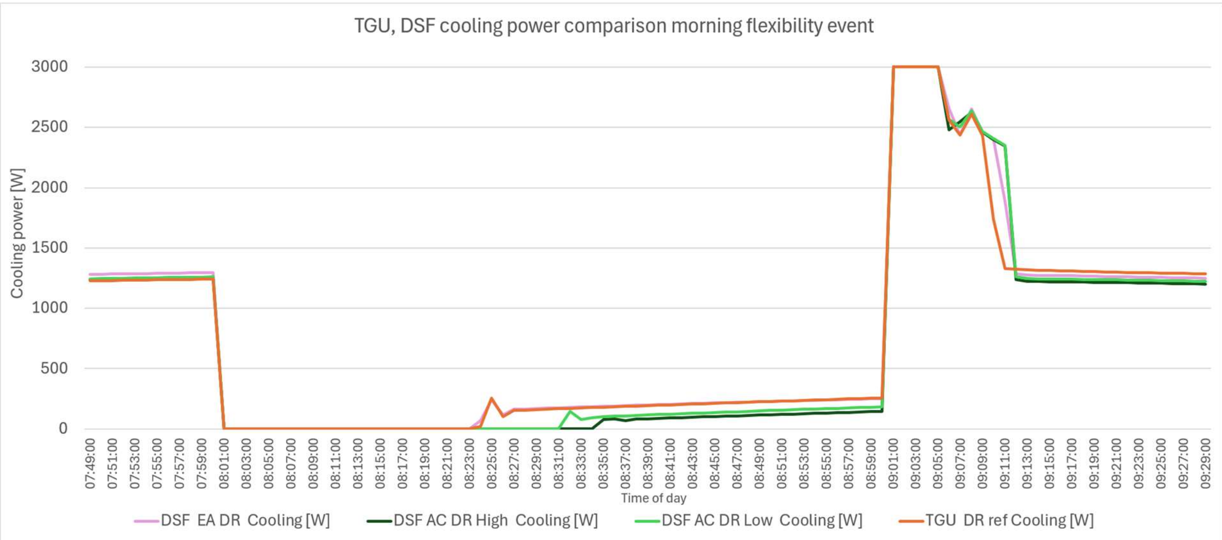

Figure 66: TGU, DSF cooling power morning DR event comparison

Figure 66 shows that, consistent with the results for the no-DR case, the DSF AC cases perform slightly better than the others.

By analysing the behaviour observed in the EC and DB-EC simulations, we can gain a better understanding of how the two devices work and the difference in their results.

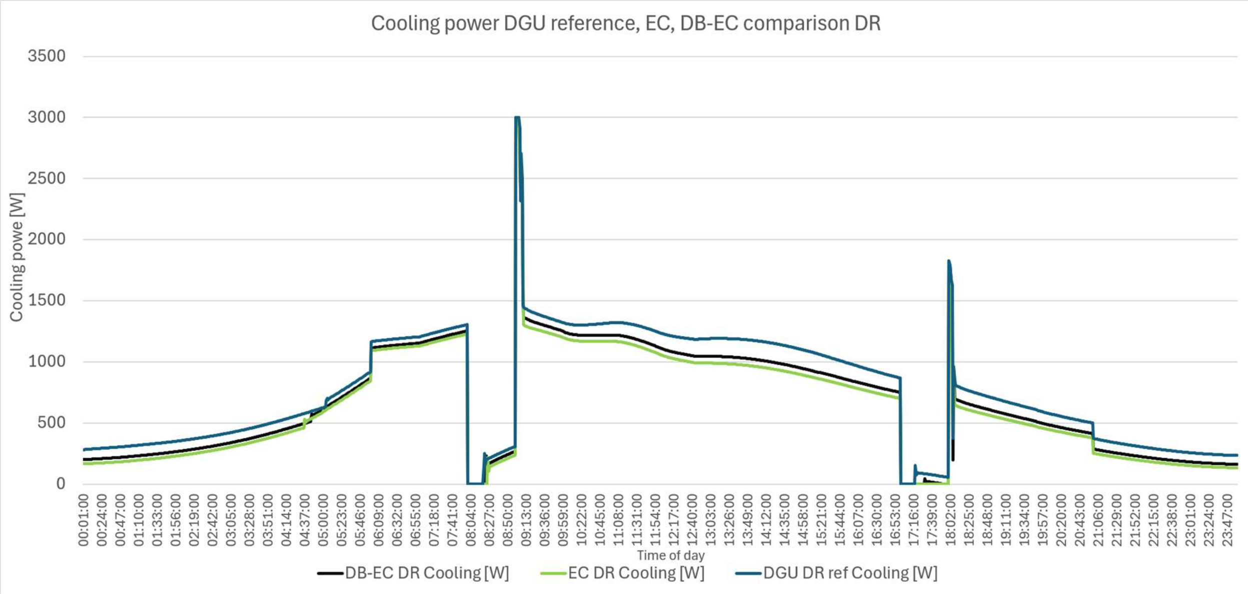

Figure 67: Summer clear cooling power DGU, EC, DB-EC case DR comparison

A comparison with the results of the DGU reference case shows an improvement in total energy consumption and, as shown in *Tables 16 and 17*, in the autonomy. This is due to the control of direct solar radiation made possible by this technology.

The graph below shows the amount of power exchanged between the indoor and outdoor environments through the transparent openings, calculated in a similar way to the FTHT parameter but without taking into account the contribution of mechanical ventilation in the room, as this is not a factor that can be controlled by this technology, unlike in the DSF case.

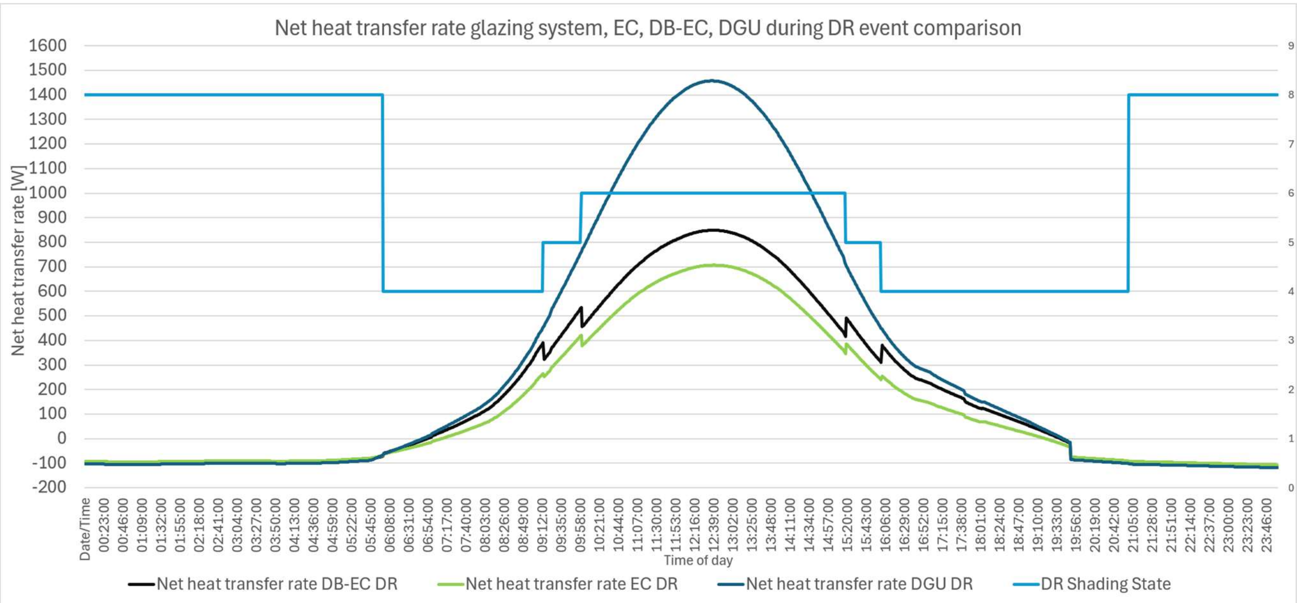

Figure 68: Net heat transfer glazing system, DGU, EC, DB-EC

As shown, the incoming energy gain in the DGU scenario during the day is greater than in the other two scenarios due to the lack of control over the transmitted direct solar radiation parameter. In the two simulations using electrochromic glazing, the total contribution is much lower; there are also some steps in the curves, coinciding with the moments when the control system changes the glazing state in response to variations in direct solar radiation.

In the DB-EC case, the total energy gain during daylight hours is consistently greater than that attributed to the EC case; this is linked to the SHGC factor characterising the two systems, which is higher in the DB-EC case even in the four darkest states featured in these simulations, motivating the difference in the results.

Finally, the PCM cases, despite the additional energy consumed during the pre-cooling period, do not demonstrate significantly better performance than the other cases; the main advantage of using this technology under these climatic conditions appears to be lower rebound energy compared with the other cases, observed in the PCM case without pre-cooling for the morning event and in the PCM 1H case for the evening event, respectively.

5.1.4. Summer clear

The final climate type analysed is classified as 'Summer Clear'; this represents the most severe summer conditions, with high outdoor temperatures and intense solar radiation.

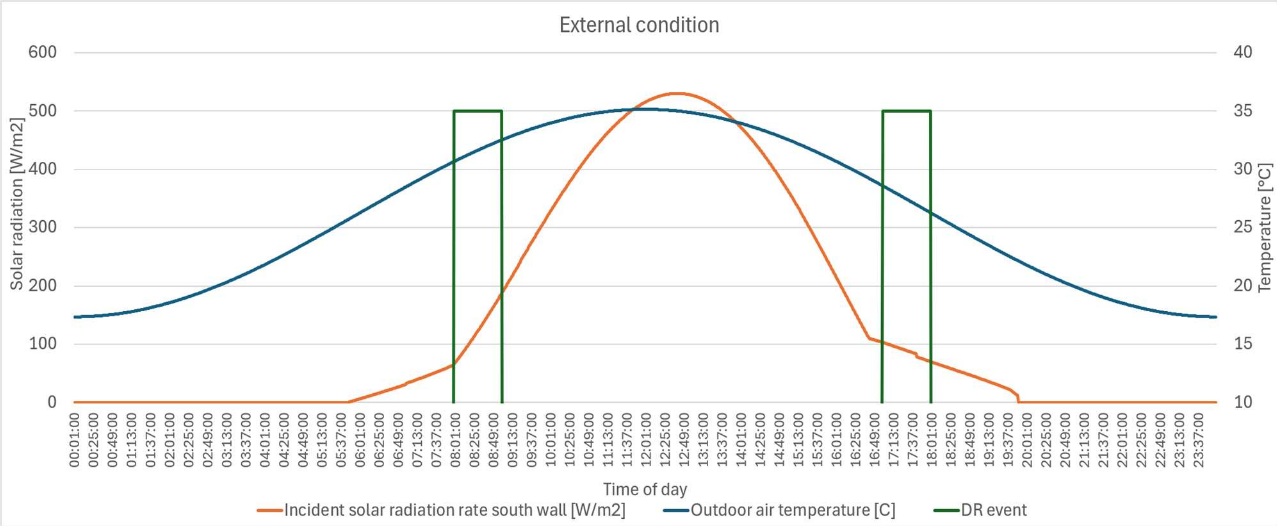

Figure 69: Summer clear external temperature and solar radiation

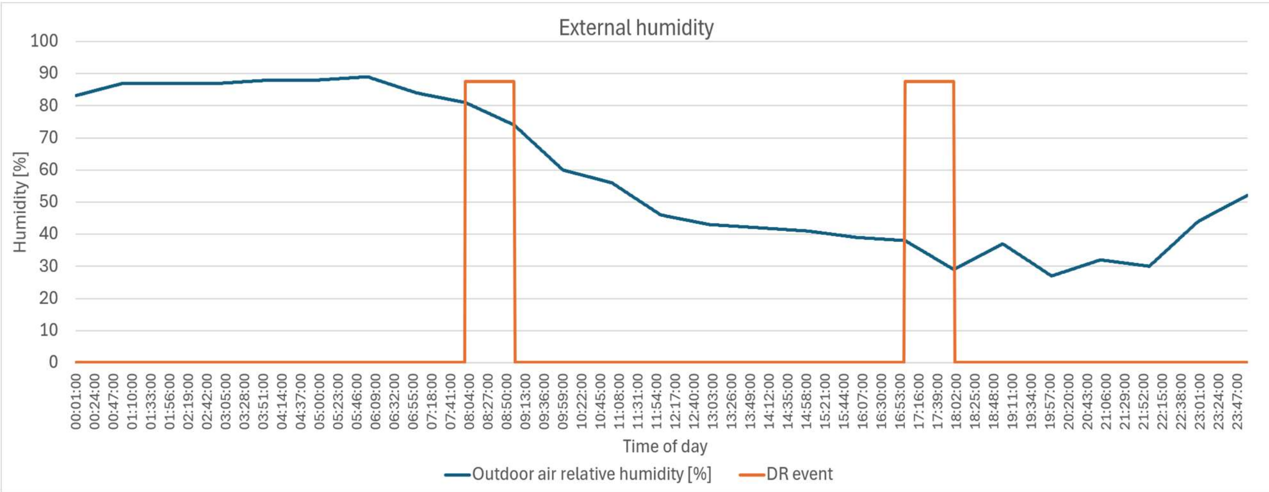

Figure 70: Summer Clear external humidity

The morning event is characterised by a temperature of 32 °C, solar radiation rising rapidly from 100 to 200 W/m² and a humidity of 75%; the evening scenario, on the other hand, features milder conditions, with an average temperature of 27 °C, a decreasing solar radiation lower than 100 W/m² and a humidity of 35%.

The thermal loads for the two reference cases are shown below, compared with those for the same scenarios without the shading system.

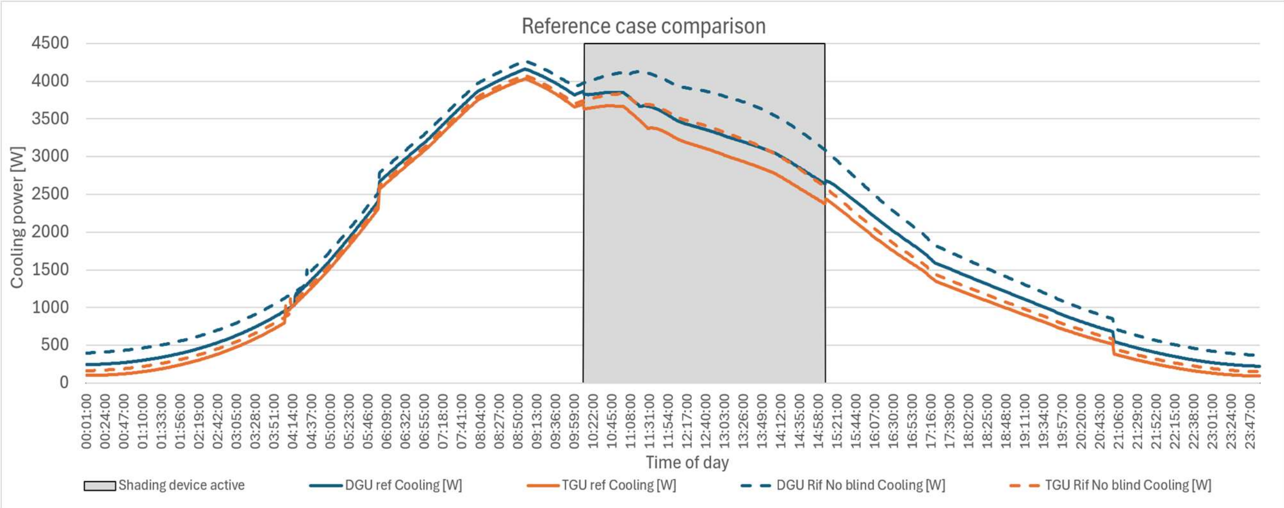

Figure 71: Summer clear reference cases power comparison

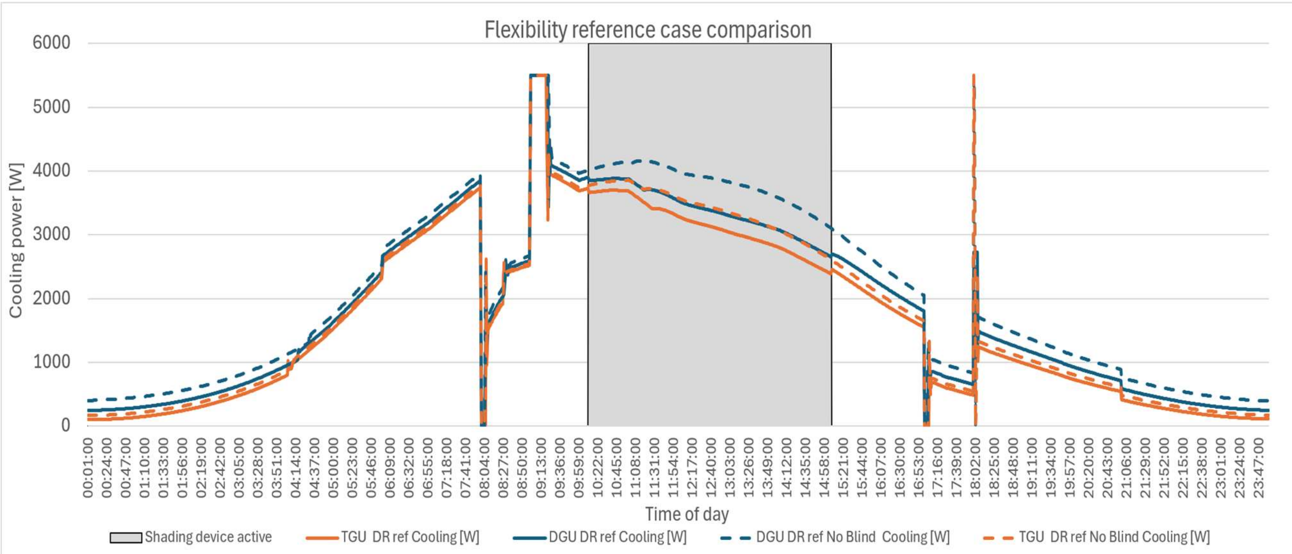

Figure 72: Summer clear reference case DR power comparison

The graphs in *Figures 71 and 72* show the trends in cooling power for the DGU and TGU reference cases, both with the shading system not in use and with it operating normally. The shape of the curves is similar to that of the 'Summer Cloudy' simulation results, but with values that are, on average, higher. The peak in energy demand occurs between 7:00 and 12:00, mainly due to the need for dehumidification and the rise in temperature and solar radiation. From 11:30 onwards, outdoor conditions no longer impose a dehumidification load on the system; as a result, the cooling load declines steadily. The DGU case without shading deviates from this behaviour: due to the high SHGC of this component, it is more significantly affected by the direct solar heat load; as a result, a particularly high heat load is observed in the middle of the day.

Energy behaviour during DR events shows little variation between the four cases analysed. During the afternoon event, particularly in the DGU case without shading, the high solar loads accumulated during the day have an impact, resulting in a higher load profile compared with the other cases.

Table 18: Summer clear morning DR event KPI results

SUMMER CLEAR						
8:00-9:00						
CASE	Autonomy [min]	Degree of partialisation [%]	Peak shaving capacity [Wh]	Precharge energy [Wh]	Rebound energy [Wh]	DR energy balance [Wh]
DGU Ref	5	50%	1999.0	-	529.4	-1469.6
DGU Ref No Blind	5	49%	2023.7	-	522.9	-1500.8
TGU Ref	5	50%	1943.5	-	533.7	-1409.8
TGU Ref No Blind	5	50%	1964.1	-	532.4	-1431.7
DSF OAC Low	6	49%	1923.7	-	526.1	-1397.6
DSF OAC High	6	49%	1935.8	-	526.0	-1409.8
DSF EA	6	49%	1911.7	-	534.0	-1377.6
PCM	6	50%	1915.2	-	385.3	-1529.9
PCM 1H	9	54%	2054.1	1223.0	441.5	-389.6
PCM 05H	9	53%	2040.9	670.1	451.1	-919.8
DB-EC	5	50%	1962.4	-	533.1	-1429.3
EC	6	50%	1948.6	-	534.2	-1414.5

The reference configurations (DGU Ref, TGU Ref, and their respective No Blind variants) exhibit the highest peak-shaving capacity in the dataset, following PCM 1H (1923.7–2023.7 Wh), alongside limited autonomy (5 minutes) and a degree of partialisation that stabilises at around 49–50%. This behaviour indicates that although these configurations remove a significant absolute amount of energy during the event, they cannot sustain this load reduction for a prolonged period before internal conditions exceed acceptable limits. Consequently, the rebound energy is the highest across the entire dataset (522.9–534.0 Wh), indicating that the substantial energy removed during the event must be largely replenished during the recovery phase.

The dynamic envelope solutions (DSF OAC Low, DSF OAC High, DSF EA) exhibit a peak shaving capacity slightly lower than the reference cases (1911.7–1935.8 Wh) but a slightly higher autonomy (6 minutes), whilst the degree of partialisation remains virtually unchanged (49%). This suggests that, under the combined load of solar radiation and dehumidification typical of the morning, the dynamic solar control strategy does not substantially alter the magnitude of the achievable load reduction, but allows it to be sustained for a marginally longer period. Rebound energy also remains high, comparable to the reference cases (526.0–534.0 Wh), indicating that the autonomy benefit does not translate into a significant reduction in the recovery burden.

The PCM, in the non-precharged configuration, stands out clearly for its rebound energy, the lowest in the entire dataset (200.4 Wh), whilst maintaining a peak shaving capacity (1915.2 Wh) and autonomy (6 minutes) in line with the other non-precharged technologies. This suggests that the phase-change material inherently mitigates the recovery phase, regardless of the energy invested in precharging. The pre-charged variants, PCM 1H and PCM 05H, on the other hand, exhibit the best absolute performance across the entire dataset in terms of autonomy (9 minutes) and degree of partialisation (53–54%), as well as the highest peak shaving capacity (2040.9–2054.1 Wh); however, the rebound energy is lower than in the reference cases (441.5–451.1 Wh) but higher than that of the non-precharged PCM, indicating that precharging improves resilience during the event without completely eliminating the recovery burden.

The electrochromic configurations (DB-EC, EC) closely replicate the behaviour of the reference cases across all four parameters (autonomy 5–6 minutes, degree of partialisation 50%, peak shaving capacity 1948.6–1962.4 Wh, rebound energy 533.1–534.2 Wh), showing no significant difference compared with the static envelope under the morning load.

Table 19: Summer clear evening DR event KPI results

SUMMER CLEAR						
17:00-18:00						
CASE	Autonomy [min]	Degree of partialisation [%]	Peak shaving capacity [Wh]	Precharge energy [Wh]	Rebound energy [Wh]	DR energy balance [Wh]
DGU Ref	5	56%	879.2	-	165.5	-713.6
DGU Ref No Blind	4	51%	924.7	-	171.3	-753.4
TGU Ref	6	60%	808.4	-	154.4	-654.0
TGU Ref No Blind	5	59%	836.9	-	158.9	-678.0
DSF OAC Low	7	63%	760.4	-	144.2	-616.1
DSF OAC High	7	64%	765.7	-	144.6	-621.1
DSF EA	7	62%	747.3	-	145.9	-601.4
PCM	6	62%	808.4	-	130.9	-677.5
PCM 1H	10	67%	881.8	1000.3	94.9	213.4
PCM 05H	10	66%	869.3	552.2	111.0	-206.1
DB-EC	6	60%	827.1	-	157.0	-670.1
EC	6	61%	814.8	-	155.0	-659.8

The overall magnitude of all KPIs in *Table 19*, except for Degree of partialisation, is significantly lower than in the morning due to the lower amount of solar radiation, the lack of dehumidification load, and slightly lower outdoor temperatures. In the reference group, the ranking of the DR energy balance is the same as in the morning, with DGU Ref No Blind (-753.4 Wh) and DGU Ref (-713.6 Wh) again having the best energy balance, although not the best autonomy.

The dynamic envelope solutions (DSF OAC Low, DSF OAC High, DSF EA) swap their relative ranking with the reference group: they are now the most autonomous (7 minutes) and the most partialized (62-64%) of all non-PCM solutions, but they are among the least favourable on DR energy balance (-601.4 to -621.1 Wh). This is consistent with the morning event and suggests a true, repeatable trade-off for this technology: DSF systems perform well at maintaining acceptable indoor conditions during the event, but at a relatively lower absolute load.

The PCM-based cases show the same split as in the morning, but the difference is increased for the precharged versions. The plain PCM case performs well (-677.5 Wh), close to the reference cases, demonstrating its ability to maintain a good energy balance without a precharge phase. Although PCM 1H has the highest autonomy (10 minutes) and degree of partialisation (67%) in the whole dataset, it has the highest DR energy balance (+213.4 Wh): the energy used during precharge (1000.3 Wh) is not compensated by the small amount of energy that can be shifted during the DR event. The PCM 05H is still energy-negative, but not as heavily penalised (-206.1 Wh), indicating that the precharge time has a significant impact on this imbalance, but does not completely remove it. The energy difference between the electrochromic cases (DB-EC, EC) and the reference envelopes is again very close, at -670.1 Wh and -659.8 Wh, respectively.

The thermal storage capacity of pre-charged PCMs appears to be the most effective technology in terms of range and degree of partialisation, in both events. DSF solutions, on the other hand, exhibit behaviour that depends on the load intensity: in the morning, under high load, they are indistinguishable from the reference cases on all four parameters; in the evening, under a lower load, they emerge as the most effective technologies for maintaining high autonomy and partialisation, precisely because the lower absolute load also proportionally reduces rebound energy. In both cases, the only advantage of the PCM without precooling is its low rebound energy, which appears to be inherent in the material and independent of seasonal or hourly load.

The graph below shows the trend in cooling power for the DGU, PCM 1H and 05H scenarios during the morning event.

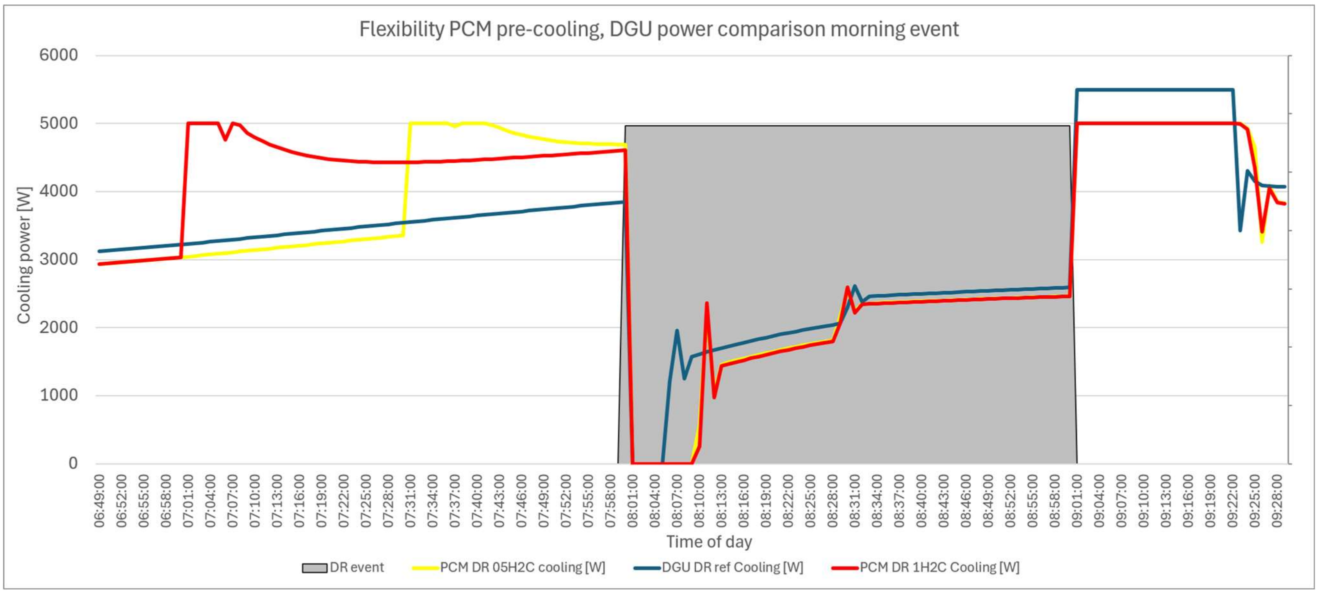

Figure 73: DGU and PCM 1H, 05H morning DR event cooling power trends

As shown in *Figure 73*, the profiles of the two PCM cases during the event are almost identical, suggesting that the longer pre-cooling time did not yield any significant improvements. By contrast, a comparison with the DGU case highlights the difference in autonomy and shows that throughout the event, the PCM cases exhibit lower energy consumption.

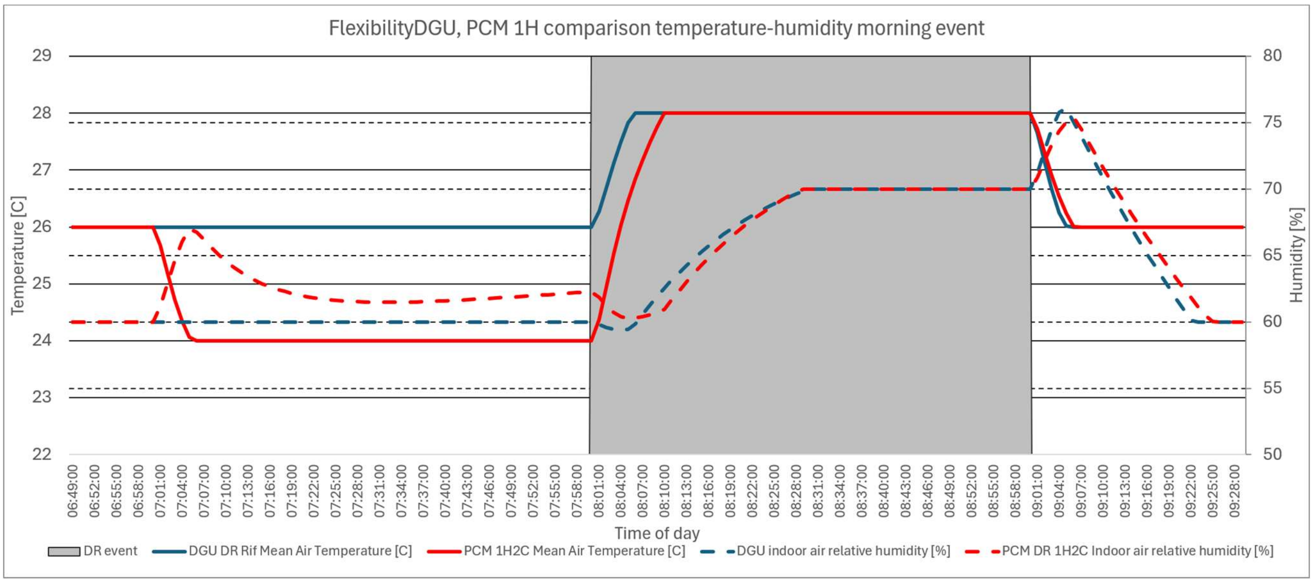

Figure 74: Temperature and relative humidity DGU, PCM 1H morning DR comparison

The comparison in *Figure 74*, which shows the indoor air temperature and relative humidity for the DGU and PCM 1H scenarios, demonstrates that in both cases, the Autonomy is limited by temperature, which rapidly reaches the 28 °C limit. Thirty minutes after the start of the event, in both cases, the humidity also reaches the 70% limit; this explains the second step visible in the power profiles shown in *Figure 73*.

The evening event is characterised by a lower energy load; the system is therefore able to ensure a higher degree of partialisation.

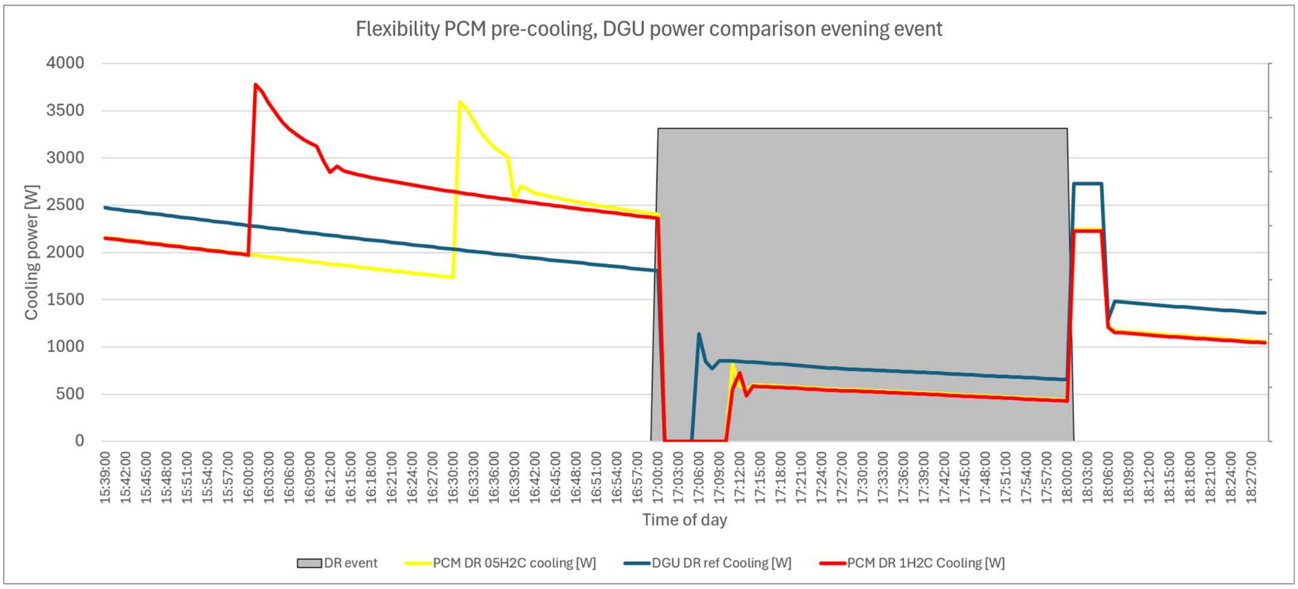

Figure 75: DGU and PCM 1H, 05H evening DR event cooling power trends

As shown in *Figure 75*, the cooling loads during the evening scenario are lower than those in the morning scenario shown in *Figure 73*; similarly, the PCM scenarios perform better than the DGU, with lower loads and greater autonomy. Once again, no benefits are observed in the scenario with greater pre-cooling.

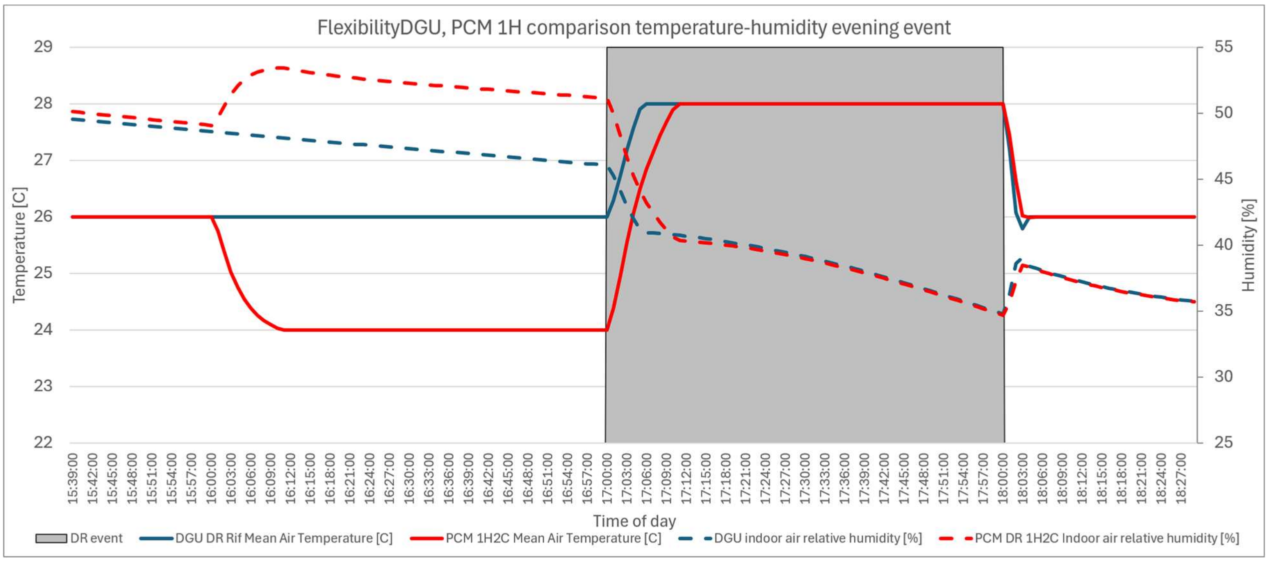

Figure 76: Temperature and relative humidity DGU, PCM 1H evening DR comparison

During the evening, as shown in *Figure 76*, the humidity falls below the setpoint and therefore does not place a load on the system.

An analysis of the results obtained from simulations using electrochromic glass shows that the results differ only slightly from the reference cases using shading systems, the greatest difference amongst the four cases is observed in the DGU case during the evening period, where the degree of partialisation is 4% lower than in the TGU and DB-EC cases and 5% lower than in the EC case, whilst the peak shaving capacity is higher; this is due to the higher energy consumption associated with this reference case, as shown in *Figure 77.*

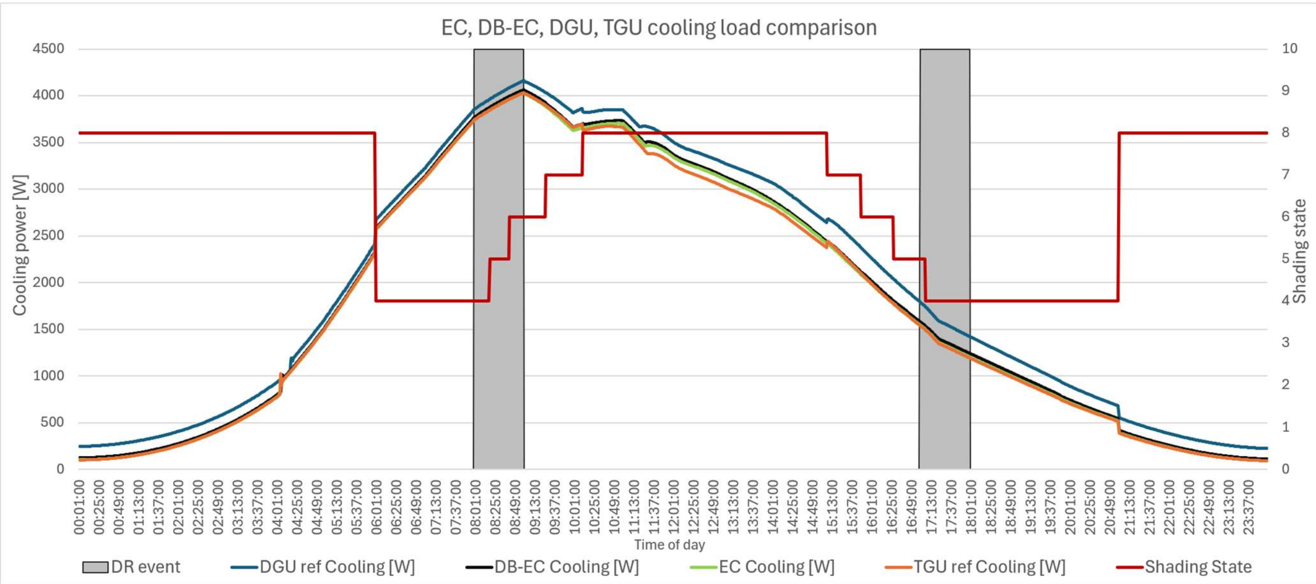

Figure 77: EC, DB-EC, DGU, TGU cooling load comparison

The difference in load between the four cases is due to the difference in energy exchange between the exterior and the interior environment through the glazed components; this depends on the shading control for the electrochromic glazing and on the use of shading elements for the DGU and TGU reference cases, as shown in *Figure 78* below.

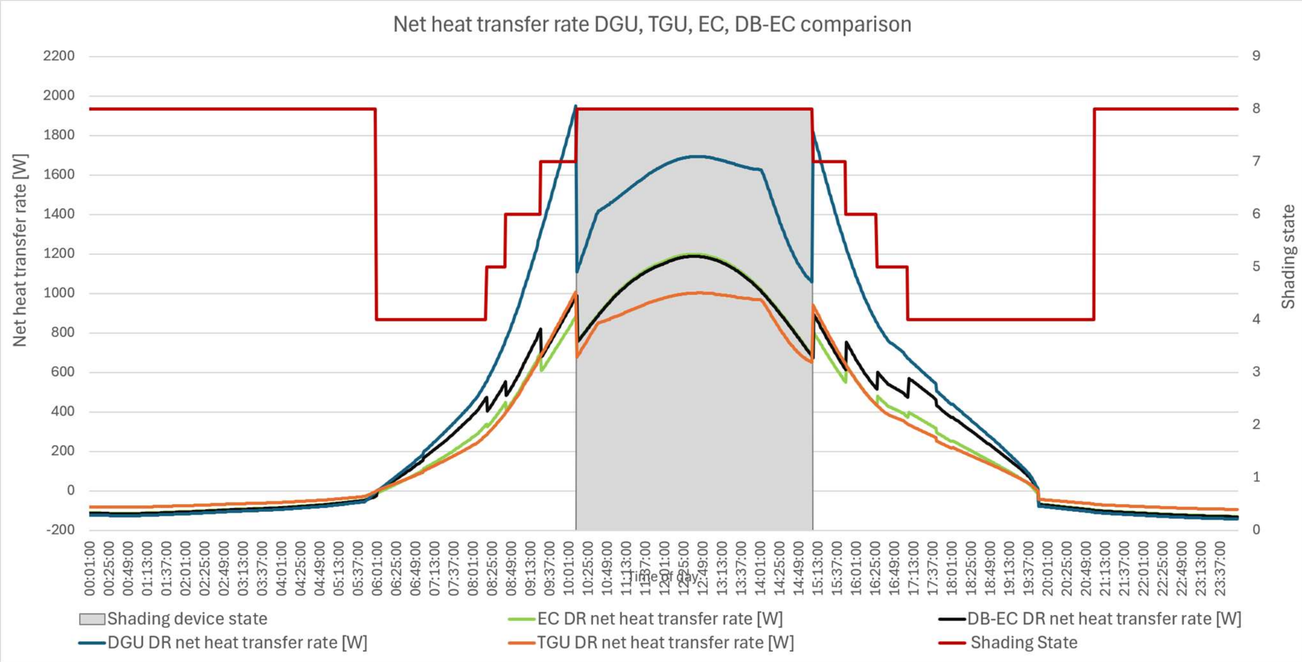

Figure 78: Net heat transfer rate DGU, TGU, EC, DB-EC comparison

The graph clearly shows how the DGU case is more affected by the external thermal load, due both to the contribution of direct radiation – mitigated by the shading element – and to the temperature. The TGU case, on the other hand, given its low SHGC value, is the least affected by external loads once the shading system is activated, thus demonstrating performance on a par with electrochromic systems in both total energy consumption and DR events.

Finally, when assessing the DSF system's results across its various modes, the three cases yield almost identical results for both events. For the morning scenario, the DSF system performs worst, with low levels of degree of partialisation and peak shaving capacity; for the evening scenario, good values for degree of partialisation are obtained, higher than those for both the baseline cases and the electrochromic glazing, whilst the peak shaving capacity is lower than in all other cases.

An analysis of the consumption profiles provides a better understanding of the reasons behind the results obtained.

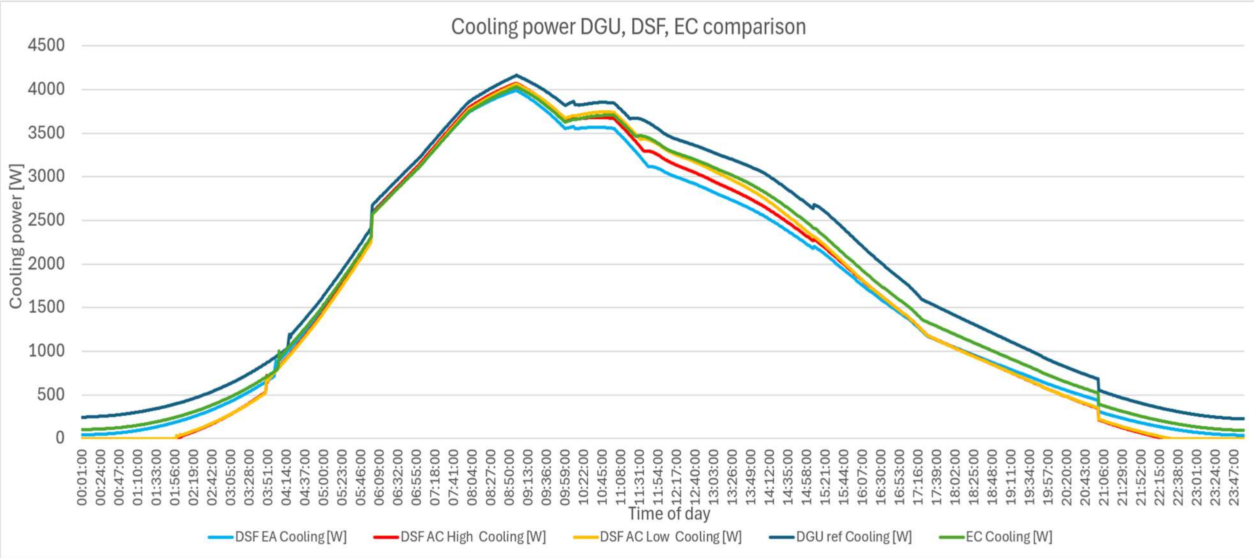

Figure 79: Cooling power DGU, DSF, EC comparison

Figure 79 shows the results of the DGU, EC and DSF simulations for the three different summer usage scenarios. In the hours leading up to the peak in energy consumption, identified at 9.00 am, all consumption profiles are almost identical; the greatest differences are observed between 11:00 am and 3:30 pm, coinciding with the hours of maximum solar exposure but not with either of the two DR events; during this period, the EA mode yields the lowest consumption profile. During the evening hours, the DSF consumption profiles converge once again, whilst remaining lower than those of DGU and EC.

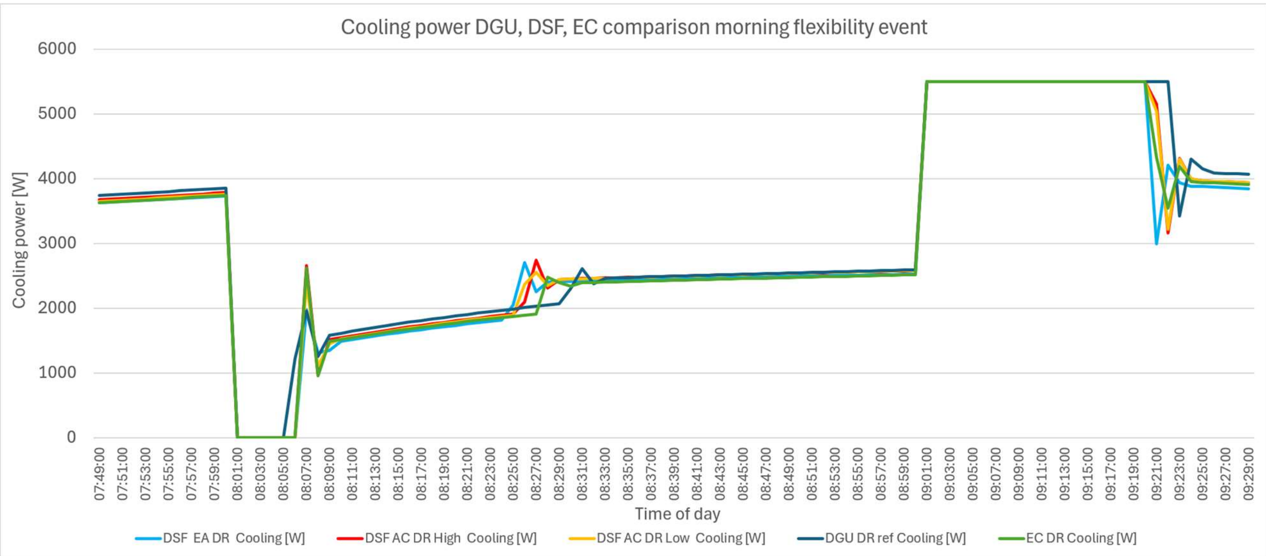

Figure 80: Cooling power DGU, DSF, EC comparison morning DR

In line with the morning consumption patterns when no DR event occurred, no significant differences were observed during the morning event.

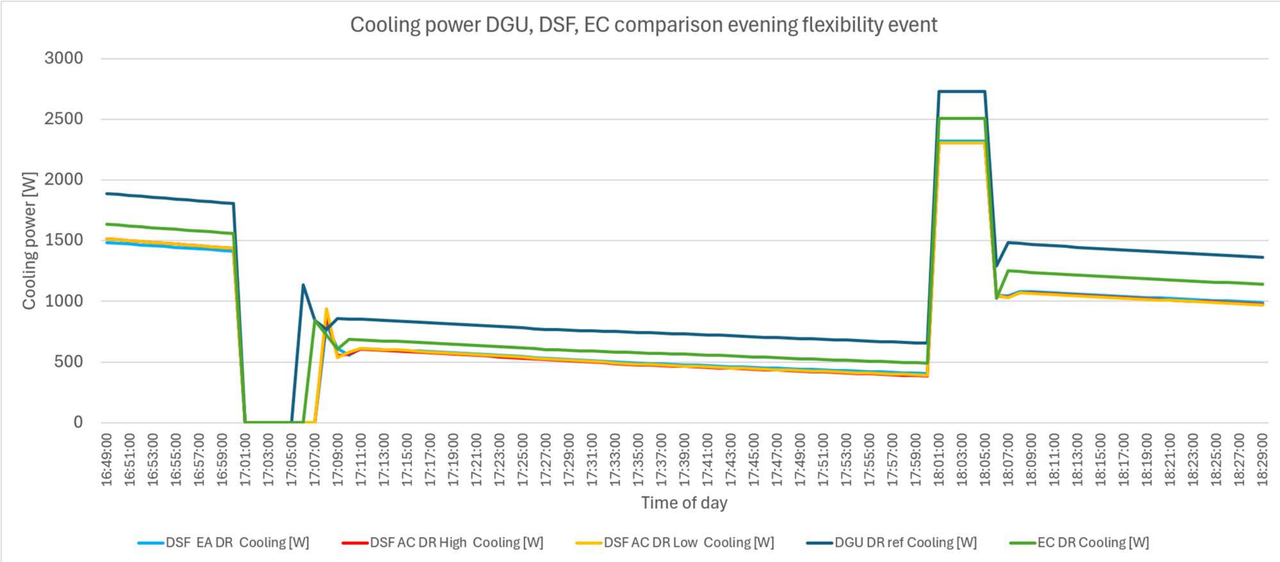

Figure 81: Cooling power DGU, DSF, EC comparison evening DR

Conversely, during the evening event, the consumption profiles associated with the use of DSF across all three modes are lower than in the EC scenario and, above all, in the DGU scenario, both during the event and in the subsequent recovery period.

In conclusion, it appears that the DSF system improves the room's thermal performance, increasing Autonomy and the Degree of Partialisation; however, whilst reducing total energy consumption even during normal use, it limits Peak Shaving Capacity.

5.1.5. Conclusions on the results

The analysis presented in this chapter has highlighted the substantial differences between fundamentally distinct systems and demonstrated that each solution provides flexibility through different physical mechanisms. Therefore, there is no single best technology, as its performance will vary depending on the climatic conditions, the nature of the demand response event and the performance indicator used. This highlights the need to use a combination of complementary KPIs to give a full picture of building energy flexibility, since technologies that are most effective on one KPI may not be most effective on another.

Considering the wide range of climatic conditions analysed, PCM materials generally showed the greatest potential for increasing flexibility under the most severe boundary conditions, particularly in the Winter Cloudy and Summer Clear scenarios. They were able to obtain the highest values of autonomy, degree of partialisation, and, in several cases, peak-shaving capacity when combined with pre-conditioning strategies. These benefits, however, need to be weighed against the high energy required during the pre-conditioning phase, which was about 7-9 times higher than the additional peak-shaving benefit obtained compared to the same cases without pre-conditioning. This imbalance is due to several factors, including numerical calculation errors discussed in Section 4.9.1, limited thermal interaction between the indoor air and the PCM-containing elements, and the use of non-optimal melting and solidification temperature ranges.

The results also showed that PCM solutions without pre-conditioning may still be a viable compromise in certain operating conditions. They tend to offer less autonomy than pre-conditioned cases but can still significantly reduce rebound energy and improve the overall energy balance, resulting in more positive DR energy balance values. This behaviour also highlights that flexibility cannot be measured by a single indicator and further emphasises the importance of a multi-KPI evaluation framework that captures the various aspects of technology performance.

The results of the simulations using electrochromic glazing highlighted differences in heat gain into the room, depending on the glazing's SHGC across its various states. Under summer conditions, where controlling solar gains is essential to controlling indoor temperatures, electrochromic glazing performed as well as selective low-SHGC glazing with external shading systems. However, the results are affected by the lack of integrated lighting control, particularly for DB-EC glazing, which is primarily used to achieve high visible-light transmittance while reducing near-infrared radiation. Coordinated control of artificial lighting and the related electricity consumption would then enable a more comprehensive quantification of the overall benefits of this technology.

The analyses also revealed that the length of flexibility events depends not only on indoor air temperature. In a few cases, the limiting factor was indoor relative humidity, highlighting the strong effect of latent loads on achievable autonomy. This emphasises the need to consider both temperature and humidity requirements when assessing the flexibility potential of envelope technologies.

Lastly, the simulations showed that the flexibility offered by the DSF system depends heavily on the control strategy used, not only on the technology itself. The four operating modes enable the façade to respond to varying climatic conditions, but they are closely tied to solar availability and the timing of the demand-response event. The Supply Air (SA) mode was found to be less suitable in the Winter Cloudy scenario, as the lack of solar radiation meant that heat recovery within the cavity was ineffective, whereas the Thermal Buffer (TB) configuration was more suitable. In contrast, the SA mode was beneficial when solar gains were high, and the TB mode was beneficial when solar gains were low, in the case of Winter Clear. The results show that the flexibility potential of DSF systems is inherently control-dependent and can only be realised through the right match between operating mode, weather conditions, and demand response event characteristics.

6 CONCLUSIONS AND FUTURE WORK

As the energy sector moves towards a more sustainable and resilient system, buildings are becoming more active participants in the electricity grid by integrating renewable energy sources. In this context, building energy flexibility has become a major concept, allowing buildings to respond to external signals by adjusting their energy demand while maintaining a satisfactory indoor environment. Advanced Building Envelopes (ABEs) are one of many strategies that can improve building flexibility, as they can affect heat transfer, solar gains, and thermal storage without relying solely on traditional HVAC systems. Although research has been conducted on each envelope technology, there is no common assessment framework that enables an objective comparison of the flexibility potential of each technology under consistent operating conditions.

This thesis aims to address this research gap by developing and applying a general methodology to assess and compare Advanced Building Envelope technologies in terms of building energy flexibility. Three representative technologies: Double Skin Façades (DSFs), Phase Change Materials (PCMs) and Electrochromic (EC) glazing, were analysed under the same boundary conditions, demand response events and performance indicators in a standardised BESTEST room using dynamic simulations in EnergyPlus. Moreover, a systematic approach was proposed to establish standardised climatic boundary conditions that represent various European climates, enabling flexible assessments under similar environmental conditions while maintaining the representativeness of each climate.

The first research question examined whether the flexibility potential of various building envelope technologies could be evaluated and compared consistently. The proposed framework was successfully applied to demonstrate that technologies with fundamentally different operating principles can be evaluated within the same analytical framework, using standardised simulation conditions, flexibility events, and a common set of Key Performance Indicators. The methodology focuses not on the specific characteristics of each technology, but on each technology's actual contribution to demand-side flexibility and can be extended to other passive and active envelope technologies. This is one of the primary contributions of the present work: a repeatable procedure for future comparative studies and technology benchmarking.

The second research question concerned the definition of standardised climatic boundary conditions that enable a generalisable assessment of building energy flexibility. The methodology developed in this work identified representative weather periods that preserve the climatic characteristics of the selected locations and provide similar operating conditions across different simulations. This is an important part of the thesis because it minimises the need to choose arbitrary weather conditions for flexibility assessments and enhances the repeatability and comparability of future studies. The proposed procedure enables objective comparison of different technologies and helps develop more robust and transferable methodologies for assessing building energy flexibility under consistent climatic boundary conditions.

The third research question focused on developing suitable Key Performance Indicators to measure the flexibility of services offered by Advanced Building Envelope technologies. The proposed set of KPIs was found to be effective at capturing various aspects of flexibility performance, such as peak demand reduction, load shifting and overall energy use. These indicators enabled a comprehensive evaluation of technologies that operate in various physical ways and demonstrated their suitability for comparative assessments within a common framework.

The outcomes of the proposed KPI set revealed substantial variations in the size of the flexibility potential and in the way flexibility is provided. In severe climatic conditions, PCMs had the highest flexibility potential among the analysed technologies due to their latent heat storage capacity and the ability to release the stored thermal energy during the demand response period. This behaviour, however, depends on an effective preconditioning phase that requires an energy investment before the flexibility event. Therefore, the overall effectiveness of PCM systems is related not only to the energy shifted during the event but also to the additional energy required to charge the thermal storage.

Double Skin Façades were found to be highly adaptable systems that can provide significant flexibility when suitable control strategies are used. Their performance was found to be highly sensitive to climatic conditions, operating modes, and control logic, reflecting the complex interactions among solar radiation, cavity ventilation, and heat transfer processes. While their flexibility potential was not always optimal, DSFs were able to deliver a range of flexibility services across various climates, emphasising the need for optimised control strategies to maximise the flexibility services they can deliver.

The contribution of electrochromic glazing to building energy flexibility was relatively small in the scenarios analysed. Dynamic solar control reduced cooling loads and improved overall energy efficiency, but its ability to shift loads or reduce demand during flexibility events was less than that of the other technologies. However, the results do not reflect the limitations of electrochromic technologies; rather, they indicate that the main advantages of these technologies are related to solar gain control, visual comfort, and energy efficiency. They could be further improved by integrating with advanced lighting control systems, predictive control methods, and broader building energy management strategies.

In general, the results show that no single envelope technology is optimal under all operating conditions. Rather, each solution has its own set of benefits for the targeted flexibility service, the climatic context, and the control strategy. Therefore, the choice of an Advanced Building Envelope should not be based solely on energy performance metrics but should also consider the desired flexibility goals and the anticipated relationship between the building and the energy system. The methodology presented in this work offers a practical approach to assist this decision-making process by allowing direct and objective comparisons of different technologies under the same assessment conditions.

Although good results have been achieved, some limitations should be noted. The analyses were conducted on the BESTEST single-zone building, which is commonly used in comparative simulation studies, but does not fully capture the complexity of real buildings with multiple thermal zones, occupant interactions and heterogeneous operating schedules. Furthermore, the Ideal Loads Air System enabled the separation of the effect of the envelope technologies from the HVAC system characteristics, but ignored the dynamic behaviour and operational limitations of actual heating and cooling systems. The flexibility events analysed in this study were also constrained to a set of one-hour demand response events and a set of control strategies, whereas real grid services may have variable durations, different activation frequencies, and more complex control requirements. Lastly, there are some limitations in the numerical models used in EnergyPlus, particularly when modelling PCM behaviour with the Conduction Finite Difference (CondFD) algorithm, which may affect predictions of thermal response under certain operating conditions.

Further research should also explore flexibility events with varying durations and activation frequencies and experimentally test the proposed methodology and simulated flexibility performance; such testing would further reinforce the applicability of the presented framework and facilitate its use in real building design and operation.

In future work, it will be necessary to adjust certain simulation and result measurement parameters.

The high ventilation rate imposed on the room during this work meant that most of the load on the air-conditioning system was due to regulating the humidity and temperature of the ventilation air, thereby limiting the contribution of the building envelope elements. Furthermore, the lack of a KPI measuring the total energy consumed by the system during the event – rather than solely the difference measured against a reference scenario (DR energy balance) – meant that, in some cases, technologies that resulted in higher energy consumption during simulations without DR events could be identified as the best choices, as they presented the highest values for peak shaving capacity and/or DR energy balance. This aspect could be advantageous for an energy provider assessing which buildings to include in DR programmes, but it limits the scope for evaluation when the objective is to choose which technology or control method to apply.

Finally, this thesis shows that Advanced Building Envelopes can contribute to building energy flexibility, but with a strong dependency on the physical mechanisms, climatic conditions and control strategies. Most significantly, the work presents a comprehensive, technology-independent approach for assessing and comparing various envelope solutions under uniform boundary conditions. The proposed framework is a valuable tool for future research on building energy flexibility and a strong foundation for developing envelope technologies that can contribute to increasingly flexible, resilient, and sustainable energy systems.

BIBLIOGRAPHY

[1] "The Paris Agreement." Accessed: May 19, 2026. [Online]. Available: https://unfccc.int/process-and-meetings/the-paris-agreement

[2] "The Eurepean Green Deal." Accessed: May 19, 2026. [Online]. Available: https://commission.europa.eu/strategy-and-policy/priorities-2019-2024/european-green-deal_en

[3] "Fit For 55." Accessed: May 19, 2026. [Online]. Available: https://www.consilium.europa.eu/en/policies/fit-for-55/

[4] "European grids package." Accessed: May 19, 2026. [Online]. Available: https://energy.ec.europa.eu/topics/infrastructure/european-grids_en

[5] "EUROSTAT European energy use." Accessed: May 19, 2026. [Online]. Available: https://ec.europa.eu/eurostat/web/interactive-publications/energy-2026

[6] "International Energy Agency Europe overview." Accessed: May 19, 2026. [Online]. Available: https://www.iea.org/regions/europe

[7] E. Hristov *et al.*, "Building energy flexibility: A systematic literature review," *Energy Strategy Reviews*, vol. 64, p. 102160, Mar. 2026, doi: 10.1016/j.esr.2026.102160.

[8] A. Arteconi, A. Mugnini, and F. Polonara, "Energy flexible buildings: A methodology for rating the flexibility performance of buildings with electric heating and cooling systems," *Appl. Energy*, vol. 251, Oct. 2019, doi: 10.1016/j.apenergy.2019.113387.

[9] "Annex 67: Energy Flexible Buildings." [Online]. Available: http://www.annex67.org

[10] G. Reynders, J. Diriken, and D. Saelens, "Generic characterization method for energy flexibility: Applied to structural thermal storage in residential buildings," *Appl. Energy*, vol. 198, pp. 192–202, 2017, doi: 10.1016/j.apenergy.2017.04.061.

[11] M. Perino, "Annex 44 -Responsive Building Elements (RBE): a state-of-the-art review", Accessed: May 14, 2026. [Online]. Available: https://www.nachhaltigwirtschaften.at/resources/pdf/annex44_rbe.pdf

[12] E. Taveres-Cachat, F. Favoino, R. Loonen, and F. Goia, "Ten questions concerning co-simulation for performance prediction of advanced building envelopes," *Build. Environ.*, vol. 191, Mar. 2021, doi: 10.1016/j.buildenv.2020.107570.

[13] N. Safer, M. Woloszyn, and J. J. Roux, "Three-dimensional simulation with a CFD tool of the airflow phenomena in single floor double-skin facade equipped with a venetian blind," in *Solar Energy*, Aug. 2005, pp. 193–203. doi: 10.1016/j.solener.2004.09.016.

[14] A. GhaffarianHoseini, A. GhaffarianHoseini, U. Berardi, J. Tookey, D. H. W. Li, and S. Kariminia, "Exploring the advantages and challenges of double-skin facądes (DSFs)," Jul. 01, 2016, *Elsevier Ltd*. doi: 10.1016/j.rser.2016.01.130.

[15] A. Jankovic and F. Goia, "Control of heat transfer in single-story mechanically ventilated double skin facades," *Energy Build.*, vol. 271, Sep. 2022, doi: 10.1016/j.enbuild.2022.112304.

[16] Y. B. Yoon, B. Seo, B. B. Koh, and S. Cho, "Performance analysis of a double-skin façade system installed at different floor levels of high-rise apartment building," *Journal of Building Engineering*, vol. 26, Nov. 2019, doi: 10.1016/j.jobe.2019.100900.

[17] "Overview on european building stock." Accessed: May 19, 2026. [Online]. Available: https://build-up.ec.europa.eu/en/resources-and-tools/articles/overview-decarbonising-non-residential-building-stock

[18] Y. Li, J. Darkwa, G. Kokogiannakis, and W. Su, "Phase change material blind system for double skin façade integration: System development and thermal performance evaluation," *Appl. Energy*, vol. 252, Oct. 2019, doi: 10.1016/j.apenergy.2019.113376.

[19] G. Li Castri, V. Serra, M. Perino, and F. Favoino, "Energy flexibility potential of transparent responsive building envelope elements", doi: 10.26868/25222708.2025.1936.

[20] H. Johra, P. Heiselberg, and J. Le Dréau, "Influence of envelope, structural thermal mass and indoor content on the building heating energy flexibility," *Energy Build.*, vol. 183, pp. 325–339, Jan. 2019, doi: 10.1016/j.enbuild.2018.11.012.

[21] S. Wijesuriya, C. Booten, M. V. A. Bianchi, and R. A. Kishore, "Building energy efficiency and load flexibility optimization using phase change materials under

futuristic grid scenario," *J. Clean. Prod.*, vol. 339, Mar. 2022, doi: 10.1016/j.jclepro.2022.130561.

[22] M. Saffari, C. Roe, and D. P. Finn, "Improving the building energy flexibility using PCM-enhanced envelopes," *Appl. Therm. Eng.*, vol. 217, Nov. 2022, doi: 10.1016/j.applthermaleng.2022.119092.

[23] "Rubitherm macroencapsulated PCM." Accessed: May 20, 2026. [Online]. Available: https://www.rubitherm.eu/en/productcategory/makroverkaspelung-csm

[24] F. Feng, Y. Fu, Z. Yang, and Z. O'Neill, "Enhancement of phase change material hysteresis model: A case study of modeling building envelope in EnergyPlus," *Energy Build.*, vol. 276, Dec. 2022, doi: 10.1016/j.enbuild.2022.112511.

[25] G. Zhou, Y. Yang, X. Wang, and S. Zhou, "Numerical analysis of effect of shape-stabilized phase change material plates in a building combined with night ventilation," *Appl. Energy*, vol. 86, no. 1, pp. 52–59, 2009, doi: 10.1016/j.apenergy.2008.03.020.

[26] S. D. Rezaei, S. Shannigrahi, and S. Ramakrishna, "A review of conventional, advanced, and smart glazing technologies and materials for improving indoor environment," *Solar Energy Materials and Solar Cells*, vol. 159, pp. 26–51, Jan. 2017, doi: 10.1016/j.solmat.2016.08.026.

[27] M. Michael, F. Favoino, Q. Jin, A. Luna-Navarro, and M. Overend, "A Systematic Review and Classification of Glazing Technologies for Building Façades," Jul. 01, 2023, *Multidisciplinary Digital Publishing Institute (MDPI)*. doi: 10.3390/en16145357.

[28] "Glazing units market size." Accessed: May 22, 2026. [Online]. Available: https://www.grandviewresearch.com/horizon/outlook/insulating-glass-windows-market/europe?utm_source=chatgpt.com

[29] M. Riganti, G. Li Castri, V. Serra, M. Manca, and F. Favoino, "Energy saving potential of advanced dual-band electrochromic smart windows for office integration," *Energy Build.*, vol. 327, Jan. 2025, doi: 10.1016/j.enbuild.2024.115084.

[30] T. Bai, W. Li, G. Fu, Q. Zhang, K. Zhou, and H. Wang, "Dual-band electrochromic smart windows towards building energy conservation," Jul. 01, 2023, *Elsevier B.V.* doi: 10.1016/j.solmat.2023.112320.

[31] R. Baetens, B. P. Jelle, and A. Gustavsen, “Properties, requirements and possibilities of smart windows for dynamic daylight and solar energy control in buildings: A state-of-the-art review,” Feb. 2010. doi: 10.1016/j.solmat.2009.08.021.

[32] TERNA, “TERNA statistiche mensili consumo energia elettrica nazionale.” Accessed: May 26, 2026. [Online]. Available: https://www.terna.it/it/sistema-elettrico/statistiche/pubblicazioni-statistiche

[33] “Gestore Mercati Energetici (GME).” Accessed: May 26, 2026. [Online]. Available: https://www.mercatoelettrico.org/

[34] “Photovoltaic Geographical Information System (PVGIS).” Accessed: May 27, 2026. [Online]. Available: https://re.jrc.ec.europa.eu/pvg_tools/it/

[35] “Climate One Building Website.” Accessed: May 27, 2026. [Online]. Available: https://climate.onebuilding.org/#gsc.tab=0

[36] *UNI 10349 Climate Data*.

[37] F. Lu, Z. Yu, Y. Zou, and X. Yang, “Cooling system energy flexibility of a nearly zero-energy office building using building thermal mass: Potential evaluation and parametric analysis,” *Energy Build.*, vol. 236, Apr. 2021, doi: 10.1016/j.enbuild.2021.110763.

[38] “EnergyPlus United States Department of Energy.” Accessed: Jun. 04, 2026. [Online]. Available: https://www.energy.gov/cmei/buildings/articles/energyplus

[39] *Minimum requirements decree 2025*.

[40] D. for byggkvalitet and N. Building Authority, “Regulations o technical requirements for construction works (TEK17) english version.”

[41] “Window Lawrence Berkeley National Laboratory.” Accessed: Jun. 08, 2026. [Online]. Available: https://windows.lbl.gov/window-software-downloads

[42] “EnergyPlus Documentation.” Accessed: Jun. 09, 2026. [Online]. Available: https://energyplus.net/documentation

[43] D. Zhilyaev, A. E. Albanesi, M. C. Demarchi, V. D. Fachinotti, H. L. M. Bakker, and H. M. Jonkers, “A shot in the dark: The current state of PCM hysteresis modelling in building energy simulation software,” *Energy Build.*, vol. 348, Dec. 2025, doi: 10.1016/j.enbuild.2025.116418.